

**Reconfigurable Wheels:  
Re-Inventing the Wheel for the Next Generation of Planetary Rovers**

by

**Brittany Baker**

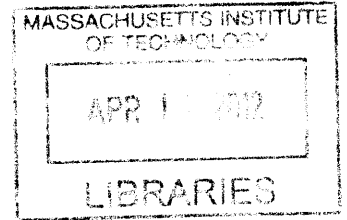
**B.S. Aeronautics and Astronautics  
Massachusetts Institute of Technology, 2008**

**ARCHIVES**

**Submitted to the Department of Aeronautics and Astronautics in Partial Fulfillment of the  
Requirements for the Degree of**

**Master of Science in Aeronautics and Astronautics  
at the  
MASSACHUSETTS INSTITUTE OF TECHNOLOGY**

**February 2012**



**© Massachusetts Institute of Technology 2012. All rights reserved.**

**Author.....**

**Department of Aeronautics and Astronautics  
February 2, 2012**

**Certified by.....**

**Olivier L. de Weck  
Associate Professor of Aeronautics and Astronautics  
Associate Professor of Engineering Systems  
Thesis Supervisor**

**Accepted by.....**

**Eytan H. Modiano  
Professor of Aeronautics and Astronautics  
Chair, Committee on Graduate Students**



# **Reconfigurable Wheels: Re-Inventing the Wheel for the Next Generation of Planetary Rovers**

by

**Brittany Baker**

Submitted to the Department of Aeronautics and Astronautics on February 2, 2012 in Partial Fulfillment of the Requirements for the Degree of Master of Science in Aeronautics and Astronautics

## **Abstract**

Experiences with Spirit and Opportunity, the twin Mars Exploration Rovers, showed that one of the major issues that needs to be addressed in order to expand the exploration capabilities of planetary rovers is that of wheel traction. The relationships governing how much traction a wheel can produce are highly dependent on both the shape of the wheel and terrain properties. These relationships are complex and not yet fully understood. The amount of power required to drive a wheel is also dependent on its shape and the terrain properties. Wheel sizes that tend to maximize traction also tend to require more power. In the past, it has always been a challenge to find the right balance between designing a rover wheel with high traction capabilities and low power requirements. More recently, researchers invented the idea of a reconfigurable wheel which would have the ability to change its shape to adapt to the type of terrain it was on. In challenging terrain environments, the wheel could configure to a size that would maximize traction. In less challenging terrain environments, the wheel could configure to a size that would minimize power. Theoretical simulation showed that the use of reconfigurable wheels could improve tractive performance and some initial prototyping and experimental testing corroborated those findings. The purpose of this project was to extend that prototyping and experimenting. Four reconfigurable wheels were designed, built, and integrated onto an actual rover platform. A control methodology whereby the wheels could autonomously reconfigure was also designed, implemented, and demonstrated. The rover was then tested in a simulated Martian environment to assess the effectiveness of the reconfigurable wheels. During the tests, the power consumption and the distance traveled by the rover were both measured and recorded. In all tests, the wheels were able to successfully reconfigure and the rover continued to advance forward; but as was expected, the reconfigurable wheel system consumed more power than a non-reconfigurable wheel system. In the end, the results showed that if maximizing vehicle traction was weighed more heavily than minimizing power consumption, the use of reconfigurable wheels yielded a net gain in performance.

Thesis Supervisor: Olivier L. de Weck

Title: Associate Professor of Aeronautics and Astronautics and Engineering Systems



## **Acknowledgements**

This project would not have been possible without the support of many people and I would be remiss if I did not publicly express my thanks to a number of individuals. First, I would like to thank my advisor, Olivier de Weck. I had the privilege of working with Professor de Weck as part of my 62x project and was grateful for the chance to continue working on this project with him as a graduate student. I am grateful for all of his support and guidance.

Secondly, I would like to thank Jessica Duda of Aurora Flight Sciences. Jessica served as a mentor for me throughout the course of this project. Her assistance and guidance were invaluable to me, especially during the time that Professor de Weck was on sabbatical. Jessica provided a lot of encouragement and support when things went wrong. She not only helped me solve technical issues specific to my project but also taught me how to be a better engineer in general.

Thirdly, I owe enormous thanks to Todd Billings, Dave Robertson, and Dick Perdichizzi. The three of them constitute the Aero/Astro technical lab staff. I never would have been able to finish my project without their advice and help. I spent many hours in the machine shop, Gelb lab, and hangar, and even when my parts broke or blew up, Todd and Dave kept me laughing the entire time and helped me push through a lot of discouraging and frustrating moments.

I owe a huge thanks to my friends Donna Hunter, Cynthia Furse, Stephanie Ketchum, David Lazzara, John Gardner, Lisa Clarke, Marytheresa Ifediba, and Bill and Jo Maitland. Each of these people has provided me with tremendous support, encouragement and love. Their small acts of kindness often came when I most needed it. In moments of self-doubt or discouragement they patiently listened to me, cheered me on, and kept believing in me even when I lost belief in myself. I am eternally in their debt.

Last, but certainly not least, I would like to thank my parents and siblings. My family is eternal and one of the greatest blessings I have ever been given in life. I was born of goodly parents who raised me in the ways of truth and righteousness. Their love for me is unconditional, their sacrifices innumerable, and I could never do enough to sufficiently repay them for all that they have done and continue to do for me.



# Table of Contents

Nomenclature .....	15
1.0 Introduction .....	17
1.1 Motivation.....	17
1.2 Objective and Goals .....	18
2.0 Background Research and Previous Work .....	19
2.1 Past Rovers and Their Wheels.....	19
2.2 Terramechanics .....	24
2.3 Concept Development .....	28
2.4 62x project .....	29
3.0 Conceptual Design and Development.....	32
3.1 General Challenges and Influence Diagram .....	32
3.2 Three Different Wheel Designs .....	33
3.3 Wheel Sizing and Simulation.....	37
3.4 Strength Modeling (Deflection and Force) .....	39
Simple Beam Theory: .....	39
Simple Beam Theory Results.....	40
3.5 Reconfigurability Metrics .....	42
3.6 Design Selection.....	44
4.0 Fabrication and Assembly .....	45
4.1 Rover Platform Selection .....	45
4.2 Material and Part Selection .....	45
4.3 Wheels and Platform Integration .....	47
4.4 Assembly .....	50
4.5 Initial Drive Testing .....	53
5.0 Integration, Autonomy, and Control.....	56
5.1 Electrical System Overview .....	56
5.2 System Integration and Preliminary Testing.....	56
5.3 Control Methodology.....	61
5.4 A Systems Engineering Perspective .....	63
6.0 Testing and Results .....	66
6.1 Test Set-Up.....	66

6.2 Testing Procedure .....	67
6.3 Test Results .....	68
6.4 Error Analysis .....	78
6.5 Summary of Results .....	80
7.0 Summary and Conclusions .....	81
7.1 Conclusion .....	81
7.2 Future Work .....	81
7.3 Closing Statement .....	83
8.0 References .....	84
9.0 Appendix .....	86



## List of Figures

Figure 1 - Opportunity's wheel stuck in the sand (Image Courtesy of NASA) .....	17
Figure 2 - Side view of a LRV wheel (Image Courtesy of NASA).....	20
Figure 4 - Astronaut Eugene Cernan driving LRV on Apollo 17 (Image courtesy of NASA) .....	21
Figure 3 - A worker hand weaves wire for LRV wheel (Image Courtesy of NASA) .....	21
Figure 5 - JPL engineer with Sojourner rover in front and one of the MERs in back (Image courtesy of NASA) .....	22
Figure 6 - Evolution of Rover Wheels: MER wheel on the left, Sojourner wheel in the center and MSL wheel on the right (Image courtesy of NASA) .....	24
Figure 7 - Diagram of wheel/soil interactions (Image courtesy of [9]) .....	26
Figure 8 - 62x Testing Apparatus .....	30
Figure 9 - 62x Test Matrix .....	30
Figure 10 - Influence Diagram .....	33
Figure 11 - SolidWorks model of first wheel design .....	34
Figure 12 - SolidWorks model of second wheel design .....	35
Figure 13 - SolidWorks model for third wheel design .....	36
Figure 14 - Objective function graph for dry sand .....	37
Figure 15 - Objective function graph for sandy loam I .....	38
Figure 16 - Graph of $J=0$ contours.....	38
Figure 17 - Pin supported arch for thin curved beam theory (Image courtesy of [15]) .....	42
Figure 18 - VEX Robot .....	45
Figure 19 - Composite tire strips made from spring steel and copper mesh .....	46
Figure 20 - Aluminum hubcap and ring flange.....	47
Figure 21 - Linear actuator used in reconfigurable wheel.....	47
Figure 22 - Wheel Attachment Design.....	48
Figure 23 - Wheel axle attachment.....	49
Figure 24 - Copper electric slip rings mounted to outside of inner hubcap .....	49
Figure 25 - Wire brushes for slip rings .....	50
Figure 26 - Wheel axle, hollow tube, and inner hubcap all pinned together .....	52
Figure 27 - Linear actuator mounted to inner hubcap .....	52
Figure 28 - Securing the tire strips.....	53
Figure 29 - The first assembled wheel .....	53
Figure 30 - Rover with four reconfigurable wheels and support bars .....	54
Figure 31 - Wheel with hand-sewn spandex cover .....	55
Figure 32 - Custom made collar to connect leadscrew, bearing/mounts, and hubcaps .....	58
Figure 33 - Bearing and bearing mount for support arch .....	58
Figure 34 - Frictionless rails mounted to rover frame .....	59
Figure 35 - Rover with new support arches .....	59
Figure 36 - Close-up of rail, cart, and arch.....	60
Figure 37 - Close-up of new hubcap attachment.....	60
Figure 38 - Charred remains of a motor driver after it exploded .....	61

Figure 39 - Flowchart for reconfiguration control algorithm.....	63
Figure 40 - Design structure matrix for rover system.....	64
Figure 41 - Testing in the homemade Mars yard filled with pea gravel and popcorn.....	67
Figure 42 - Text matrix of testing procedures.....	68
Figure 43 - Total average distance with reconfiguration for test scenarios.....	70
Figure 44 - Average additional distance traveled due to reconfiguration for test scenarios.....	70
Figure 45 - Average percentage increase in distance due to reconfiguration for test scenarios.....	71
Figure 46 - Average power consumed with reconfiguration for test scenarios.....	72
Figure 47 - Average increase in power due to reconfiguration for test scenarios.....	72
Figure 48 - Average percentage increase in power due to reconfiguration for test scenarios.....	73
Figure 49 - J* values for different alpha values in test scenarios.....	75
Figure 50 - Efficiency calculations for all testing scenarios.....	76
Figure 51 - Relative efficiency values for all test scenarios.....	77
Figure 52 - Potential test diagram for future testing.....	82
Figure 53 - Image Collage: MER on the left, reconfigurable wheel rover on the right, Apollo 1 Hills in the background (MER and Apollo 1 Hills pictures courtesy of NASA).....	83
Figure 54 - Earlier version of the influence diagram.....	86
Figure 55 - Influence diagram with variables.....	87
Figure 56 - Incidence matrix showing dependencies between relevant variables.....	88
Figure 57 - Simple beam theory deflection results for 3hubcap wheel design. The different colors represent different tire strip lengths. The x-axis is the distance along the length of the tire strip and the y-axis is the amount of deflection.....	91
Figure 58 - Simple beam theory deflection results for 62x_ver2 wheel design. The different colors represent different tire strip lengths. The x-axis is the distance along the length of the tire strip and the y-axis is the amount of deflection.....	91
Figure 59 - Thin curved beam theory deflection results for the 3hubcap wheel design. The different colors represent different tire strip lengths. The x-axis is the distance along the length of the tire strip and the y-axis is the amount of deflection.....	92
Figure 60 - Thin curved beam theory results for the 62x_ver2 wheel design. The different colors represent different tire strip lengths. The x-axis is the distance along the length of the tire strip and the y-axis is the amount of deflection.....	92
Figure 61 - Dimensional drawings of inner hubcap and aluminum plug.....	96
Figure 62 - Dimensional drawing for bearings for hollow steel tube.....	97
Figure 63 - Dimensional drawing for support arms.....	97
Figure 64 - Dimensional drawing of collars and vertical mounts for outside hubcaps.....	98
Figure 65 - Specification sheet for linear actuator.....	99
Figure 66 - Specification sheet for stepper motor driver.....	100
Figure 67 - Stepper motor diagrams.....	101
Figure 68 - All of the connections for the electrical system.....	102
Figure 69 - Power and distance data for slow, easy, no tilt scenario.....	104
Figure 70 - Power and distance data for slow, easy, tilted scenario.....	105
Figure 71 - Power and distance data for slow, bumpy, tilted scenario.....	106

Figure 72 - Power and distance data for slow, bumpy, no tilt scenario .....	107
Figure 73 - Power and distance data for fast, easy, no tilt scenario.....	108
Figure 74 - Power and distance data for fast, easy, tilted scenario.....	109
Figure 75 - Power and distance data for fast, bumpy, tilted scenario.....	110
Figure 76 - Power and distance data for fast, bumpy, no tilt scenario.....	111
Figure 77 - Power difference vs. distance difference for all tests .....	112



## List of Tables

Table 1 - Design Comparison of LRV, Sojourner, and MERs .....	23
Table 2 - List of Variables for Equation 2 .....	25
Table 3 - List of Variables for Equations 4–6.....	27
Table 4 - Properties of Soils Used in Wheel Simulation.....	39
Table 5 - List of Variables for Equations 12–15.....	40
Table 6 - Axial Strengths for Modified 62x Design.....	40
Table 7 - Axial Strengths for 3hubcap Design .....	41
Table 8 - Scenario Rankings for All Values .....	78
Table 9 - Statistical Values for Set of 25 Samples .....	79
Table 10 - Wheel Design Comparison .....	89
Table 11 - Material properties for tire strips .....	90
Table 12 – Manufacturability assessment for the 62x_ver2 and 3hubcap wheel designs.....	93
Table 13 - Parts List.....	94
Table 14 - Statistics for slow, easy, no tilt scenario .....	104
Table 15 – Statistics for slow, easy, tilted scenario .....	105
Table 16 - Statistics for slow, bumpy, tilted scenario .....	106
Table 17 - Statistics for slow, bumpy, no tilt scenario .....	107
Table 18 - Statistics for fast, easy, no tilt scenario.....	108
Table 19 - Statistics for fast, easy, tilted scenario.....	109
Table 20 - Statistics for fast, bumpy, tilted scenario.....	110
Table 21 - Statistics for fast, bumpy, no tilt scenario.....	111



# Nomenclature

## Abbreviations

CAD	computer aided design
GMDRL	General Motors Defense Research Laboratory
JPL	Jet Propulsion Laboratory
LRV	Lunar Roving Vehicle
MER	Mars Exploration Rover
MIT	Massachusetts Institute of Technology
MSFC	Marshall Space Flight Center
MSL	Mars Science Laboratory
NASA	National Aeronautics and Space Administration

## Roman Symbols

A	contact area of wheel (for terramechanics)
A	closed area of wire mesh (for simple beam theory)
$A_{ss}$	relative area of spring steel
b	wheel width
$b_1$	length of beam
$b_2$	spring steel width
$b_3$	wire mesh width
c	cohesion
D	wheel diameter
$D^*$	distance
DP	drawbar pull
E	modulus
$E_{ss}$	spring steel modulus
$E_{cw}$	copper wire modulus
$E_f$	relative functional efficiency
$E_p$	relative performance efficiency
F	tractive force
$h_1$	spring steel thickness
$h_2$	wire mesh thickness
I	inertia
$I_{cw}$	copper wire inertia
$I_{ss}$	spring steel inertia
J	objective function
$J^*$	alternative objective function
K	shear deformation modulus
$K_{pc}, K_{pT}$	Terzaghi soil factors
$k_c$	cohesive modulus of deformation

$k_{\phi}$	frictional modulus of deformation
L	length of contact area (for terramechanics)
L	length of beam (for simple beam theory)
n	soil constant
P	power
P	load on beam (for thin curved beam theory)
$P_r$	buckling force
q	uniform load on beam
R	effective radius
$R_b$	bulldozing resistance
$R_c$	compaction resistance
s	wheel slip
T	torque
W	wheel load
w	deflection
z	sinkage

#### **Greek Symbols**

$\alpha$	weighting function (for wheel performance)
$\alpha$	angle between horizontal surface and pin location (for thin curved beam theory)
$\Upsilon$	soil density
$\theta_1$	angle from vertical to point of soil contact
$\theta_2$	angle from vertical to point of loss of soil contact
$\sigma$	normal stress
$\omega$	angular velocity
$\tau$	soil shear strength
$\phi$	internal friction angle



## 1.0 Introduction

### 1.1 Motivation

Forty three years ago, man successfully walked on a world other than the one that we call home. Since that monumental moment, many have dreamed of the day when the world would watch man walk on the surface of Mars. The challenges associated with getting to Mars are much greater than those required for getting to the moon, but that does not mean the planet cannot still be explored in the meantime. Probes and planetary rovers offer promising alternatives for exploring not only the moon and Mars, but other celestial bodies as well.

These probes and rovers come with their own set of unique challenges. Issues of control, vision, navigation, and communication must be handled differently for robotic exploration compared with human exploration. In terms of navigation, it is much easier for a human explorer to assess terrain conditions, decide how to navigate to their desired destination, or adapt to changing conditions than it is for a rover to carry out those same tasks. However, successful navigation is imperative to effective exploration, so the success of a robotic-based mission is largely dependent on the navigational capabilities of the rover. For example, in 2005 one of the Mars Exploration Rovers (MERs), Opportunity, got stuck in a sand pit (see Figure 1). It took engineers a month of painstaking effort to remove the rover, which was almost lost in the process [1].

More recently, in May of 2009, Opportunity's twin, Spirit, also got trapped in the sand and has remained trapped there ever since. [2] Engineers eventually lost communication with the rover and it was officially retired in May 2011. [3] Neither of the MERs can be considered a failure because they significantly outperformed what they were initially designed to do. However, if robotic exploration of Mars is to



**Figure 1 - Opportunity's wheel stuck in the sand  
(Image Courtesy of NASA)**

continue, rovers need to have better capability to traverse challenging terrain, particularly soft soils such as sand. There are multiple ways to enhance the mobility of these rovers. One of the most promising avenues is to design more effective wheels. This endeavor, though, is complicated by the trade-offs that accompany any engineering design problem. It would be easy to install all-powerful, all-terrain wheels, but not without significant setbacks in terms of weight, cost, and complexity. As researchers reach toward the future and look for ways to explore more interesting and challenging places on the moon and Mars, it is clear that new and more innovative engineering solutions need to be developed to enhance the mobility of robotic explorers.

## **1.2 Objective and Goals**

In response to the need to enhance robotic mobility, the purpose of this thesis is to investigate the use of reconfigurable wheels on planetary rovers. Performing a complete evaluation of this concept is not within the scope of this Master's project. Rather, this thesis will seek to fulfill the following important objectives:

1. Explore new design concepts for reconfigurable wheels
2. Select the best design and then build four working prototypes of that design
3. Integrate the four wheels onto a simulated rover platform to demonstrate proof of concept
4. Demonstrate ability of rover to autonomously reconfigure its wheels
5. Demonstrate and assess the effectiveness of using reconfigurable wheels while traversing a simulated Martian environment

The first objective will be completed mainly through software-based analysis and assessment. The remaining objectives will be hardware intensive and focus on the fabrication, assembly, integration, and testing of the wheels.

This thesis will report on each successive phase of the project. The first section has outlined the project goals. The second section will focus on past design considerations that have served as the foundation for this work. The third section will describe the design process for this project. The building and assembly procedures for the mechanical system will be set forth in the fourth section. The fifth section will focus on the design and development of the electrical system. In the sixth section, the testing procedure will be outlined followed by a discussion of the testing results. The seventh and final section will include a project summary, conclusion, and discussion of future work.

## **2.0 Background Research and Previous Work**

### **2.1 Past Rovers and Their Wheels**

#### **Lunar Rovers**

Work on the first planetary rovers began in the early 1960s as the U.S. turned its sights toward landing men on the moon. Development of the lunar rover was mainly conducted under the direction of NASA's Marshall Space Flight Center (MSFC). Although development of the lunar rover was managed by MSFC, many other major contractors, including Boeing Aircraft Corp., Bendix Corp., Grumman Aircraft Engineering Corp., and Northrop Space Laboratories Inc., developed concepts for a lunar rover. At the time, Dr. Mieczyslaw G. Bekker was regarded as the leading authority on land locomotion. He was in charge of the Mobility Research Laboratory at General Motors Defense Research Laboratory (GMDRL) in Santa Barbara, California, and was a key player in the development of some of the first concepts for a lunar rover. Working with him were Samuel Romano, chief of Lunar and Planetary Programs at GMDRL, and Ferenc Pavlics, a chief engineer in Romano's group [4].

The first vehicle design concepts were being developed simultaneously with the logistics of actually getting to the moon, so rover researchers originally operated under the assumption that a moon voyage would consist of two separate launches—one to carry the crew and another to carry equipment. This meant that weight restrictions were much more lenient and initial designs for lunar rovers were very large—many on the order of about 3,000 kg. A critical development in the mid-1960s significantly altered the rover designs: NASA decided that earth orbit rendezvous would be preferred over dual-mode missions. This meant that the astronauts and their equipment would be transported together. As a result, strict weight limits were imposed and the lunar rover could weigh no more than 227 kg (500 lbs) [4].

In the summer of 1965, a two-week conference was held in Falmouth, Massachusetts to outline a ten-year plan for lunar exploration. As part of that plan, engineers and program managers agreed that any surface roving vehicle would need to transport one to two crew members plus a scientific payload a distance of at least 8 km. Design concepts and mobility studies continued to be carried out, but it was not until four years later—only a few days before the historic Apollo 11 landing, in fact—that NASA issued a formal request for proposals for a Lunar Roving Vehicle (LRV). There were 22 specific requirements for the LRV [4]. Those relevant to the wheels included:

- the maximum weight of the vehicle was to be no more than 400 lbs
- the vehicle would have four wheels and each wheel would be individually driven using battery powered electric motors
- the carrying capacity was to be 840 lbs
- the total range of the LRV had to be 120 km
- the LRV had to have an operational lifetime of 78 hours on the lunar surface
- the speed range of the fully loaded vehicle was to be 0–16 km/hr
- the vehicle had to be capable of traversing slopes of up to 25 degrees

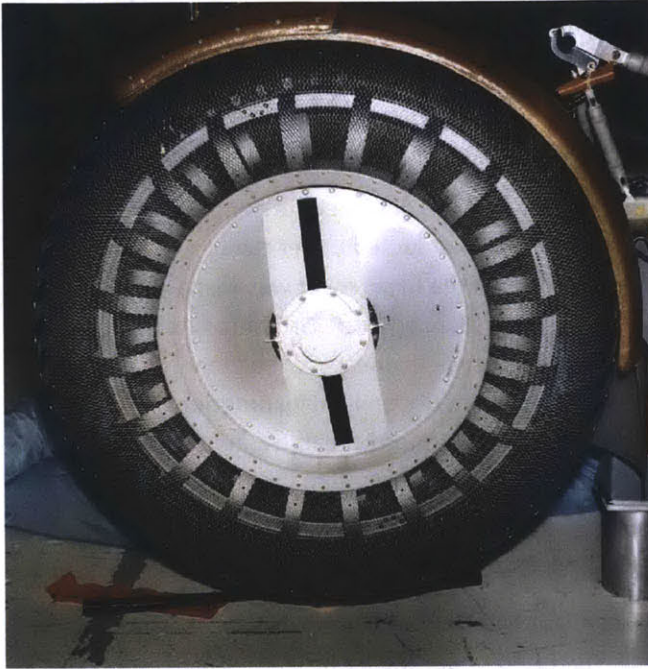


Figure 2 - Side view of a LRV wheel (Image Courtesy of NASA)

- the vehicle had to be capable of negotiating obstacles up to 30 cm high and crevasses 70 cm wide

Four different contractors submitted proposals for the LRV; ultimately the Boeing Co. won the contract. They had less than two years to design, build, and test the LRV, which needed to be delivered to Kennedy Space Center in April 1971.

The entire LRV was a work of engineering genius (see Figure 2). The vehicle worked virtually flawlessly on all of its missions despite the fact that there was limited knowledge available regarding the surface and soil conditions on the moon. The

vehicle's mobility success was largely attributed to the eloquent wheel design.

The design came largely from the initial research and development conducted during the early 1960s as part of NASA's various lunar mobility programs. A major portion of this work was done at GM's Defense Research Laboratories (GMDRL) in Santa Barbara [4].

Two different designs were initially considered for the final product. The first design was a metal-elastic wheel with a flat metal tread and a complex of interior circular cross-section metal springs. The second design consisted of a wire frame with interior hoops and a solid aluminum rim. The second design was eventually selected. Ferenc Pavlics, one of the chief engineers at GMDRL, described the challenges of the wheel design as such: "We had to invent an all-metallic but still flexible wheel. Since this was a manned vehicle going at a reasonable speed over rugged terrain, it had to provide the astronauts with a good ride quality. So, the wheel had to be flexible and have good flotation over the soft lunar terrain....We tried many different types and different materials, and finally nailed down this configuration which was a flexible wire frame-type of wheel. The behavior of the wheel was like a low-pressure pneumatic tire. It was flexible and it had a good footprint over the soft terrain so it didn't sink into the soil. At the same time, it provided a certain amount of damping because the interwoven tires, as they deformed, had a friction at the joints, so it didn't bounce like a spring would." [4]

The wheel diameter was 81.3 cm and the width was 22.8 cm. The finished wheel weighed a mere 5.4 kg and the nominal static load on each wheel, including the weight of the vehicle, the astronauts, and the equipment, was 147 kg. The tire's wire frame was made out of 0.84 mm diameter steel spring wire. 800 strands, each 81.3 cm long, were hand-woven using a special loom so that there was no seam anywhere along the curved surface (see Figure 3). Riveted to the wire mesh were titanium tread strips in a specific chevron pattern that provided 50 percent coverage of the contact patch. The inner circumferential ring

and titanium hoop springs created a secondary frame that helped prevent wheel collapse under the impact of lunar rocks. Extensive testing was done on the LRV wheels, including tests involving lunar soil simulants and tests on a KC-135 flying a parabolic profile to simulate the moon's one-sixth gravity environment [4].

The LRV was successfully used on the last three Apollo flights—Apollo 15, 16, and 17. This vehicle greatly enhanced the scientific capability of these last three missions, permitting the astronauts to cover seven times more distance than previous missions, carry more scientific tools, and collect and return twice the amount of moon rock and soil

samples (see Figure 4). To date, the LRV remains the first and the last human-rated rover, but the lessons learned from that first rover experience were important as the U.S. prepared to send its first rovers to Mars, and they continue to provide valuable insight for current challenges related to rover design [4].



**Figure 3 - A worker hand weaves wire for LRV wheel (Image Courtesy of NASA)**

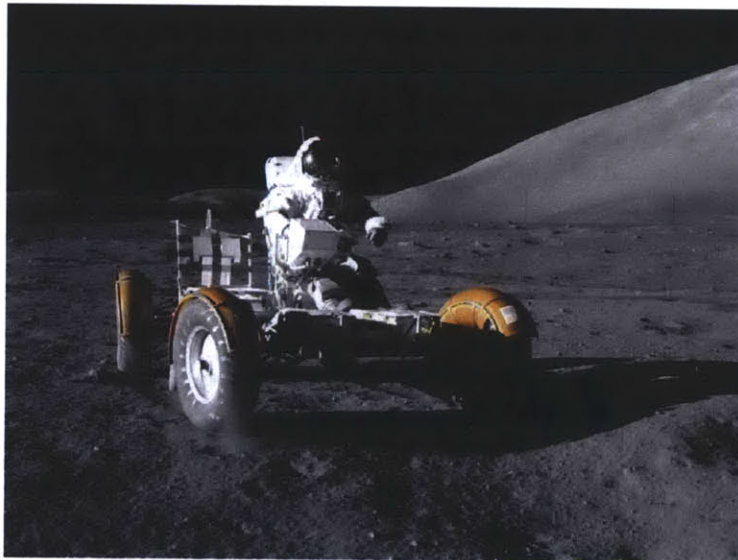


**Figure 4 - Astronaut Eugene Cernan driving LRV on Apollo 17 (Image courtesy of NASA)**

### **Mars Rovers**

Before the Apollo program was over, researchers and engineers had already turned their sights towards landing on Mars. Several successful and unsuccessful attempts at sending landers and probes to Mars began in the 1960s, but the first planetary rover didn't make it to Mars until the late 1990s. The rover was named Sojourner and was part of the Mars Pathfinder mission. The goals of this mission were to demonstrate the feasibility of low-cost landings and exploration of the Martian surface, and characterize the Martian environment for further exploration. Although the Pathfinder lander did much of this work, the ability of the Sojourner rover to explore places outside of the reach of the lander's probes and

cameras was invaluable. This rover was relatively small, with a total mass of 10.5 kg and wheels that were only 13 cm in diameter and 7 cm wide. The speed of the rover was also slow, traveling only 1 cm per second. The most notable feature of this rover was the rocker-bogie suspension system. This was a six-wheeled suspension system developed in the garage of a JPL engineer, Don Bickler. This ingenious design permitted a rover to surmount virtually all potential obstacles while remaining stable.

The Sojourner rover roamed around the Martian surface for about two and a half months before engineers lost contact with it. During that time, it traveled 104 meters and collected a plethora of pictures and data that it relayed back to scientists on earth. The successful demonstration of the Sojourner rover paved the way for the next, much larger Mars Exploration Rover (MER) program [4, 5].

Spirit and Opportunity were the twin rovers that debuted after Sojourner. These rovers were much larger, each weighing 174 kg. Similar to Sojourner, these rovers had six individually-driven wheels and a rocker-bogie suspension system (see Figure 5). Chris Vorhees, one of the primary engineers in charge of the MERs mobility system, described the process and challenge of designing new wheels for these rovers: “We started with the Sojourner wheels as a base to work from. Because of many different engineering demands on the wheels, the wheels for our new rovers didn’t mature until late in the game. A big challenge was to be able to get enough traction to get through soil and over rocks but also to be benign enough to get off the lander without getting tangled in the deflated airbags.” [4]

After lots of modeling, simulation, analysis, prototyping, and testing, the mobility team settled on a final design for the wheels. Each wheel was machined from a single solid piece of aluminum and curved along the entire circumferential surface to maintain uniform contact with the Martian surface. The wheels were 26 cm in diameter and featured spiral flexures in the hubs that served as built-in shock absorbers. The flexures were filled with a special foam material called solimide that remained flexible even in the extreme Martian temperatures. The foam also protected the drive and steering actuators inside the wheel [4, 5].



Figure 5 - JPL engineer with Sojourner rover in front and one of the MERs in back (Image courtesy of NASA)

Spirit was launched first in July of 2003. Opportunity followed three months later, and both rovers successfully landed on the Martian surface in 2004. The mission lifetime of the rovers was designed to be only 90 days, but both rovers far outlasted that time frame [5]. Engineers recently lost contact with Spirit and it was officially retired in May 2011, but as of this writing, Opportunity continues to operate on the red planet's surface, more than eight years after its landing [6]. Together these two rovers have traveled more than 20 km on the Martian surface and explored a variety of terrain, rocks, hills and craters. They have sent back more than a quarter million images and thousands of scientific spectra. Arguably, their most noteworthy contribution is that their analysis and findings have led to the conclusion that at one time water was present on the planet's surface. Although these rovers have been highly successful and able to explore an exceptional amount of terrain, both have faced numerous mobility problems. There are still many locations on the planet's surface that scientists desire to explore, but doing so requires that future rovers be equipped with better mobility systems. Table 1 provides a side by side design comparison for the LRV, Sojourner, and the MERs (also see Figure 6).

The most recent Mars rover is the Mars Science Laboratory (MSL). It launched in November 2011 and is scheduled to land on Mars in August 2012. It is much bigger than the MERs, with an estimated mass of approximately 775 kg. This rover features an even more efficient rocker-bogie suspension system with wheel diameters of 40 cm and the capability to roll over 75 cm-high obstacles. These wheels are very similar to the wheels on the MERs and their effectiveness at navigating through the rough Martian soil is yet to be determined [5].

**Table 1 - Design Comparison of LRV, Sojourner, and MERs**

<b>Rover</b>	<b>Physical Sizes</b>	<b>Notable Features</b>
Sojourner	b = 7 cm D = 13 cm Rover mass: 10.5 kg	- Traction provided by metal wheels with metal spikes - Rocker-bogie suspension system
MERs (Mars Exploration Rovers)	D = 26 cm Rover mass: 174 kg	- Aluminum wheels - Shock-absorption provided by spiral flexures in wheel hubs - Uniform contact with planet surface maintained due to uniform curvature of entire circumferential surface - Rocker-bogie suspension system
LRV (Lunar Roving Vehicle)	b = 22.8 cm D = 81.3 cm Wheel mass: 5.5 kg Rover mass: 210 kg Static load per wheel: 147 kg	- Wheel rim made out of 2024-T4 aluminum alloy - Seamless wire mesh for tire were hand-woven in special loom using 800 strands of wire, each 81.3 cm long and 0.84 mm in diameter - Titanium tread strips were riveted to wire mesh in a specific chevron pattern to provide 50% coverage of contact patch - Wire mesh and titanium tread were riveted to wheel disc - Dynamic impact forces absorbed by a secondary wheel made out of circumferential ring and titanium hoop springs

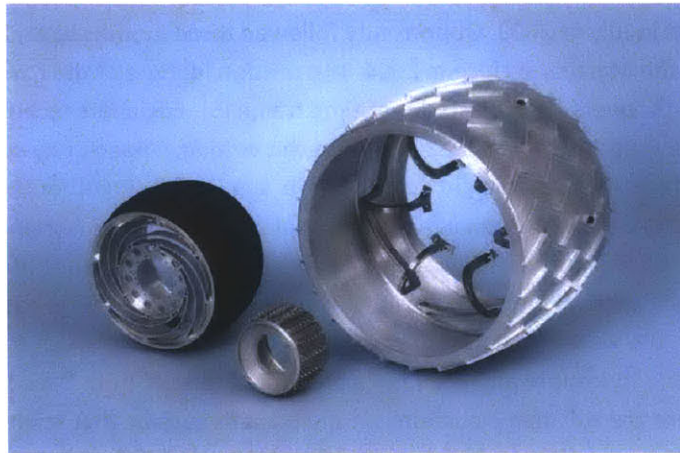


Figure 6 - Evolution of Rover Wheels: MER wheel on the left, Sojourner wheel in the center and MSL wheel on the right  
(Image courtesy of NASA)

## 2.2 Terramechanics

In order to design an effective wheel, it is imperative to understand the interactions that occur between a wheel and the ground it is in contact with. This field of study is called terramechanics. This field can be further divided into other sub-categories. For instance, the equations that describe wheel behavior for pneumatic wheels are different than those for non-pneumatic (i.e., rigid) wheels. Additionally, the parameters most significant for road-based wheels differ from those most significant for off-road vehicles [7-10]. The equations and principles discussed here will focus on rigid wheels for off-road vehicles.

In general, there are three principal elements that control or contribute to vehicle mobility:

- vehicle type and loading conditions
- surface cover and surface layer properties
- geometric terrain features

In order to achieve optimum mobility, the vehicle must be able to move from one point to another with the least amount of wasted motion and energy. The vehicle must be able to “float” on top of the terrain, which requires that the terrain provide sufficient support and strength. Otherwise, the wheels sink into the soil. The wheel must also provide sufficient resistance (i.e., friction) so that thrust can develop between the wheels and terrain with minimal loss due to slippage. The greater the ability of these wheel-terrain interactions to transfer the thrust into the substrate, the more traction the vehicle is able to generate. Vehicle slip happens when the vehicle cannot propel itself forward because it is unable to “grip” the substrate by transferring the surface slip motion to substrate thrust. There are three main ways that the vehicle can become immobilized [7-10]:

- there is too much sinkage due to lack of terrain strength



- excessive slippage occurs even though adequate flotation exists
- slip-sinkage behavior occurs where continued slippage causes the wheels to “dig” into the soil and exacerbate sinkage

All of these interactions are quite complex and developing equations to accurately model them remains an active area of research. One of the reasons why modeling these behaviors is so difficult is because there are many variables that play a role in these interactions. Everything from the geometry and structural properties of the wheel to the environmental conditions and structural properties of the soil influence how much traction the wheel is able to create. To date, the most commonly accepted and used model for off-road vehicles is that developed by Bekker, one of the engineers who was an active participant in the development of the lunar rover. The net force or thrust generated by a wheel is called drawbar pull (*DP*) and is defined as the difference between the tractive force (*F*) generated by the wheel and the sum of resistances from the soil ( $\Sigma R$ ) [7-10].

$$DP = F - \Sigma R \quad (1)$$

The traction created by the wheel-soil interaction is a function of soil properties, the contact area of the wheel, the wheel load, and the amount of slippage. Its exact equation is shown in Equation 2 and Table 2 identifies all of the variables (also see Figure 7).

$$F = (Ac + W \tan \phi) \left( 1 - \frac{K}{sL} \left( 1 - e^{-\frac{sL}{K}} \right) \right) \quad (2)$$

**Table 2 - List of Variables for Equation 2**

<b>Symbol</b>	<b>Variable</b>
<i>A</i>	contact area of wheel
<i>c</i>	cohesion
<i>W</i>	wheel load
$\phi$	internal friction angle
<i>K</i>	shear deformation modulus
<i>s</i>	wheel slip
<i>L</i>	length of contact area

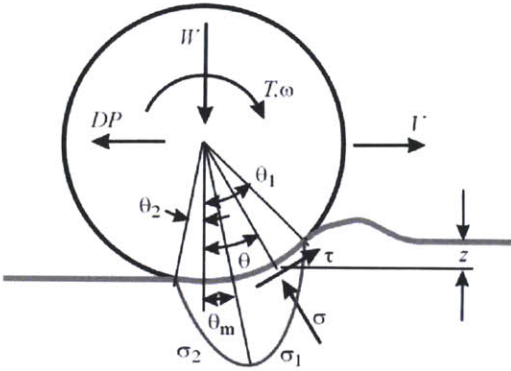


Figure 7 - Diagram of wheel/soil interactions (Image courtesy of [9])

It is important to note that there is a limit to how much tractive force or thrust can be exerted from the soil. Every soil has a failure point—the equivalent to hitting a region of plastic deformation. As a vehicle attempts to drive forward, it exerts a certain amount of stress on the soil. However, if the stress level exceeds a certain point, the soil will experience a structural failure and thrust will not be generated from the wheel-soil interaction. One of the more commonly used metrics to describe

this failure point is the Mohr-Coulomb Criterion, which estimates the shear strength of soil ( $\tau$ ) as a function of soil cohesion ( $c$ ), internal friction angle ( $\phi$ ), and the normal stress exerted on the surface ( $\sigma$ ). Cohesion describes the bond that cements particles together irrespective of internal normal pressures between individual particles. Some soils, such as clay, have very high cohesion; in fact, their shear strength mostly comes from cohesion. Other soils, particularly dry sand, have very little cohesion and their shear strength only comes from the internal normal pressures that exist between individual particles [8]. The failure point is described as follows:

$$\tau = c + \sigma \tan\phi \quad (3)$$

This failure point, which is mostly dependent on soil properties, bounds the amount of traction that can be generated from wheel-soil interactions. Therefore, attempting to minimize soil resistances is arguably a better strategy for maximizing drawbar pull rather than trying to continually increase the thrust from wheel-soil interactions.

There are several different types of soil resistances. These include grade resistance due to a vehicle trying to climb up a slope; obstacle resistance due to stumps, stones, or other objects that the vehicle may have to climb over; bulldozing resistance, which represents the horizontal resistance due to terrain deformation; and compaction resistance, which represents the vertical resistance due to terrain deformation. For off-road conditions, the most prevalent of these resistances are bulldozing resistance ( $R_b$ ) and compaction resistance ( $R_c$ ). Their equations can be seen below [7-10] and variable names are listed in Table 3.

$$R_b = b(czK_{pc} + 0.5z^2\gamma K_{py}) \quad (4)$$

$$R_c = \frac{z^{n+1}}{n+1}(k_c + bk_\phi) \quad (5)$$

$$z = \left[ \frac{3W}{(3-n)(k_c + bk_\phi)\sqrt{D}} \right]^{\frac{2}{2n+1}} \quad (6)$$

**Table 3 - List of Variables for Equations 4–6**

<b>Symbol</b>	<b>Variable</b>
<i>b</i>	wheel width
<i>D</i>	wheel diameter
<i>z</i>	sinkage
<i>n</i>	soil constant
<i>k<sub>c</sub></i>	cohesive modulus of deformation
<i>k<sub>φ</sub></i>	frictional modulus of deformation
<i>W</i>	wheel load
<i>γ</i>	soil density
<i>K<sub>pc</sub>, K<sub>pγ</sub></i>	Terzaghi soil factors
<i>c</i>	cohesion

As can be seen from Equations 4–6, the amount of resistance exerted by the soil is highly dependent on both the shape of the wheel and soil properties. One of the reasons why optimizing a wheel for a variety of soil types is so challenging is because these soil properties vary widely depending on the type of soil. Additionally, there is great variability even within the same type of soil. For example, there are several different types of sand that have different frictional moduli, cohesive moduli and soil deformation exponents. Many of these soil properties also change depending on temperature, humidity, moisture content, and other factors. Even on the Martian surface, there are a wide variety of soils [11]. Despite these challenges, it is still possible to decrease the magnitude of soil resistances by changing the width and/or diameter of the wheel. For example, compaction resistance can be reduced by increasing wheel diameter or wheel width. However, there are many limitations associated with these terramechanic equations and it is important to note the following [7-10]:

- the sinkage equation only works well for  $n \leq 1.3$  and  $z \leq D/6$
- predictions are more accurate for larger wheel diameters and smaller sinkages
- predictions for wheels smaller than 50 cm in diameter become less accurate
- predictions for sinkage in dry, sandy soil are not accurate if there is significant slip-sinkage
- according to the theory used to develop these equations, maximum normal pressure should occur at the lowest point of contact where sinkage is a maximum. However, experiments show that maximum normal pressure occurs at the junction of two flow zones, which is actually in front of the lowest point of contact. Additionally, the location of maximum normal pressure varies with slip.
- it is assumed that normal pressure distribution on the tire-terrain interface is uniform and that shear stress acts along the projected horizontal surface. In reality, the normal pressure distribution is not uniform and the shear stress acts in the direction tangential to the interface.

Although these models are still useful in making design decisions, the discrepancy between theoretical and experiment results indicate that actual interactions between the wheel and terrain are much more complicated than what is being modeled. It is important to be aware of this when using these equations and it is important to rely on both theoretical and experimental results when making design decisions. Furthermore, the complexities of these wheel-soil behaviors and the challenge of finding ways to accurately model them highlight why designing wheels for off-road applications presents so many difficulties.

### 2.3 Concept Development

The concept of a reconfigurable wheel was first proposed by a group of researchers at MIT. One member of that group, Professor Olivier de Weck, worked with engineers from JPL to free the rover Opportunity from its almost catastrophic encounter with a sand pit in 2005. That incident brought to light many of the limitations of the current rover wheels and more attention was given to investigating what could be done to improve rover mobility.

Scrutiny of wheel designs must be viewed from a cost perspective in addition to a performance perspective. From a performance standpoint, the optimal wheel design is one that generates the most drawbar pull, and the terramechanic equations suggests that such a wheel would have a large diameter and a large width. However, the amount of drawbar pull the wheel can generate is only one consideration. The amount of power required to drive the wheels is another metric used to evaluate cost. Power is calculated in relation to the amount of torque ( $T$ ) required to drive a wheel, which is given by [9]:

$$T = \left(\frac{D}{2}\right)^2 b \int_{\theta_1}^{\theta_2} \tau(\theta) d\theta \quad (7)$$

$D$  and  $b$  are still the wheel diameter and width, respectively,  $\tau$  is soil shear strength,  $\theta_1$  is the angle from vertical at which the wheel first comes into contact with the soil and  $\theta_2$  is the angle from vertical at which the wheel loses contact with the soil. Power ( $P$ ) is the product of torque ( $T$ ) and angular velocity ( $\omega$ ):

$$P = T\omega \quad (8)$$

For space applications, more power means more weight—in the form of batteries, solar panels, or other power sources. More weight is always unwelcome for space hardware because it translates into higher launch costs. Adding even a small amount of weight can translate into hundreds or thousands of dollars in increased costs. In order to minimize the amount of power consumed (and hence the weight of the rover) it is desirable to minimize the amount of torque required to drive the wheel. Like drawbar pull, torque is a function of both soil properties and wheel size. As can be seen from equations 7 and 8, larger wheels require more power. This is unfortunate because, as noted earlier, larger wheels tend to optimize drawbar pull. Thus most current wheel designs do not optimize performance, but were selected in part because they fit within power, mass, and cost budgets.

With these additional constraints in mind, de Weck and his fellow researchers proposed a wheel design capable of changing its shape depending on the type of terrain it was traversing which would optimize performance without significantly driving up costs. Based on the lessons learned from the MERs, standard size wheels usually provide sufficient drawbar pull; the rovers did not face mobility issues for most terrain. However, in order to reach all desired destinations, there is still some terrain the rover must traverse where standard wheels are insufficient. It would be inefficient to design the wheels for the most challenging terrain because the rover would also use more power on less challenging terrain. However, if a wheel was capable of changing shape, it could operate in a state of minimal power consumption and then change its shape to increase the amount of drawbar pull when it encountered more difficult terrain conditions [12].

In order to test their new concept, this group of researchers performed a software simulation of a rover with reconfigurable wheels. An objective function,  $J$ , was designed to represent the desire to simultaneously maximize drawbar pull and minimize power.

$$J = \alpha DP - (1 - \alpha)T \quad (9)$$

$\alpha$  was a weighting constant whose value could vary between 0 and 1. A vehicle with wheels whose diameter could vary from 0.8 to 1.1 m and whose width could vary from 0.24 to 0.66 m was simulated to drive over six different types of soil whose properties were all known. When the rover encountered a new soil type, the objective function for all possible wheel states was calculated and the probability that the wheel transitioned to a different wheel state was modeled using Markov Chains. The results of this simulation showed that the use of reconfigurable wheels on a planetary rover could increase its tractive performance by 35 percent. Since the results of this study were supportive of the use of reconfigurable wheels, the next step was to design a wheel capable of changing its shape [12].

## 2.4 62x project

The next major work on reconfigurable wheels took place as part of an undergraduate experimental/senior capstone project (i.e. 62x project) in 2007-2008. I and another undergraduate student set out to build the first working prototype of a reconfigurable wheel, test its performance in a variety of soils, and compare the experimental results to the simulation results of de Weck's research group. The wheel featured two aluminum hubcaps connected by an axial linear actuator and a tire of partially overlapping segments made from copper wire mesh and spring steel. The idea was that on soft terrain the wheel would move to its widest position, providing the largest possible contact area and minimal sinkage. On hard terrain the wheels would become narrow and minimize power, similar to a racing bicycle wheel on a paved road.

A test apparatus was constructed and the prototype wheel design was tested in three different soil types—sand, gravel and rock. These tests were performed using only one wheel. The wheel was not attached to a rover, but was suspended from a support structure and driven using an electric motor and bicycle chain (see Figure 8). In each soil type, two different tests were performed—one to measure drawbar pull and another to measure power. For the drawbar pull tests, an extensional spring was

attached to the wheel rig and test apparatus. Drawbar pull was calculated by measuring the distance the wheel could pull the spring and then converting that value to force using Hooke's law ( $F = kx$ ). For the power tests, the wheel was allowed to travel the length of the test bed (approximately 1.8 m) and the average current required to run the motor was recorded. Power was then calculated using the relation  $P = VI$ . For each soil type, the wheel was tested in three different configurations and three different loading conditions. Figure 9 outlines the 62x test matrix. Each test was repeated multiple times; in total 195 power tests and 465 drawbar pull tests were performed [13].



Figure 8 - 62x Testing Apparatus

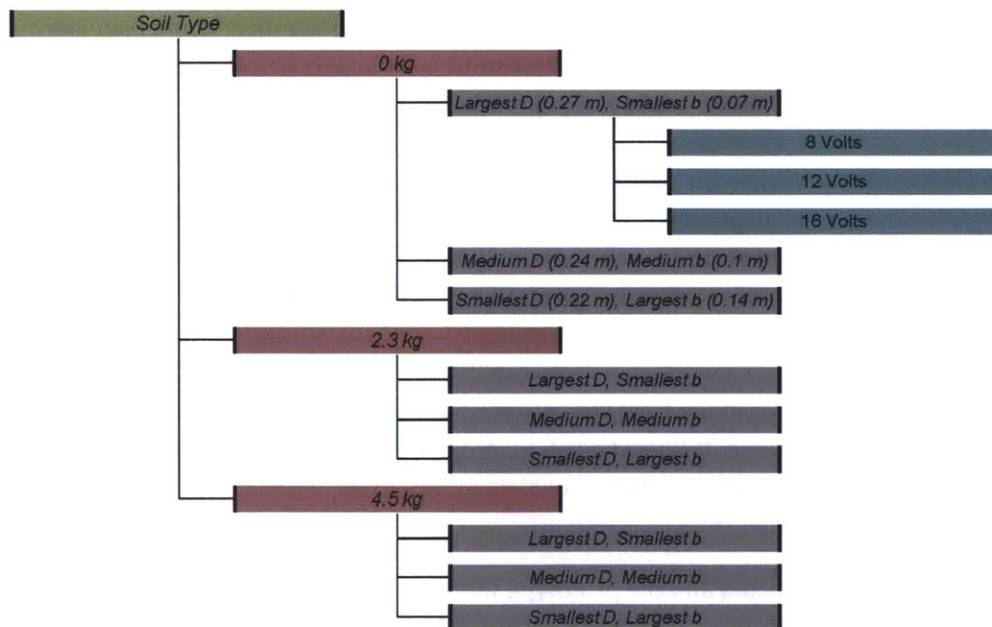


Figure 9 - 62x Test Matrix

The experimental results from this project did not match the simulation results exactly, but they were nevertheless very encouraging. When compared to a standard wheel, the reconfigurable wheel had lower power consumption in sand and gravel, but not rock. The reconfigurable wheel always had better drawbar pull performance in sand and better performance in rock for about 50 percent of the tests. Overall, this project successfully demonstrated the proof of concept for a reconfigurable wheel and provided sufficient experimental evidence to support the notion that a reconfigurable wheel could improve a rover's mobility [13].

## **3.0 Conceptual Design and Development**

### **3.1 General Challenges and Influence Diagram**

The focus of this project is to design, build, and integrate reconfigurable wheels as a proof of concept, but as will be seen later on, the optimal design of a reconfigurable wheel is dependent on the specific kind of rover that those wheels are designed for. Although only one wheel was built for this project, the overarching design process for a reconfigurable wheel will be examined in order to facilitate application to a variety of different rovers and missions.

The first step was to create an influence diagram outlining the relationships between all of the key parameters involved in the design of a reconfigurable wheel; see Figure 10 for this diagram. The green box represents outside factors that the designer has no direct control over—in this case, the variety of terrain and the properties of the different soil types. The purple boxes represent potential rover requirements—a mass budget, the number of wheels the rover must have, and how fast it must be able to travel. It is likely that rovers will have other requirements that are also relevant for the wheels, but for this project those three requirements were deemed the most relevant. The yellow boxes represent the parameters that the designer can choose—how big the wheels should be and what materials will be used to build them.

Those initial inputs and requirements then break down into and affect other parameters in the wheel design. For example, power will be needed for the regular motors used to drive the rover, but power will also be needed to actuate the wheel when it is changing shape. The amount of power available will influence what kind of drive motors can be used and what type of actuation method is most prudent. The type of terrain the rover encounters, the mass of the rover, how many wheels it has and the size of its wheels will all determine how much drawbar pull can be generated, which is ultimately a measure of wheel performance. Similarly, the weight of the rover and the material of the tire will dictate how strong the tire must be, which will influence the physical design of the tire itself.

The two main outputs or measurable metrics of the design are the wheel performance and cost. Wheel performance represents the effectiveness of the reconfigurable wheels and whether or not they are successfully improving the ability of the rover to navigate challenging terrain. Cost is a driving factor in any engineering project and if the design is overly complex or particularly difficult to manufacture, it will be evident in the cost associated with the design. The goal is not to create invincible wheels, but rather to create more effective wheels at a reasonable cost. Considering all of these internal relationships is extremely important when designing the reconfigurable wheels (see appendix for additional figures).

In general, the two main challenges associated with designing a reconfigurable wheel deal with power and strength. The wheel design must provide strength and rigidity to support the full weight of the rover and simultaneously be sufficiently flexible to change their shape. The power challenge is coupled with strength. The goal of the reconfigurable wheel is to minimize power, but changing the shape of the wheel requires additional power. Therefore the optimal design will be one that provides sufficient strength while minimizing the amount of power required for reconfiguration.



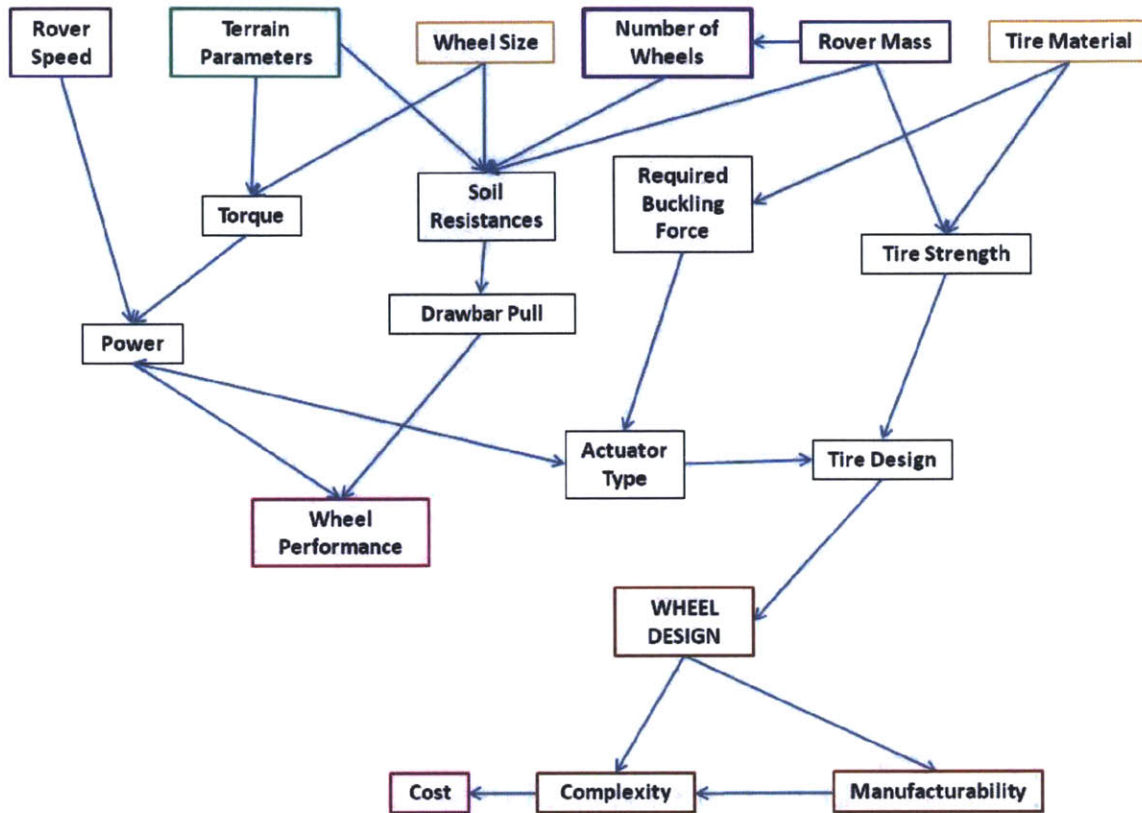


Figure 10 - Influence Diagram

### 3.2 Three Different Wheel Designs

Once all of the internal relationships were defined, the next step was to create feasible designs for the wheels. The process began with general brainstorming regarding different shapes, materials, and actuation methods. Some initial prototyping using cardboard, duct tape, thread, and wire ties was done to test out design ideas. This initial prototyping helped to identify which concepts and ideas were promising and which ones were obviously problematic. This brainstorming and prototyping resulted in three main wheel designs that were subsequently modeled using the SolidWorks computer aided design (CAD) system.

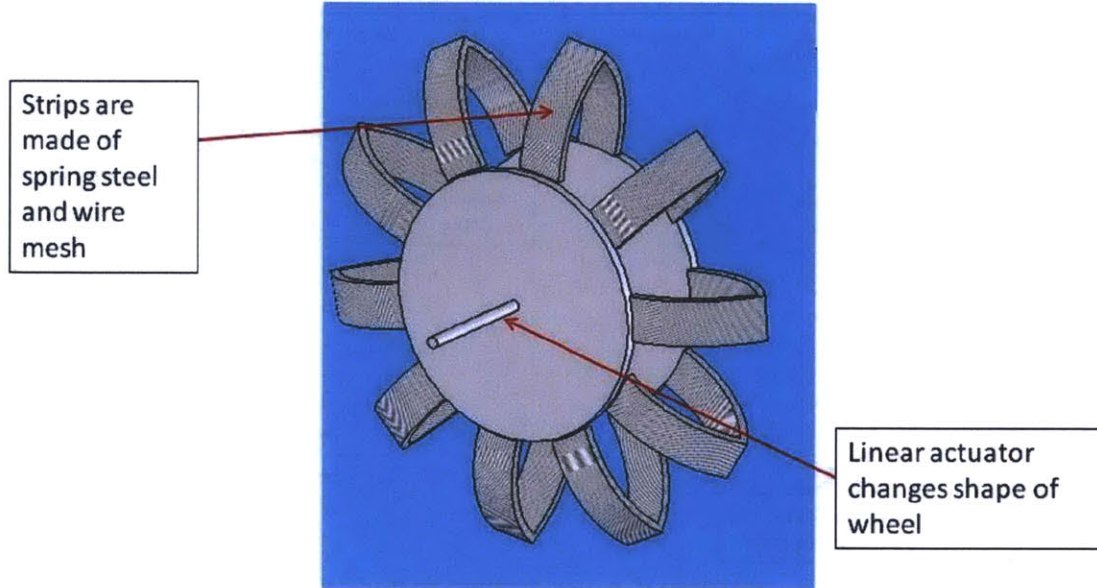


Figure 11 - SolidWorks model of first wheel design

The first design is a modified version of the 62x wheel (Figure 11). There are two aluminum hubcaps connected by a linear actuator. The tire of the wheel is made from composite strips of copper wire mesh and spring steel. These strips span the circumference of the wheel. The spring steel increases the strength of the tire and the copper strips increase the surface area and rigidity of the tire. When the linear actuator pulls the hubcaps closer together, the strips buckle to create a smaller wheel width but larger wheel diameter.

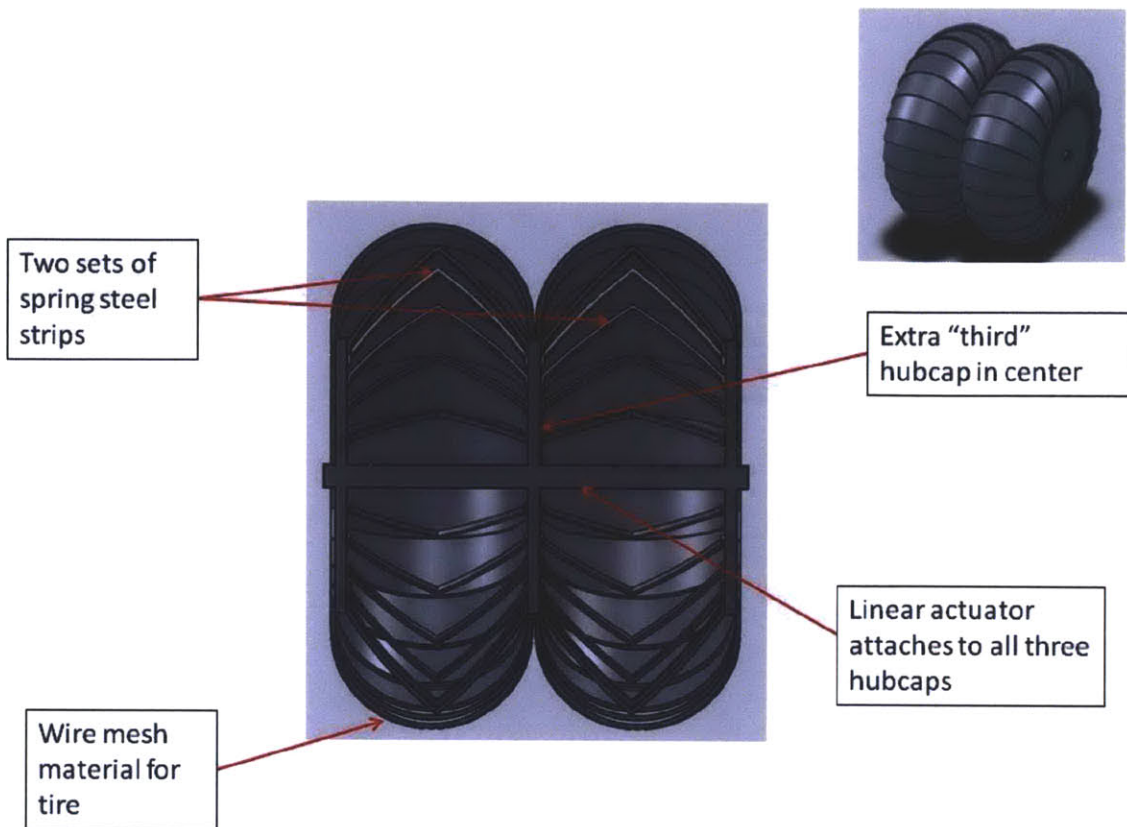


Figure 12 - SolidWorks model of second wheel design

The second design, nicknamed the 3hubcap design, is essentially two narrow wheels connected as one (Figure 12). There are three hubcaps connected to the linear actuator. As in the first design, when the linear actuator pulls the hubcaps closer together, the strips buckle to create a smaller wheel width and larger diameter. One of the major concerns with the first design was whether it would be strong enough to support the weight of a large rover. The shorter composite strips in this design increase the strength of the tire, making it less likely to collapse under larger loads.

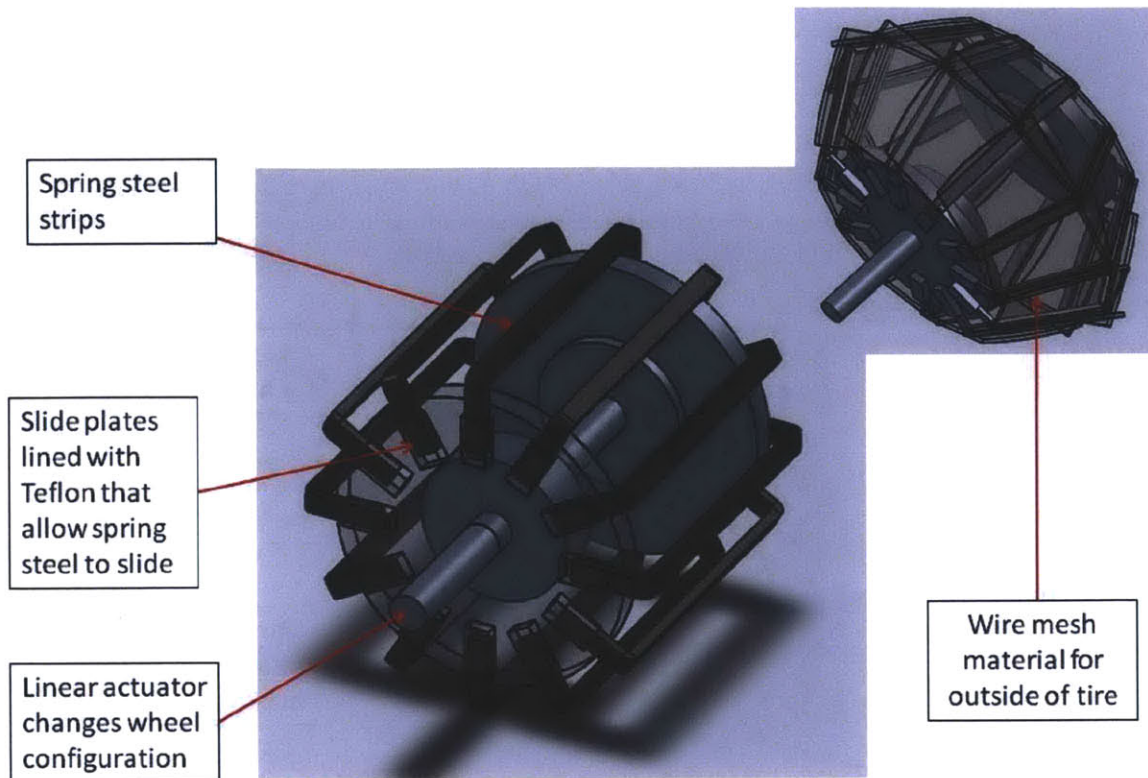


Figure 13 - SolidWorks model for third wheel design

For the final design (Figure 13), two aluminum hubcaps are connected by a linear actuator. However, instead of buckling the spring steel strips slide in and out of the hubcap to change the wheel size. The small transparent fixtures on the side of the wheel are Teflon coated plates that allow the spring steel to slide with as little friction as possible.

Once these three concept designs were created, they were compared using several figures of merit, including cost, weight, complexity, ease of manufacturing, susceptibility to environment, and failure modes/risk (see appendix). After consulting with the head of the MIT Aero/Astro machine shop, it was concluded that the third design would not be robust in a sandy environment because the sand granules would most likely cause the Teflon plates to become clogged and possibly deteriorate. Additionally, after building prototypes of the design it was discovered that a second mechanism beside the linear actuator would most likely be needed to initiate the sliding motion in and out of the Teflon plates. Based on these considerations, it was decided that this concept would not be used as the final design.

The 3hubcap design would cost and weigh slightly more than the modified 62x design because the third hubcap requires extra material. The design would be more complex and harder to assemble because the actuator would have to be secured to the intermediate hubcap. However, both designs are equally

susceptible to the environment and one design does not have significantly greater risk of failure than the other. Therefore the most important comparisons between these two designs was how strong they would be and how much force would be required for actuation. As mentioned previously, these are the two key challenges in the wheel design. As such it was desirable to find a way to model and quantify these two important parameters.

### 3.3 Wheel Sizing and Simulation

Before computing the respective strengths of these designs it was necessary to determine the actual dimensions of the wheel. The size of the wheel should obviously depend on the size of the rover, but it should depend on other factors as well. Another important question to address for reconfigurable wheels is what range of wheel size is most appropriate. The answer to this question is also dependent on the type of soils the vehicle would navigate. One soil might require only a small change in wheel size while another soil might require a much larger change in wheel size. There are so many different kinds of soils that it would be impossible to design a reconfigurable wheel capable of traversing all types. Since these wheels are for Mars rovers, a simulation was developed to examine the range of wheel sizes needed for several different types of soil for a rover approximately the same size as Spirit and Opportunity.

For this simulation, the terramechanic equations outlined in Equations 1-7 were used to compute drawbar pull (DP) and torque (T) for five different types of soil and a range of wheel sizes. The objective function developed by de Weck et al. (Equation 9) was also computed for each of these different soil and wheel combinations. For each of the soil types, a minimum J point was identified at the point where J was zero. A negative J could be caused by a negative DP value or by a DP value that was less than the torque value. Since either situation is undesirable, the  $J = 0$  point represents the minimum acceptable wheel size. Graphical results of the simulation can be seen in Figures 14 and 15. The width in the simulation ranged from 5 to 25 cm and the diameter ranged from 15 to 35 cm. The J value is dimensionless because the DP and T values were normalized.

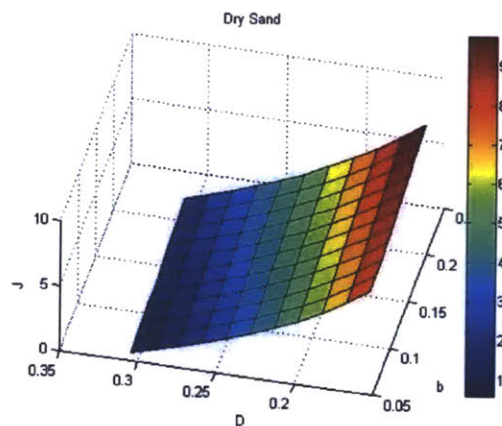


Figure 14 - Objective function graph for dry sand

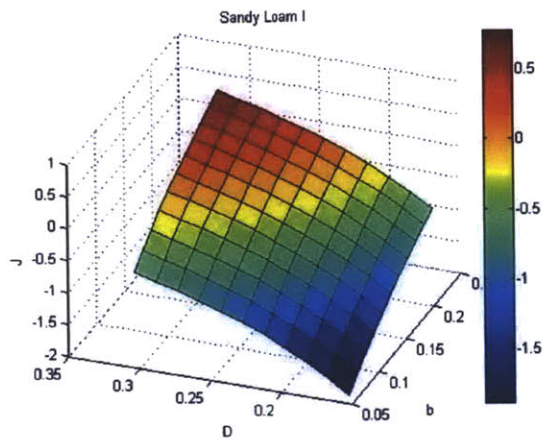


Figure 15 - Objective function graph for sandy loam I

By identifying the  $J=0$  boundaries for a variety of soil types, it was then possible to pick wheel dimensions. In order to be effective in multiple soil types, the wheel needed to be capable of changing its size to cross the  $J=0$  boundary for as many soils as possible. Figure 16 shows  $J = 0$  contours for different types of soil and different alpha values. After running this simulation for five different soil types whose soil properties were obtained from [10] and can be seen in Table 4, the maximum wheel width was identified as 20.3 cm (8 in.) and the minimum wheel diameter was identified as 19.8 cm (7.8 in.).

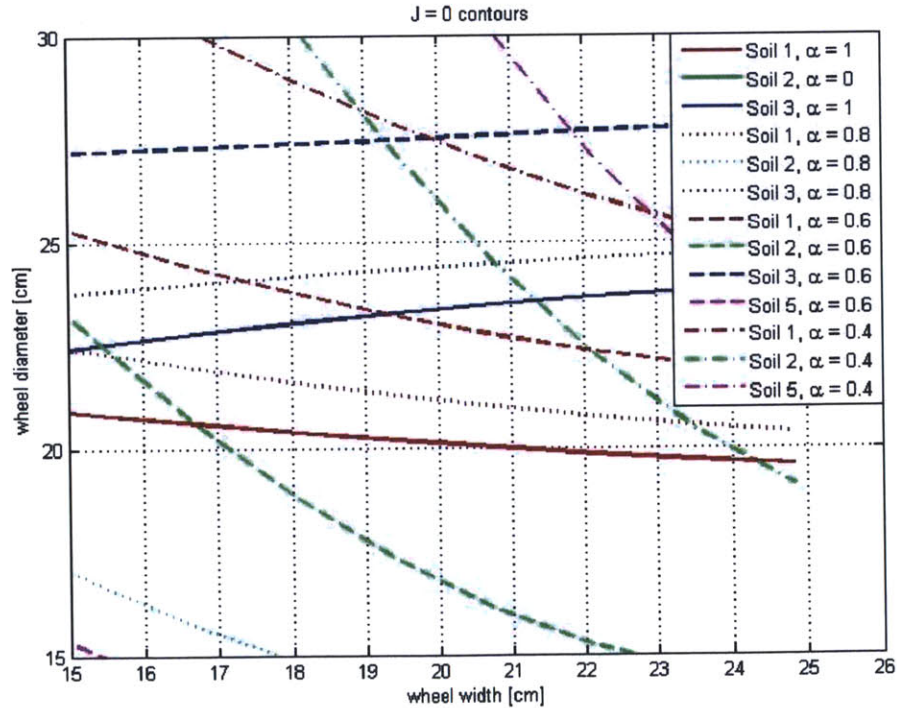


Figure 16 - Graph of  $J=0$  contours

Table 4 - Properties of Soils Used in Wheel Simulation

Soil Type	$k_c$ [kN/m <sup>n+1</sup> ]	$k_\phi$ [kN/m <sup>n+2</sup> ]	$c$ [kPa]	$\phi$ [deg]	$n$	$K$ [m]	Density [kg/m <sup>3</sup> ]
LETE Sand	6.49	505.8	1.15	31.5	0.7	1.15	1600
Clayey Soil	13.19	692.15	4.14	13	0.5	1.15	1520
Sandy Loam I	2.79	141.11	15	25	0.3	1.13	1500
Dry Sand	0.99	1528.43	1.04	28	1.1	3	1600
Sandy Loam II	74.6	2080	0.22	33.1	1.1	2.54	1650

### 3.4 Strength Modeling (Deflection and Force)

As can be seen from the influence diagram (Figure 10), one of the key relationships is the link between the tire material and the actuators. The tire material dictates the strength of the tire. The tire strength can be separated into axial and radial directions. The strength of the tire in the radial sense must be strong enough to support the weight of the rover. The strength of the tire in the axial direction is important because it dictates how much actuation force must be applied in order to change the shape of the wheel. Greater force requirements also translate into greater power requirements, which must be carefully monitored to fit within budget restrictions. Since both the axial and radial strengths are so vital to the overall design and performance of the wheel, it was desirable to find a way to model them. For the purposes of modeling, the tire strips were considered as individual components. The strength of each strip was then calculated using simple beam theory. The weight of the rover acts downwards and the natural tendency of the tire material will be to deflect under this weight. Therefore, the metric used to evaluate the radial strength of the tire will be how much deflection occurs due to the weight of the rover. A similar metric must also be used to evaluate the axial strength of the tire. When the hubcaps are pushed together it causes the wire strips to buckle, therefore the metric used to measure axial strength is the buckling force of the material. This is also a quantity that can be calculated from simple beam theory [14].

#### Simple Beam Theory:

The equation from simple beam theory that describes the deflection in a beam is as follows:

$$w(x) = \left(\frac{q}{48EI}\right)(x^4 - 2Lx^3 + L^3x) \quad (10)$$

$w$  is the deflection,  $L$  is the length of the beam,  $q$  is the uniform load on the beam,  $E$  is the beam's modulus, and  $I$  is the beam's inertia.

The equation for the buckling force is:

$$P_r = \frac{4\pi^2 EI}{b_1^2} \quad (11)$$

$P_r$  is the buckling force and  $b_1$  is the length of the beam. An additional consideration that must be taken into account for both equations is that the wire strips or “beams” are made of two different materials that consequently must be modeled as composites. This requires that the overall material modulus be weighted according to the relative area of the two materials and the overall material inertia must be the combined inertia of both materials (Relevant material properties are listed in the appendix).

$$E = A_{ss}E_{ss} + (1 - A_{ss})E_{cw} \quad (12)$$

$$I = I_{ss} + I_{cw} \quad (13)$$

$$I_{ss} = \frac{b_2 h_1^3}{12} \quad (14)$$

$$I_{cw} = \frac{A b_3 h_2^3}{12} \quad (15)$$

**Table 5 - List of Variables for Equations 12–15**

Symbol	Variable
$E_{ss}$	spring steel modulus
$E_{cw}$	copper wire modulus
$A_{ss}$	relative area of spring steel
$I_{ss}$	spring steel inertia
$I_{cw}$	copper wire inertia
$b_2$	spring steel width
$h_1$	spring steel thickness
$A$	closed area of wire mesh
$b_3$	wire mesh width
$h_2$	wire mesh thickness

### Simple Beam Theory Results

The length of the strips for the 62x design was 8.25 inches and the length of the strips for the 3hubcap design was 4.5 inches. The width of the copper wire was 1.5 inches and the width of the spring steel was 0.25 inches. The buckling force required for two different spring steel thicknesses and two different wire mesh densities can be seen in Tables 6 and 7.

**Table 6 - Axial Strengths for Modified 62x Design**

62x ver2	0.012" spring steel	0.015" spring steel
8 Mesh	12.91 N	13.30 N
10 Mesh	10.08 N	10.47 N



**Table 7 - Axial Strengths for 3hubcap Design**

<b>3hubcap</b>	<i>0.012" spring steel</i>	<i>0.015" spring steel</i>
<i>8 Mesh</i>	85.34 N	87.93 N
<i>10 Mesh</i>	66.67 N	69.22 N

To verify that these were reasonable results, a quick comparison was made with the initial 62x wheel. That wheel was made from 10 Mesh copper wire and 0.012 inch spring steel. Both the spring steel and the copper wire strips were 7 inches long. The actual wheel consisted of 16 composite strips and required approximately 110 N of force to cause the strips to buckle. When the buckling force model is run with the dimensions for the initial 62x wheel, the buckling force required for one strip is 14 N. Multiplying that by 16 yields an estimated required buckling force of 224 N. There is about a 100 N difference between the calculated buckling force and the actual buckling force. This shows that there is room for improvement in the buckling model, so this model could only be used as a coarse first order approximation. Since the main purpose of modeling the required buckling force is to have reasonable force estimates with which the two different wheel designs can be compared rather than to exactly determine the required buckling force, this simple beam model is sufficient for the purposes of model comparison.

The buckling force estimates suggest that the density of the wire mesh has a greater effect on axial strength than the thickness of the spring steel. More importantly, it can be seen that the 3hubcap design requires approximately 6.5 times more buckling force than the modified 62x design. From a power conservation standpoint, the 62x design is favorable over the 3hubcap design.

### **Thin Curved Beam Theory**

As noted earlier, the metric used to evaluate the tire strength was the amount of deflection that would occur in the tire material. Simple beam theory was initially used to compute this quantity. Equation 10 shows the deflection equation for simple beam theory. Deflection estimates made using this equation yielded results that did not make sense since the deflection amounts were actually larger than the length of the beam (see appendix). Therefore, another theory was found to more accurately model the material deflection: thin curved beam theory [15]. This theory describes the deflection for a thin arch, which is precisely what the tire material for the reconfigurable wheels is. Under this theory, the deflection is given by:

$$w_{max} = \frac{PR^3}{EI} G_3 \quad (16)$$

$$G_3 = G_1 - \frac{[4\sin(\alpha) + 3\cos(2\alpha) - (\pi - 2\alpha)\sin(2\alpha) - 1]^2}{8(\pi - 2\alpha)(1 + 2\sin^2(\alpha)) - 24\sin(2\alpha)} \quad (17)$$

$$G_1 = 0.125[(\pi - 2\alpha)(1 + 2\cos^2(\alpha)) - 8\cos(\alpha) + 3\sin(2\alpha)] \quad (18)$$

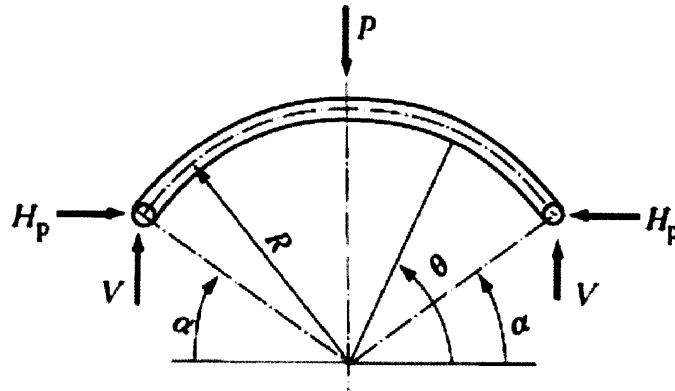


Figure 17 - Pin supported arch for thin curved beam theory (Image courtesy of [15])

$P$  is the load on the beam,  $R$  is the effective radius of the beam,  $\alpha$  is the angle between the horizontal surface and the pin location, and  $w$  is the amount of deflection (Figure 17). Using this theory to compute estimates for the amount of deflection in the beam yielded much more reasonable results. For the 62x design, the maximum deflection was 6.22 cm and for the 3hubcap design the maximum deflection was 0.54 cm. These numbers suggested that the 3hubcap design was significantly stronger than the 62x design, which was not unexpected. In the 3hubcap design, each wheel is essentially two wheels, so the weight of the rover was effectively distributed across eight wheels rather than only four. The effective radius for this design is much smaller as well since the total width of a single wheel is essentially spread across two wheels. So whereas the 62x design is more favorable than the 3hubcap design from a power conservation perspective, the 3hubcap design is more favorable from a strength perspective.

### 3.5 Reconfigurability Metrics

While the concept of a reconfigurable wheel holds potential for improving a rover's ability to traverse challenging terrain, the idea is not without downsides. Additional power and hardware is required to change the wheel's shape and a reconfigurable wheel is certainly more complex than a non-reconfigurable wheel. It is necessary to assess whether the net benefits from a reconfigurable wheel outweigh the disadvantages. Siddiqi, de Weck, and Hoffman reviewed this concept of reconfigurability in space systems and designed two important reconfigurability metrics to be used in determining whether the net benefit of a particular reconfigurable system is positive or negative [16-17]. The first metric defines a relative function efficiency ( $E_f$ ) that compares the efficiency of the reconfigurable system to the efficiency of a non-reconfigurable system whose capability is equivalent to the reconfigurable system:

$$E_f = \frac{\text{Functional efficiency of reconfigurable system}}{\text{Functional efficiency of non-reconfigurable system}} \quad (19)$$

The functional efficiency of each system is defined as the ratio of the functional capability to the resources required for that capability. The specific parameters that best quantify those metrics must be individually defined for each system. For the reconfigurable wheels, it was decided that the functional capability of the reconfigurable wheels was the ability to achieve multiple wheel states, and the resource required to achieve that capability was the necessary wheel mass. In other words:

$$\text{Functional Efficiency} = \frac{\# \text{ of wheel states}}{\text{wheel mass}} \quad (20)$$

The functional efficiency of a non-reconfigurable wheel for a MER-sized rover was calculated. The functional efficiency of a reconfigurable wheel for a similar sized rover with three wheel states was also calculated. The relative functional efficiency ( $E_f$ ) of this MER-sized system was 3.688. Any value greater than one indicates that the reconfigurable system is favorable because it is more functionally efficient than the non-reconfigurable system. In this case, the value is much greater than one, which suggests that despite the need for additional resources, the reconfigurable wheels provide substantial functional advantages over non-reconfigurable wheels.

The second reconfigurability metric defined by Siddiqi et al. was relative performance efficiency ( $E_p$ ). Similar to before, this metric compares the performance efficiency of a reconfigurable and non-reconfigurable system.

$$E_p = \frac{\text{Performance efficiency of reconfigurable system}}{\text{Performance efficiency of non - reconfigurable system}} \quad (21)$$

Once more, the exact definition of performance efficiency is dependent on the particular application, but in general the performance efficiency for each system is a ratio of performance to resources. For reconfigurable wheels, the performance efficiency was defined as the ratio of the net drawbar pull of each system (i.e. a performance metric) compared to the power required for each system (i.e., a resources metric):

$$\text{Performance Efficiency} = \sum_{i=0}^n \frac{DP_i}{P_i} \quad (22)$$

$n$  represents the total number of states in the system. The relative performance efficiency was calculated for the same reconfigurable, MER-sized system described above. Drawbar pull and power values were averaged for five different soil types and calculated using Equations 1–8. The relative performance efficiency for this system was 1.323. Again, this value is greater than one, which indicates that the reconfigurable system provides a net gain in performance. Hence, the results from both reconfigurability metrics suggest that there is a net benefit in using reconfigurable wheels for planetary rovers.

### **3.6 Design Selection**

At this point, it has been quantitatively shown that using either the 3hubcap reconfigurable wheels or the 62x reconfigurable wheels is more efficient than using non-reconfigurable wheels. The 3hubcap design and the 62x design have both been analyzed and compared according to cost, weight, complexity, ease of manufacturing, susceptibility to environment, failure modes/risk, and strength. As explained earlier, strength is the most critical figure of merit. For the specific case of a MER-sized wheel, the best design choice is the 3hubcap design. This design requires more force to actuate (i.e., more axial strength), but its radial strength is significantly greater. The radial strength is more important than the axial strength because the primary requirement of the wheel is that it is capable of supporting the weight of the rover.

From the analysis it is also possible to make design selections in a more general sense. As robotic exploration expands, rovers will undoubtedly be used more extensively and there will be many different sizes of rovers needed. The results presented in this section were all based on using a MER-sized rover model, but it is hoped that the software tools developed here will aid in the design of reconfigurable wheels for other rover sizes as well, since it is possible to change the rover size in the simulation codes. While the 3hubcap design is the optimal choice for a MER-sized rover, it is important to note that the 62x design would be sufficiently strong to support the weight of smaller rovers. Based on the analysis completed in this project, for smaller rovers (i.e., < 25 kg) the 62x reconfigurable wheel design would be recommended because it provides sufficient strength while minimizing power, but for larger rovers (such as MER-type rovers) the 3hubcap reconfigurable wheel design is the best choice to ensure sufficient wheel strength.

## 4.0 Fabrication and Assembly

### 4.1 Rover Platform Selection

Once the design analysis had been completed, the next step was to make material and part selections. The first part selection regarded which rover platform the wheels would be installed on. Originally it was hoped that the K-REX rover from ProtoInnovations would be available for use. The K-REX rover is an actual rover used for earth-based rover testing. Unfortunately, the K-REX rover could not be used due to some legal issues so it became necessary to find an alternative rover platform. Several options were considered. The most promising options were a large RC “monster truck”, a child’s ride-on electric car, or a VEX robot. After weighing the pros and cons of these different options, the VEX robot was selected as the rover platform (Figure 18). Although significantly smaller than a MER type platform, this platform could be purchased as part of a kit that included drive motors, a microcontroller, and a number of different sensors—all necessary items to make the rover autonomous. The rover base is approximately 7.5 inches wide and 12.5 inches long. The rover came with 5 inch diameter wheels, but rather than using these wheels, the reconfigurable wheels were attached to the rover platform instead. The size of this rover platform was comparable to the Sojourner rover, and its mass was within the small rover category, therefore the modified 62x wheels were the best design choice for this platform.

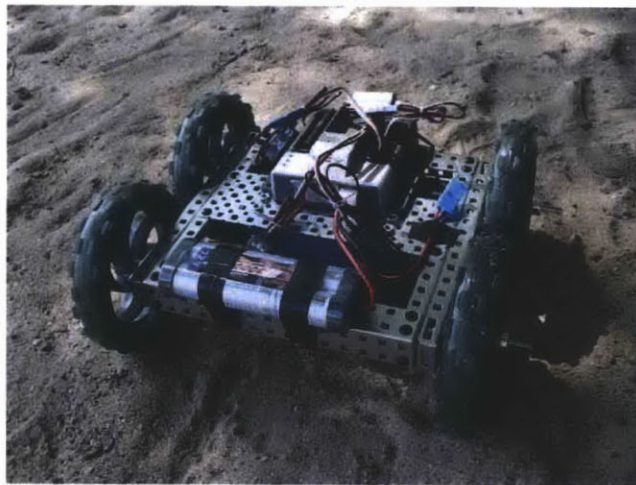
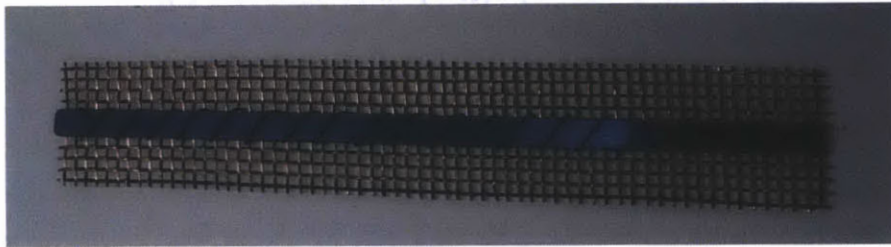


Figure 18 - VEX Robot

### 4.2 Material and Part Selection

Once the wheel design and rover platform were chosen, the details of the wheel size and type of materials could be determined. Since the purchased robot was about the same size as the Sojourner rover, the wheels were sized similar to the Sojourner wheels. The hubcaps were 4.5 inches in diameter and the tire strips were 6.5 inches long. After assembly, the minimum wheel width was 2.75 inches and the corresponding maximum diameter was 8.75 inches. The maximum wheel width was 3.75 inches and the corresponding minimum diameter was 8.5 inches.

Hardened (spring tempered) spring steel and a copper wire mesh were used for the tire strips. The spring steel had a thickness of 0.012 inches, a width of 0.25 inches, and a length of 6.5 inches. The spring steel strips were cut using a waterjet cutting machine. The copper wire mesh was made from 0.025 inch diameter copper wire and had a 10 mesh density (i.e. 10 x 10 mesh/square inch). This thickness for the spring steel and density for the copper wiring were chosen because both provided the best balance between flexibility and strength. The copper strips were 1 inch wide and 6.5 inches long. The copper mesh came in a large sheet so the strips were cut by hand using heavy-duty cutting shears. The spring steel strips were centered on the copper mesh strips and hand-sewn together using steel wire (Figure 19). Each wheel had thirteen tire strips.



**Figure 19 - Composite tire strips made from spring steel and copper mesh**

The hubcaps were made out of aluminum. This material was chosen because it is light-weight and cost effective, and the Aero/Astro machine shop has the proper tools needed for cutting and shaping it. The outer hubcaps were 0.125 inches thick and the inner hubcaps were 0.1875 inches thick. The inner hubcap was slightly thicker because the actuator was mounted to this hubcap; having a slightly thicker hubcap permitted deeper screw holes and a more secure mounting. In order to attach the tire strips to the hubcaps, a ring flange was made to go along with each hubcap. The ring flanges were also made out of 0.125 inch thick aluminum. Eight evenly-spaced holes were drilled and tapped into the hubcaps. Eight corresponding clearance holes were drilled in the ring flanges so the flanges and hubcaps could be screwed together (Figure 20). The tire strips were secured to the hubcaps by placing them in between the hubcap and ring flange and screwing the hubcap and ring flange together as tightly as possible.

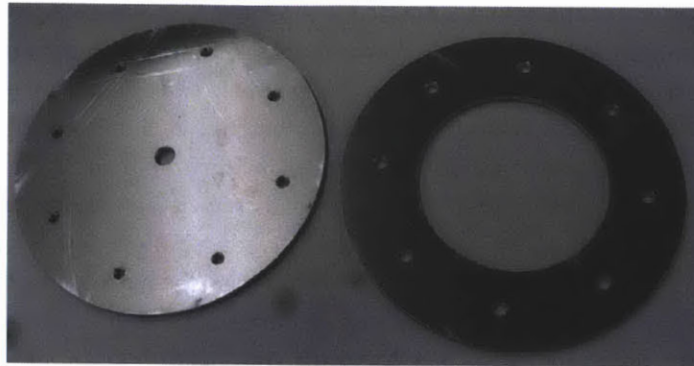


**Figure 20 - Aluminum hubcap and ring flange**

The biggest challenge in selecting the parts was finding an acceptable linear actuator. A very extensive on-line search was conducted, but most available linear actuators were either not strong enough or lacked the needed range of motion. Another problem was finding cost effective actuators that would fit within the limited budget of this project. In the end, the only actuator that provided enough strength, fit within the budget, and had an adequate range of motion was a linear actuator from a company called Anaheim Automation. This actuator consists of a stepper motor and leadscrew (Figure 21). The motor screws the leadscrew in and out creating a translational motion. The range of available travel for the actuator is 4.5 inches and it is capable of exerting 24 lbs of force.

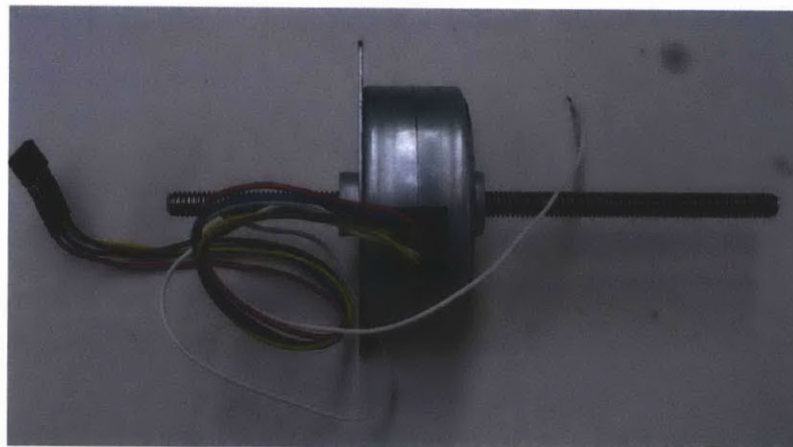


**Figure 21 - Linear actuator used in reconfigurable wheel**

### **4.3 Wheels and Platform Integration**

After the parts and materials were selected and acquired, the next step was to determine the details of the rover/wheel integration. The integration design presented several challenges, especially in regard to the linear actuator. As discussed above, the linear actuator was mounted to the inside of the hubcap closest to the rover frame (i.e., the inner hubcap). A hole was drilled through the center of the hubcap to allow room for the leadscrew to pass through. The outer hubcap also had a hole drilled in its center

through which the other end of the actuator leadscrew emerged. This end of the leadscrew was attached to the outer hubcap by placing a collar on both sides of the hubcap. When the wheel was in its largest width configuration, the leadscrew for the actuator would sit entirely on the inside of the wheel, but when the actuator pulled the hubcaps together, the leadscrew would extend outside the wheel. This meant that the wheel needed to be offset approximately 3 inches from the rover frame. The wheel axle also needed to be longer and avoid interfering with the leadscrew. It was decided that a hollow tube would be attached to the outside of the inner hubcap to provide a protective case for the leadscrew and extend the length of the wheel axle (Figure 22). In order to attach the hollow tube to the hubcap, the hubcap needed to have a built-in flange. This element of the design was accomplished by turning a solid piece of aluminum on a lathe to create the inner hubcaps; the outside hubcaps did not require a flange and were cut using the waterjet.

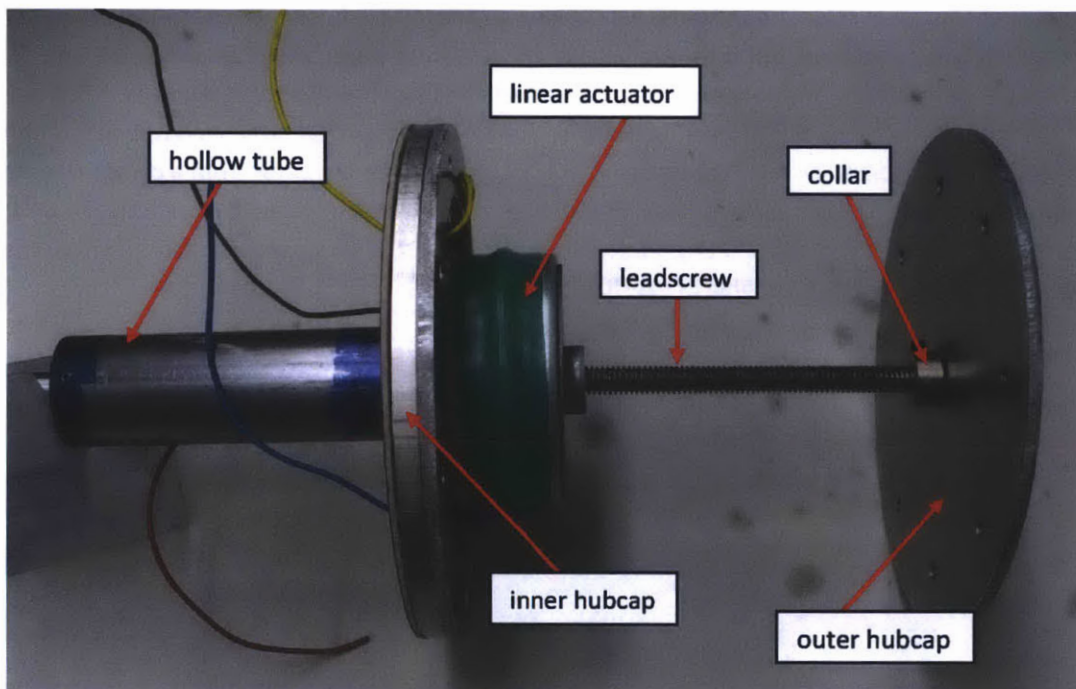


Figure 22 - Wheel Attachment Design

The hubcaps were 4.5 inches in diameter. The outer hubcap was 0.125 inches thick and the inner hubcap was 0.1875 inches thick. The flange for the inner hubcap was 0.375 inches thick and 0.875 inches in diameter. The axles for the wheels and drive motors that came with the robot kit were 0.125 inch square axles, so in order to use these drive motors, it was necessary to also use 0.125 inch square axles. The outer diameter of the tube was 1 inch, thus a tapered aluminum plug was made to gradually decrease the size of the axle. The 0.125 inch axle was made out of steel stock and press fitted into the aluminum plug. The hollow tube was pinned to the flange on the hubcap and the aluminum plug was pinned to the tube (Figure 23).



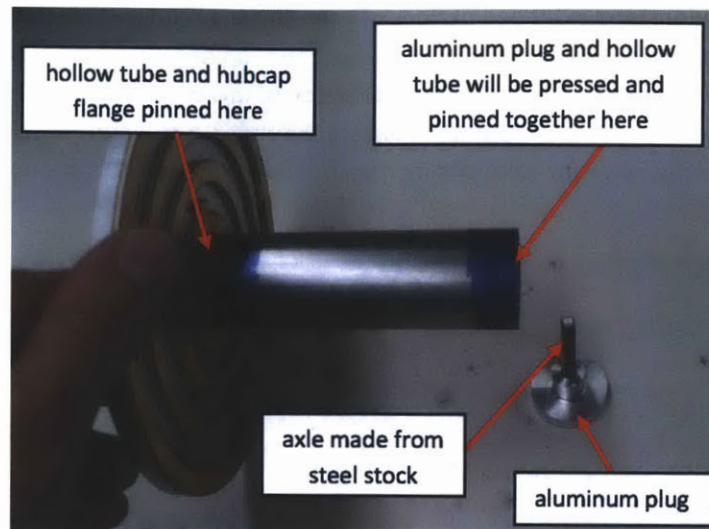


Figure 23 - Wheel axle attachment

The next major integration issue that was addressed was related to electrical wiring. Since the stepper motor was on the inside of the hubcap it rotated with the wheel. This presented a problem because the electrical wires that powered the stepper motor got tangled as they also rotated with the wheel. One of the technical instructors suggested that an electrical slip ring could be used to solve this problem. Price quotes from several companies were obtained for electrical slip rings, but the prices were outside the budget range for this project. Therefore it was decided that the slip rings would be manufactured instead.

A company was identified that sold PCBs (printed circuit boards) which are very thin copper sheets with a composite laminate on the bottom. The plan was to cut concentric circles out of this material using the waterjet and then epoxy the circles onto the outside of the inner hubcap (Figure 24). The stepper motor has four wires so four circles were needed. For each wire, a small hole was drilled through the hubcap and the wire was fed through this hole and then soldered to one of the copper rings on the outside of



Figure 24 - Copper electric slip rings mounted to outside of inner hubcap

the hubcap. Small metal brushes then sat against the copper circles with the wheel (and stepper motor wires) free to rotate. Wires were soldered to the brushes, which maintained constant contact with the copper circles and provided a pathway whereby electrical signals could be sent from outside to inside the wheel (Figure 25). Some experimentation was required to figure out what size the circles should be and what settings should be used for the waterjet when cutting the PCB material. The material tended to delaminate under normal settings so low pressure and very brittle material settings had to be used instead. The metal brushes were made from

RFI EMI shielding gasket fingers from a company called OmegaShielding. This was not the most robust design—the brushes

were not expected to withstand extended periods of use—but the total cost for these slip rings was only about \$20 and cost was the driving factor for this design. The slip rings successfully worked the first time they were tested and have performed well for the duration of this project. These slip rings are sufficiently robust for demonstrating a proof of concept; however, a real rover would probably need more robust parts (See appendix for a list of major parts, dimensional drawings, and hardware specification sheets).

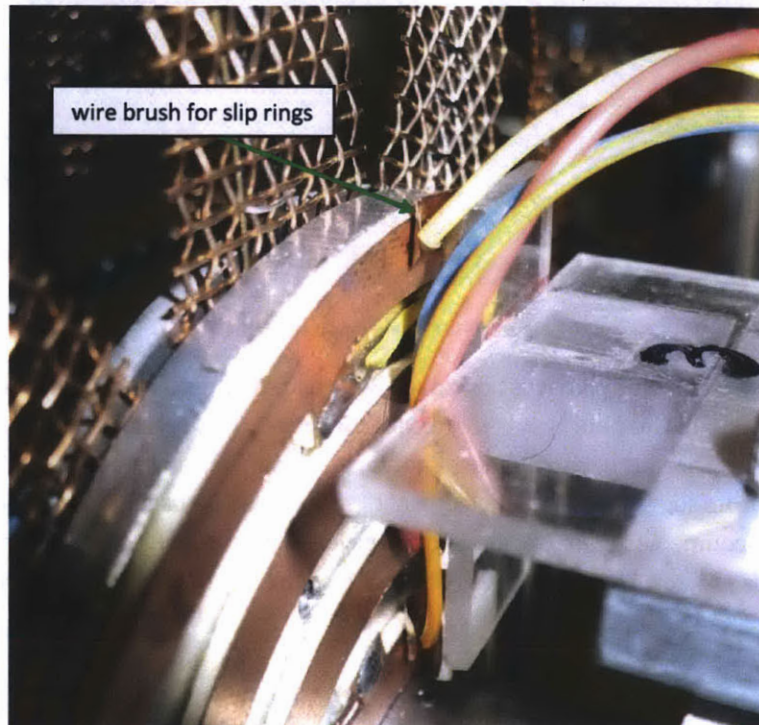


Figure 25 - Wire brushes for slip rings

#### 4.4 Assembly

Assembling the wheel after manufacturing was completed was not an easy task. It was critical to do some tasks in a specific order. Before assembly, the following tasks were completed first:

1. Cut spring steel strips using the waterjet and cut copper strips using cutting shears.
2. Sew spring steel strips and copper strips together using steel wire.
3. Cut outer hubcap and ring flanges using the waterjet.
4. Make inner hubcap using a lathe.
5. For the outer hubcap, drill a center hole that actuator leadscrew can fit through, and drill and tap eight evenly spaced holes around the outer edge.
6. For hubcap rings, drill eight evenly spaced clearance bolt holes around the outer edge.
7. For the inner hubcap, drill center hole for leadscrew, drill and tap mounting holes for actuator, drill clearance holes for actuator wires, and drill and tap eight evenly spaced holes around the outer edge.
8. Cut hollow steel tube that will extend wheel axle and enclose actuator leadscrew.

9. Make tapered aluminum plug for connecting wheel axle to steel tube using a lathe.
10. Drill starter hole for wheel axle into tapered plug.
11. Cut wheel axle from steel stock.
12. Cut electrical slip rings using the waterjet.

The above items do not necessarily have to be performed in that order. After all the tasks have been completed, the wheel is ready to be assembled by completing the following steps in the order listed:

1. Press outer hubcap onto one end of steel tube.
2. Drill two 0.0625 inch holes through steel tube and aluminum hubcap (holes should be 180 degrees apart).
3. Hammer spring-loaded pins into holes (this task may require two people).
4. Install grommets in wire holes for outer hubcap.
5. Epoxy electric slip rings onto outside edge of inner hubcap with copper side up. Allow 24 hours for epoxy to dry.
6. Press fit wheel axle into tapered plug.
7. Press tapered aluminum plug into open end of steel tube and then drill two 0.0625 holes through steel tube and aluminum plug (holes should be 180 degrees apart).
8. Hammer spring-loaded pins into holes (this task may require two people).
9. Once epoxy has dried, mount actuator to inside of inner hubcap and then thread actuator wires through wire holes.
10. Place ring flange on the inside of inner hubcap and attach to hubcap by loosely screwing together.
11. Evenly space 13 tire strips around inner hubcap. The strips should sit in between the hubcap and ring flange.
12. Once all the strips are in place, tighten all screws. This is best done by tightening screws gradually in a star pattern similar to tightening lug nuts on a tire.
13. Attach outer hubcap to leadscrew by securing it between two collar attachments.
14. If necessary, screw in leadscrew so that only 2.5–3.0 inches are exposed.
15. Place ring flange on the outside of outer hubcap and attach to hubcap by loosely screwing them together.
16. Gently bend each tire strip and place the free end in between the outer hubcap and its ring flange.
17. Once all strips are in place, gradually tighten all screws again following a star pattern.
18. Solder actuator wires to the tabs on the electrical slip rings.

Figures 26-29 show various steps in the assembly process. It should be noted that it can take several hours to assemble one wheel. For some of the steps it is helpful to have another person available to assist in holding and securing parts. In particular, getting all the tire strips correctly situated can be an arduous task and will likely take several attempts and some patience to accomplish.

Initially, only one wheel was built and assembled. This attempt was a trial-and-error experiment that allowed me to learn how to use all the machines necessary to make the parts, what order to assemble things in, and decide if any size adjustments were necessary for the individual pieces. Once the first wheel was successfully built and the fabrication and assembly process was “de-bugged,” three more

wheels were built. Once all four wheels were assembled, they were attached to the rover platform (i.e., the wheel axles were secured in the shafts of the drive motors) and the rover was ready for its first test drive.

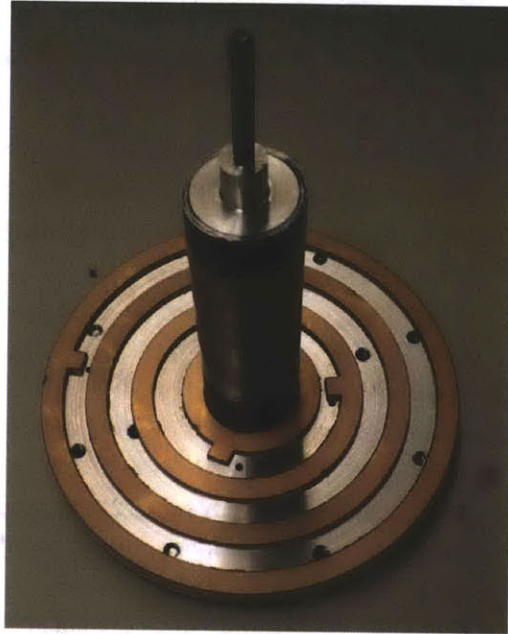


**Figure 26 - Wheel axle, hollow tube, and inner hubcap all pinned together**

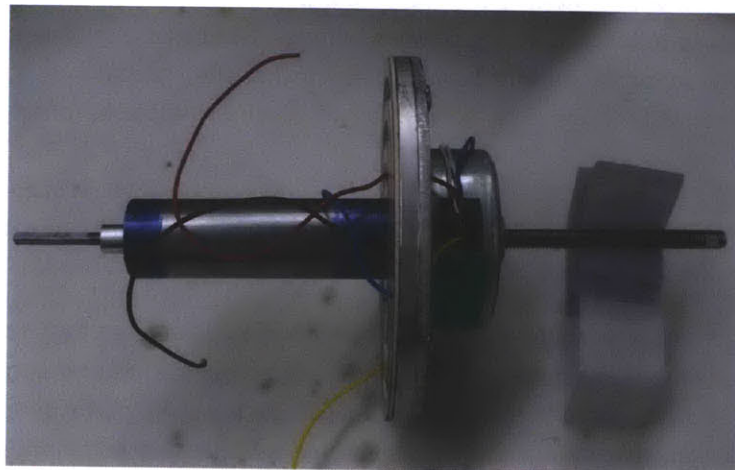


**Figure 27 - Linear actuator mounted to inner hubcap**

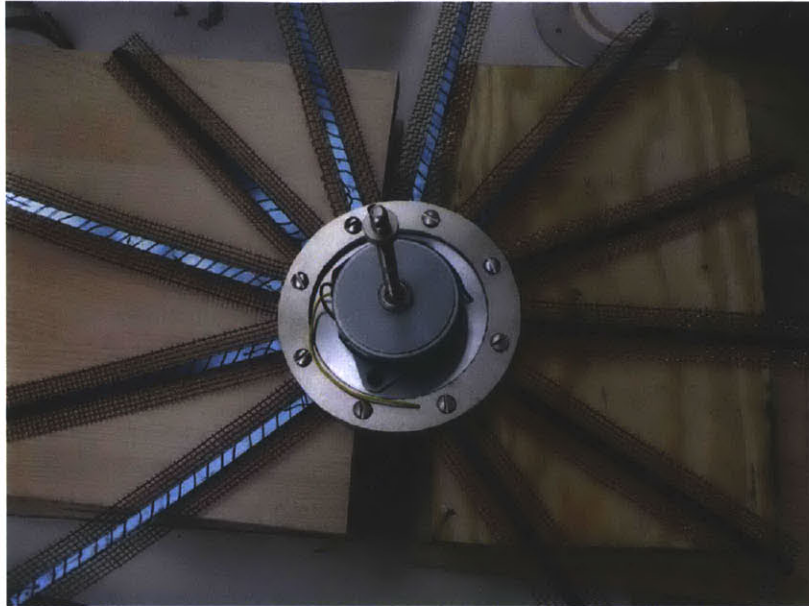


**Figure 28 - Securing the tire strips**

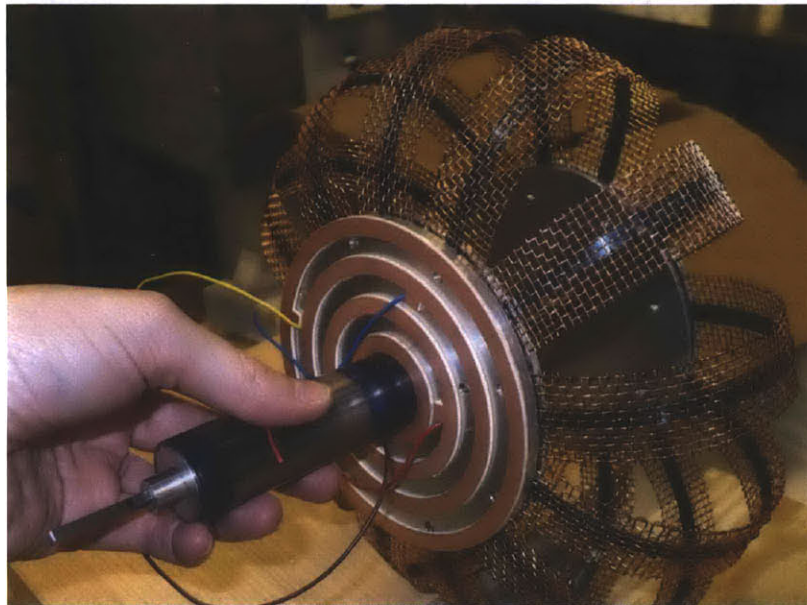


**Figure 29 - The first assembled wheel**

#### **4.5 Initial Drive Testing**

After the assembly was complete, some initial drive tests were conducted to verify that the wheels could support the weight of the rover. During the initial tests, there was a large bending moment

occurring at the wheel axles because they were situated so far from the rover frame. The fact that the wheel axles were small compared to the wheels also exacerbated this problem. After several initial driving tests, the axles on one of the wheels broke off. In order to fix the broken wheel, a new axle was cut, the old aluminum plug was cut off of the steel tube, a new aluminum plug was turned on the lathe, the new plug had to be pinned to the steel tube, and the new axle had to be pressed into the new plug.

To provide more structural support and prevent more broken axles in the future, support bars were designed and built to take some of the stress off the axles. There was one bar for the front wheels and one bar for the back wheels. Both bars were cut from 0.25 inch thick aluminum stock. They were 14.5 inches long and 2.0 inches wide. Clearance bolt holes were drilled into the support bars and then offsets were used to attach the bars to the frame. Bearings were needed to attach the bars to the wheels. Small mounts with holes for the bearings were cut out of aluminum using the waterjet and the bearings were pressed into the mounts. The steel tubes sat inside the bearings and then the bearing mount was screwed into the support arms (Figure 30). Additional drive testing conducted after the support arms were built demonstrated that they were able to resolve the bending moment issues.

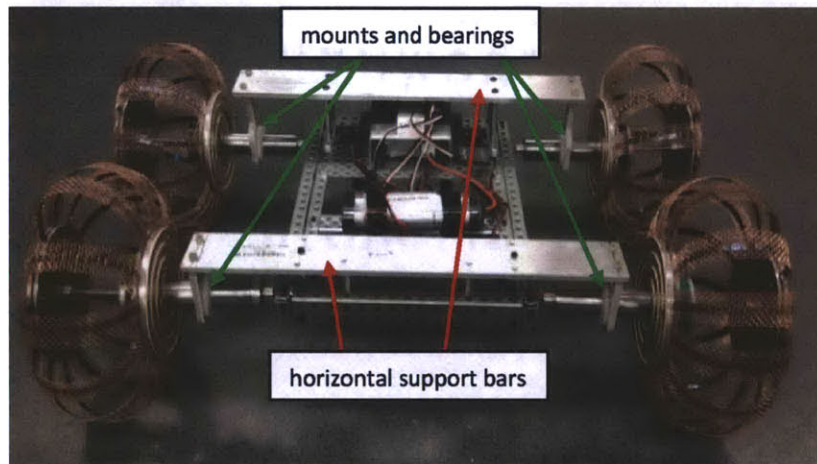


**Figure 30 - Rover with four reconfigurable wheels and support bars**

One other minor issue was identified during the initial drive testing. Because of the are gaps between the tire strips and the holes in the copper mesh itself, if the rover was driving on sand or some other loose, dusty terrain, small soil particles would sometimes get stuck in the leadscrew and motor gears. To protect against soil and dust contamination, covers for the wheels were sewn using a sewing machine. The covers were made out of spandex in order to stretch and conform to the shape of the wheel as it changed to different configurations (Figure 31). Different patterns were experimented with until finally one was made that matched the contour of the tire strips.

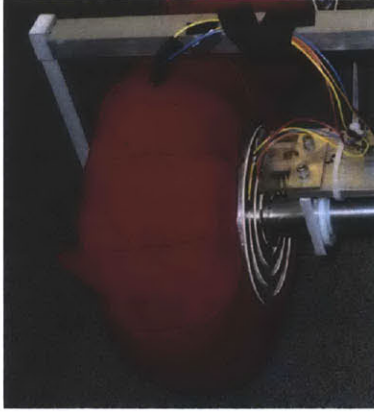


**Figure 31 - Wheel with hand-sewn spandex cover**

## **5.0 Integration, Autonomy, and Control**

### **5.1 Electrical System Overview**

At this point, the project objectives to build four reconfigurable wheels and integrate them onto a rover platform were complete. The next goal was to demonstrate that the wheels could autonomously reconfigure. This required a working electrical system, and eventually that the mechanical and electrical systems be integrated to successfully work together. The electrical system for the rover can be considered as two subsystems. One subsystem is responsible for controlling the wheel as it drives and the other subsystem is responsible for reconfiguring the wheels. The wheels are independently driven so each wheel requires its own drive motor. The drive motors are controlled by a microcontroller, though initially the drivers were tested independent of each other using power supplies and a signal generator. This was done to test out the wheels and stepper motors, and to ensure proper usage.

The drive motors and their accompanying microcontroller were included in the robotics kit that was purchased for the rover platform. The microcontroller came with built-in ports designed specifically for the drive motors. Once plugged in, their power setting could be controlled via the microcontroller. Eventually the drivers would need to be powered by batteries and the microcontroller. The microcontroller had its own battery, but the drivers needed their own power source. The reconfigurable wheels were much larger (in both size and weight) than the wheels that came with the robot kit, so it was necessary to find the minimum power required for the rover to drive forward using the reconfigurable wheels. Through experimentation, it was discovered that the minimum power setting was 40% on a hard floor.

Controlling the stepper motors (i.e. linear actuators) used to reconfigure the wheels is more challenging than controlling the drive motors. A driver is required to interface between the stepper motor and the microcontroller. The stepper motor's shaft is a permanent magnet surrounded by electromagnets. The shaft is turned by energizing the electromagnets in a specific pattern. If given direction and speed commands, the motor driver will translate those commands into the appropriate input signals to power the electromagnets. The direction command is either hi (1) or lo (0). To control the speed, the driver must receive a square pulse. The higher the frequency of the pulse, the faster the stepper motors will turn (see appendix for more details).

### **5.2 System Integration and Preliminary Testing**

The first step in the integration process was learning to program the microcontroller. This was a trial-and-error process. The microcontroller had a number of digital input/output pins (I/O pins) capable of receiving or sending either hi signals (1) or lo signals (0). A lo signal causes the linear actuator (i.e., stepper motor) to pull the hubcaps together while a hi signal pushes the hubcaps apart. The square pulse is generated by pulling the same pin lo and then hi. There is a programmed time delay in between the lo and hi commands. The frequency of the square pulse can be altered by changing the length of this time delay. A program was written to generate a square pulse and the output was verified by hooking up the microcontroller to an oscilloscope.



Once the driver could be controlled using the microcontroller and powered using batteries, initial reconfiguration testing was conducted. The initial testing was, in short, unsuccessful due to two main problems. The first problem was mechanical in nature. The correct signals were being sent to the drivers and the stepper motors would turn, but the leadscrew struggled to move in or out. After troubleshooting, it was observed that when the wheels supported the entire weight of the rover, the hubcaps became misaligned. Since the hubcaps are attached solely by the linear actuator, it plays both a structural role and a dynamic role. Although the linear actuator can provide enough force to actuate the wheel, it cannot provide sufficient structural support. The misalignment of the hubcaps caused the leadscrew to sit at an angle to the motor which was not powerful enough to overcome the misalignment and still turn the screw.

If the hubcaps were supported by me, however, the wheel would successfully reconfigure. Given this observation, it was clear that either manual intervention would be necessary during the testing or additional support structures would be required to fix the misalignment. After consulting with the project advisor, it was decided that demonstrating the autonomy of the wheel warranted that additional support structures should be built. Designing these support structures was difficult because it required supporting the outside hubcap. Since the outside hubcap moves when the wheel reconfigures, the support structure would need to move along with it. Additionally, the support structure must require little or no power to move or else the linear actuators may not be able to move the hubcaps and the supports.

After brainstorming, the project mentor suggested the use of (nearly) frictionless rails. The rails would be mounted to the rover's frame. Support arches could then be built that would attach to the outside hubcaps at one end and the rails on the other end. The arches would keep the hubcaps aligned and the rails would allow the arches to move back and forth with minimal additional power. Similar to the support arms previously made, bearings and bearing mounts were needed to attach the arches to the hubcaps. Special bearings capable of withstanding both radial and axial loads were purchased and new collars were custom made on the lathe to fit inside the bearings (Figure 32). The support arches and additional aluminum bearing mounts were designed and cut using the waterjet. The bearings were glued into the mounts using Loctite adhesive (Figure 33), and bolt holes were drilled and tapped into the ends of the support arches so that they could be screwed together with the bearing mounts. The frictionless rails were screwed to the horizontal support arms, with specially designed carts that could slide back and forth with relative ease (Figure 34). The support arches were mounted to these carts and then they extended over the tops of the wheels where they met the bearing mounts (Figures 35–37). Care was taken when making measurements for these new pieces to ensure that each remained properly aligned. Designing these support arms was an involved process, but after they were implemented, the actuator leadscrew misalignments were no longer a problem.



**Figure 32 - Custom made collar to connect leadscrew, bearing/mounts, and hubcaps**

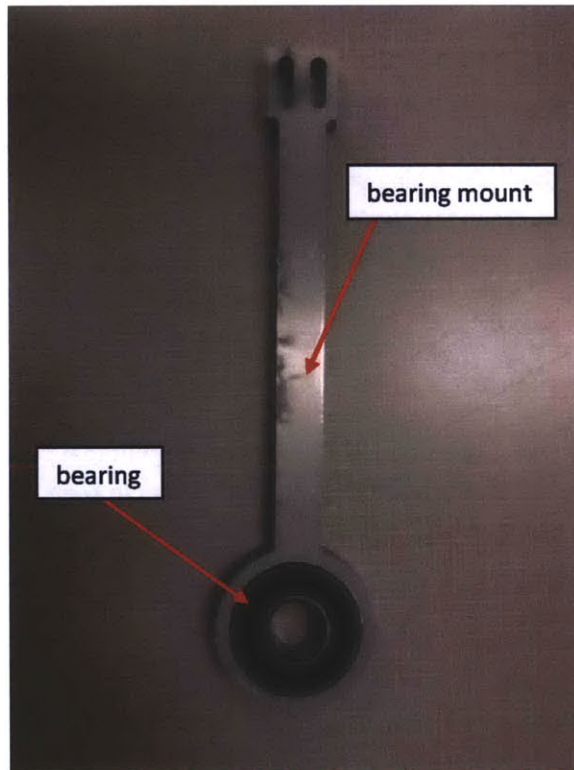


**Figure 33 - Bearing and bearing mount for support arch**

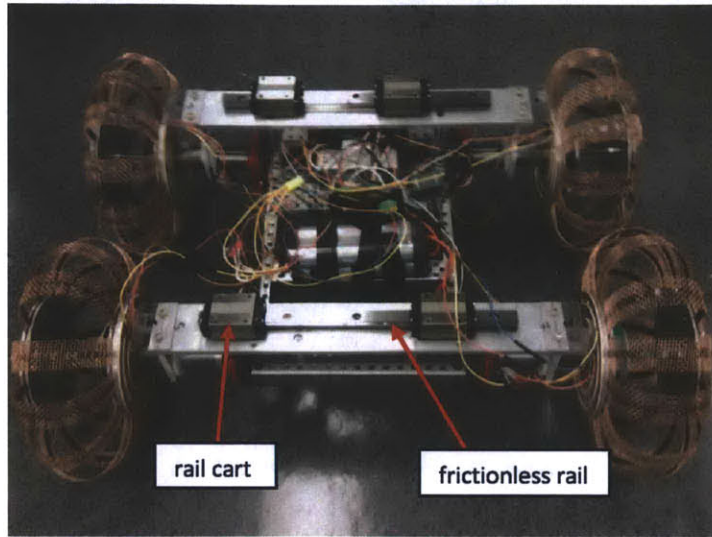


**Figure 34 - Frictionless rails mounted to rover frame**

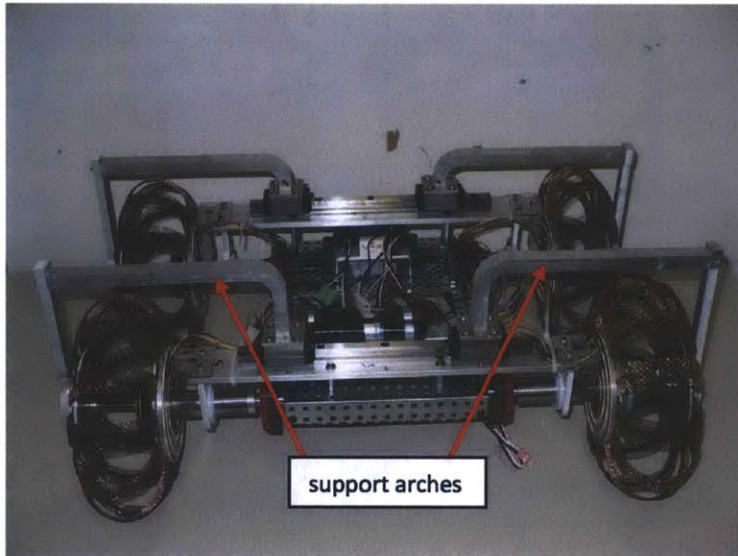


**Figure 35 - Rover with new support arches**

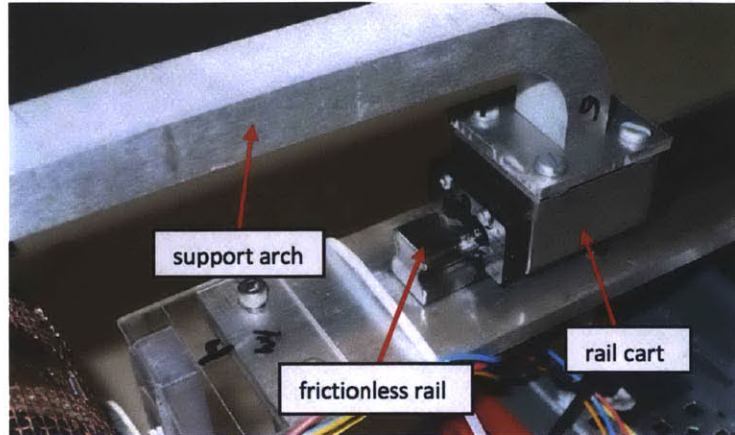


**Figure 36 - Close-up of rail, cart, and arch**

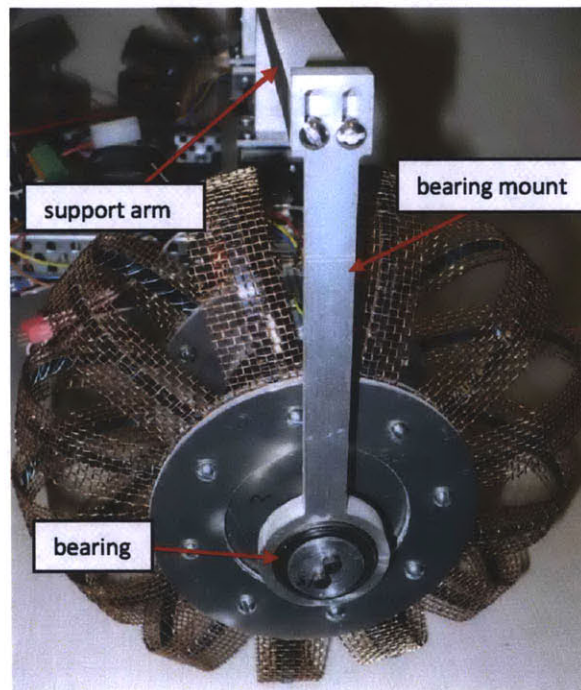


**Figure 37 - Close-up of new hubcap attachment**

The second major problem during the initial reconfiguration testing happened while troubleshooting the misalignment problem. It is not known exactly when or why this happened, but at some point the drivers for the stepper motors burned out and stopped working. There did not seem to be any major electronic malfunction so it was hypothesized that the drivers, which were fairly low quality, were too small or inefficient to power the motors. Some higher-quality drivers were purchased, but installing them required that all the electrical connections be re-done. These new drivers were also significantly more expensive than the previous drivers, so in an effort to save money only two drivers were

purchased and each driver was connected to two wheels. According to all the product specifications this should have been a viable option, but the new drivers exploded on the first testing attempt after they were installed (Figure 38). It is still not understood what caused this malfunction. New, even more heavy-duty drivers were again bought, and in an effort to avoid destroying any more motor drivers, it was decided that each wheel would have its own driver. These new drivers were incrementally tested and set-up. After a labor-intensive effort and a third re-work of the electrical system, the rover finally had four working drivers to go along with its wheels.



**Figure 38 - Charred remains of a motor driver after it exploded**

Unfortunately this was not the end of the electrical system problems. The drivers and motors could successfully operate off of a signal generator, but when the microcontroller was hooked up instead the drivers (and hence the motors) stopped working. After another painstaking troubleshooting procedure it was discovered that the new drivers operated on a 5V electrical standard, but the microcontroller operated on a 3.3V standard. The new motor drivers were therefore incompatible with the microcontroller. Some small translator chips were bought, but this too ended in failure because even with the translator chips, the microcontroller was incapable of producing the amount of current required for the drivers. It was decided that the easiest solution was to use a different microcontroller for reconfiguring the wheels. The Arduino Uno, a small microcontroller that operates on a 5V standard, was obtained, programmed, and successfully used to reconfigure the wheels (see appendix for detailed diagram of the electrical set-up).

### **5.3 Control Methodology**

With working mechanical and electrical systems, the final issue to address was determining how the rover would decide when it needed to reconfigure. Designing the optimal control algorithm for this is an

entire project in itself. Several researchers have developed in-depth control strategies for identifying and controlling wheel slip and traction [18-19]. The purpose of this project was not to optimize a control strategy for a rover with reconfigurable wheels, but a working control algorithm was necessary to demonstrate the autonomous capability of the rover. Time limitations permitted only a very simple control algorithm to be developed. While the reconfigurable wheels were being built, initial testing with the wheels that came with the robot kit was being conducted on various terrains to investigate what happens prior to the rover getting stuck. Video was taken of the rover in these different terrains and the film was studied as part of the control algorithm development process. It was observed that the most likely indicator of the rover becoming stuck was wheel slip. Therefore, wheel slip was selected as the event that would be measured and used to indicate when the wheels should reconfigure.

Wheel slip occurs when a wheel is rotating but the rotation fails to move the vehicle forward. In most cases, not all the wheels begin to slip at the same time, so an easy way to detect wheel slip is by measuring and comparing the rotation rates of two or more wheels. If the rotation rates are not the same, then wheel slip is beginning. Although the rover wheels are all independently driven, the front wheels and back wheels still tend to work in pairs, similar to cars operating on rear wheel drive. Because the two back wheels pull together and the two front wheels pull together, the best way to detect wheel slippage is by comparing the front wheels to each other and the back wheels to each other (as opposed to comparing the right wheels to each other and the left wheels to each other).

Rotation rates can be measured using simple sensors called encoders. Two such sensors were purchased and installed on the back wheels of the rover. While comparing both sets of wheels is likely more optimal than comparing only one set of wheels, the project's need for an effective yet simple control algorithm could be met with just one comparison. From a software engineering perspective, writing a program to compare two sets of wheels is more complex than one to compare just one set of wheels. The back wheels were chosen for comparison because in the preliminary testing they tended to get stuck more often than the front wheels. The algorithm was programmed to have the encoders continuously measure the rotation rates of the wheels as the rover drove forward. The rotation rate information would be sent to the microcontroller, which would continuously compare the rotation rates. If the rates differed too much, the microcontroller would stop the rover because it would mean the wheels were slipping and needed to be reconfigured to improve traction (Figure 39).

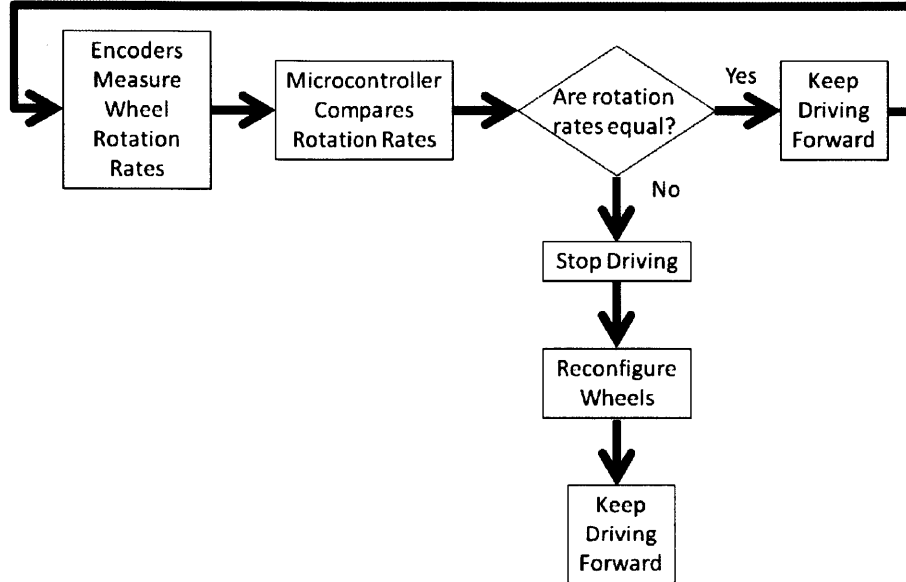


Figure 39 - Flowchart for reconfiguration control algorithm

#### 5.4 A Systems Engineering Perspective

With the control algorithm completed, it was time to enter the testing phase of the project. Before doing so, however, it is worthwhile to make a few closing comments about the rover itself. As this project progressed from the initial design and building phases into the integration phases it became clear that this project was indeed a systems engineering project. There were certainly design and fabrication challenges, but the greatest difficulties in this project were associated with integrating all of the mechanical, electrical, and software systems together. These subsystems could not be thought of as individual entities; rather design decisions for one system had to also consider the effects on the other subsystems. An outstanding subsystem is useless if it is incompatible with the system at-large. A design structure matrix shown in Figure 40 diagrams the different interactions that exist between different components of the rover system. Black boxes indicate structural connections, green boxes indicate signal flows, and red boxes indicate energy flows.

	Wheel	Axle	Rover Frame	Actuator	Drivers	Drive Motors	VEX Microcontroller	Arduino Microcontroller	Horizontal Support Bars	Rails	Support Arches	Encoders	Battery (LiPo)	Battery (NiMH)
Wheel	█	█		█							█			
Axle	█	█	█						█			█		
Rover Frame		█	█		█	█	█	█	█				█	█
Actuator	█			█	█	█								
Drivers			█	█	█	█		█					█	
Drive Motors			█			█	█	█						
VEX Microcontroller			█			█	█					█		█
Arduino Microcontroller			█		█		█	█						
Horizontal Support Bars		█	█						█	█				
Rails									█	█	█			
Support Arches	█									█	█			
Encoders		█					█					█		
Battery (LiPo)			█		█								█	
Battery (NiMH)			█					█						█

Figure 40 - Design structure matrix for rover system

Some of the biggest mistakes made during the course of the project related to integration. At first, everything was assembled all in one step, but this strategy only resulted in things not working or in the most extreme cases, exploding. One of the most significant lessons learned from this project was that the key to successful integration is taking small, incremental steps. A system is made from many different components, and it must be built and tested one component at a time. Systems engineering is a delicate balancing act that requires a focus on the subsystems while simultaneously maintaining a view of the entire system. In order to achieve that balance with the rover, it had to be thought of as a system. The individual components of subsystems had to work correctly, but the sub-systems themselves also had to be thought of as components that must be compatible with each other. Issues related to mass, power, design, performance, and cost all had to be considered from the perspective of the entire rover, not just a particular subsystem.

During the course of development, this project demonstrated that even small problems or changes within a subsystem can have rippling effects. For example, the choice to use linear actuators for reconfiguration affected not only the mechanical design of the system but also the electrical design of the system by requiring the use of slip rings and microcontrollers. The failure to anticipate bending



moment problems led to a series of design add-ons, increased costs, and as will be seen later, changes to the testing environment and procedure. Similarly, issues with the original motor drivers eventually led to incompatibilities within other aspects of the electrical system and required several redesigns.

As the engineering world takes on greater challenges and as systems become increasingly complex, it is imperative to understand engineering from a systems perspective as well as a micro fluidic or resistor and transistor perspectives. Similar to an orchestra conductor who must be aware of individual instruments while also creating a symphonic whole, engineers must pay attention to individual components while also ensuring that all subsystems are working in harmony to create an engineering masterpiece.

## **6.0 Testing and Results**

### **6.1 Test Set-Up**

In order to demonstrate and assess the effectiveness of autonomous reconfigurability, it was necessary to create a Mars-like environment for the rover, which is non-trivial. The natural choice for a Mars-like soil is sand, but using sand was very risky because the rails that were added to keep the wheel hubcaps aligned are very sensitive to sand and dust. In order to maintain their nearly frictionless state, the rails must be kept free of sand and dust. If the rails were to become contaminated, the autonomous reconfigurable capability of the rover would be compromised. Considering the project time constraints and the high risks associated with testing in sand, it was decided that sand should be strictly avoided. However, it was still desirable to use a material that would mimic the behavior of sand.

The first sand replacement material that was tried was pea gravel. A “sandbox” three feet wide, ten feet long, and three inches deep was constructed out of plywood. The box was filled with 500 pounds of fine-grained pea gravel purchased from a home improvement store. Several test drives with the rover were conducted in the gravel but no slippage was occurring. As a result, it was decided that the pea gravel would not be a suitable substitute for sand. Two more materials were experimented with—rice and popcorn seeds. These may sound like odd materials to use as sand substitutes, but keep in mind that the main goal of the test set-up was not to exactly replicate the Martian surface, but rather to simulate a Mars-like environment where the rover would likely slip due to the nature of the terrain. The rice and popcorn simulate a sand-like environment in that both consist of small grains that can easily slide against each other. As it would in sand, the rover tended to sink into the rice, but the sinkage was not deep enough that the rover ever lost traction. The popcorn seeds, however, were much more successful. Prior to testing in the alternative soils, testing had been conducted to calibrate how much wheel slippage occurred on a flat solid floor. This amount of slippage was designated as a normal or acceptable level. In the alternative soils, the rover was commanded to drive forward but stop if it detected that the wheel slippage became greater than the acceptable amount. The rover experienced above average slippage in the popcorn seeds, therefore it was decided that these would be the material of choice for the homemade Mars yard (Figure 41).

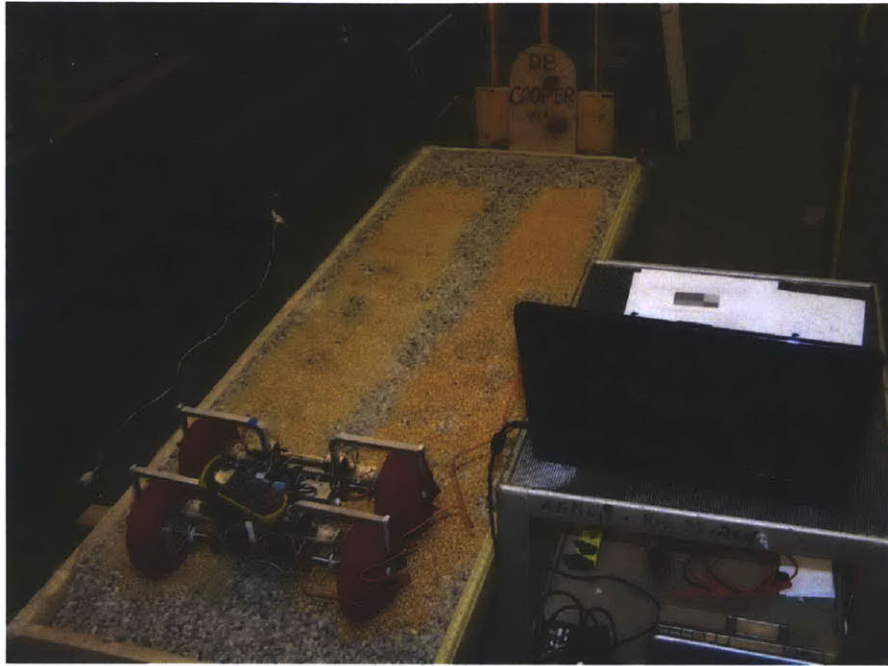


Figure 41 - Testing in the homemade Mars yard filled with pea gravel and popcorn

## 6.2 Testing Procedure

The purpose of the testing was to fulfill the last two objectives of the project, namely, to demonstrate the ability of the rover to autonomously reconfigure its wheels and to assess the effectiveness of using reconfigurable wheels in a simulated Martian environment. The first objective was documented via video. To fulfill the second and final objective, data for the reconfigurable wheels was collected by recording relevant measurements as part of the testing.

Recall that the basic motivation behind designing a reconfigurable wheel was to find a better trade-off between the competing metrics of drawbar pull and power. Measuring drawbar pull is very difficult, but in this case a related metric is distance. If the rover gets stuck it will not travel very far; with the aid of reconfigurable wheels the rover will be able to travel greater distances in challenging terrain. Given this, the first measurement that was collected in the tests is the distance traveled by the rover. The second measurement that was collected is power. The distance was measured using a measuring tape. The amount of current used to drive the motors was also measured and then multiplied by the battery voltage to calculate power. The tests were conducted using different rover speeds (slow vs. fast), inclinations (flat vs. tilted), and terrain types (easy/flat vs. hard/bumpy). Results using the reconfigurable wheels were compared against results without reconfiguring the wheels. In the non-reconfigurable system testing, the wheels began in the smallest width configuration and the rover drove as far forward as it could before it exceeded slippage limits described earlier. For the reconfigurable system testing, the wheels again began in the smallest width configuration. Once the rover exceeded its slippage limits, the wheels were allowed to reconfigure to the largest width configuration and the rover continued driving

forward until it again exceeded its slippage limit, hence the tests only focused on reconfiguration from smallest to largest width. A copy of the test procedure can be viewed in the appendix. Figure 42 is a test matrix that outlines all the different tests that were conducted. A slow speed meant that the motor power was set at 70% and a fast speed meant it was set at 80%. For the inclined scenarios, the far end of the test bed was raised up by two inches. The easy terrain scenario meant that the surface was flat. For the hard terrain scenario, small craters were manually introduced to the test environment to create a bumpy surface. Five tests were conducted in each test scenario with the exception of the fast speed/no tilt/easy terrain scenario. For that scenario, a set of 25 tests was done so that a larger sample size would be available to conduct an error analysis. For each scenario, the results from the individual tests were averaged together. These results are discussed in the next section.

Speed		Terrain			
		easy		hard	
Tilt	none	slow	fast	slow	fast
	inclined	slow	fast	slow	fast

Figure 42 - Text matrix of testing procedures

### 6.3 Test Results

The first metric that was examined was the average distance achieved using the reconfigurable wheels for each of the test scenarios. These results can be seen in Figure 43. The slow, bumpy, tilted scenario had the smallest distance and the fast, easy, no tilt scenario had the largest. These results are not surprising. An inclined surface and a bumpy surface both create additional soil resistances, which impede the progress of the rover. Additionally, a rover moving at faster speeds will have more momentum which can assist in navigating the terrain. It is interesting to rank the different scenarios according to their distance achieved. From smallest to largest, the order is:

- 1) slow, bumpy, tilted
- 2) slow, bumpy, no tilt
- 3) fast, bumpy, tilted
- 4) fast, bumpy, no tilt
- 5) slow, easy, tilted
- 6) slow, easy, no tilt
- 7) fast, easy, tilted
- 8) fast, easy, no tilt

This ranking can be further divided into three distinct groups: small distances (scenarios 1 and 2), medium distances (scenarios 3–5), and large distances (scenarios 6–8). It is interesting to note that the

common characteristic of the high distance group is the easy terrain which suggests that distance was most heavily influenced by terrain difficulty. Further examination of the ranking suggests that the next most influential factor was speed and inclination was the least influential factor.

Performing similar analysis from a different data perspective is also revealing. The difference between the distance achieved by the non-reconfigurable system and the distance achieved by the reconfigurable system was also examined. Figure 44 outlines the additional distance achieved in each test scenario thanks to the reconfigurable wheels. The ranking of these scenarios, again from lowest to highest, is as follows:

- 1) slow, bumpy, tilted
- 2) slow, bumpy, no tilt
- 3) slow, easy, tilted
- 4) fast, easy, tilted
- 5) fast, bumpy, tilted
- 6) fast, bumpy, no tilt
- 7) slow, easy, no tilt
- 8) fast, easy, no tilt

In this case, the larger distance is grouped by speed more than terrain. The most likely explanation for this is that for the reconfigurable system, the rover has more trouble restarting after it has reconfigured its wheels than when it is first starting. When the rover initially begins to move forward it has good flotation over the surface. However, as it moves forward the sinkage of the rover increases. The rover stops to reconfigure its wheels after it has started to get stuck in the soil, so when the rover attempts to drive forward again after reconfiguring its wheels, it must now overcome not only its natural inertia but the additional resistance due to more sinkage. Since a higher speed translates into more power, the rover is more capable of overcoming the additional resistances and traveling farther distances when moving at a higher speed.

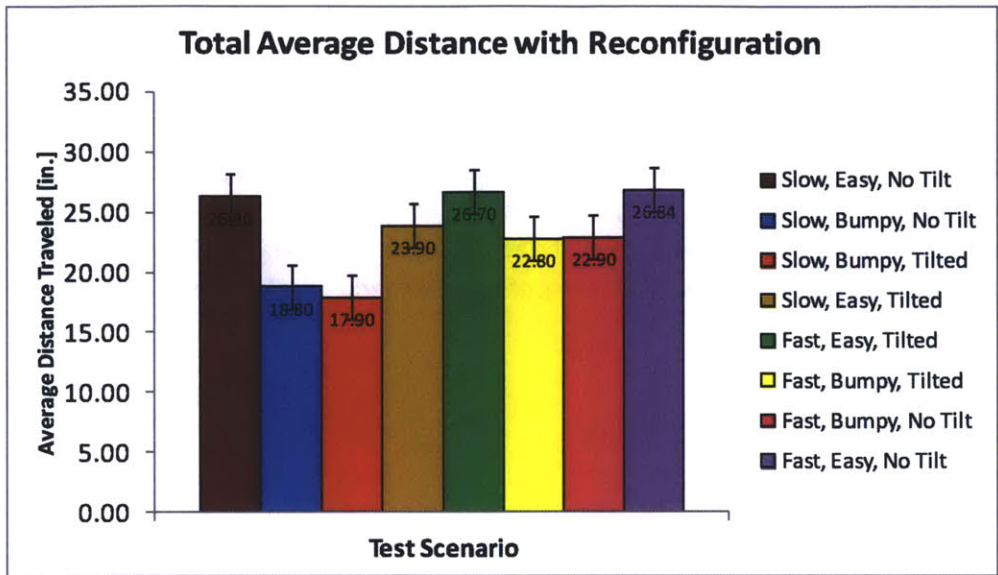


Figure 43 - Total average distance with reconfiguration for test scenarios

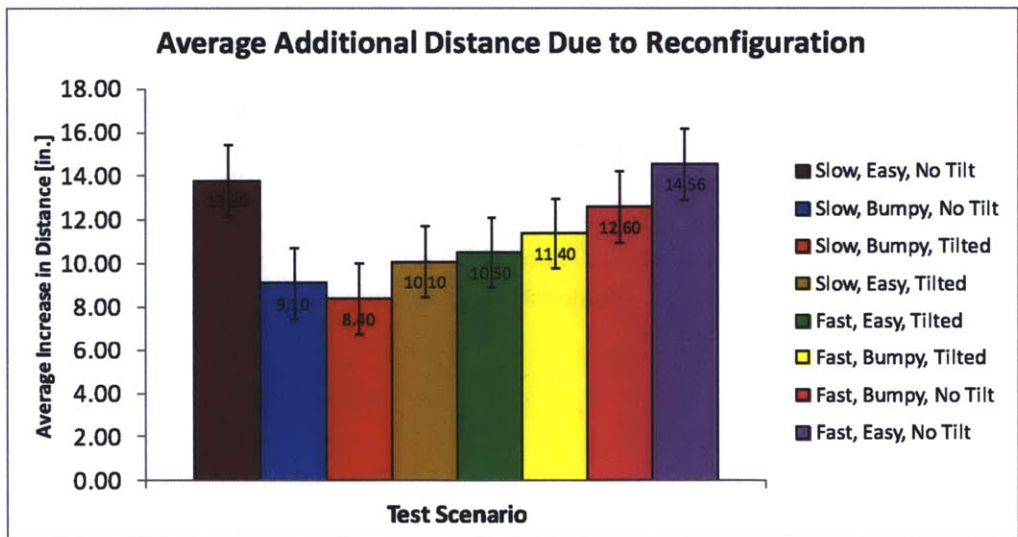


Figure 44 - Average additional distance traveled due to reconfiguration for test scenarios

It was also interesting to examine the increase in distance from a percentage standpoint. There is some consistency between the overall distance achieved by the rover and the additional distance achieved from using the reconfigurable wheels. However, when examined from a percentage standpoint there tends to be little, if any, consistency. Figure 45 shows the percentage increase in distance for all the test scenarios. The ranking, again from lowest to highest, is:

- 1) fast, easy, tilted
- 2) slow, easy, tilted
- 3) slow, bumpy, no tilt
- 4) slow, bumpy, tilted
- 5) fast, bumpy, tilted
- 6) slow, easy, no tilt
- 7) fast, bumpy, no tilt
- 8) fast, easy, no tilt

From these results it is not clear if one factor is more influential than the others. Additionally, there are large differences between the ordering of scenarios for the percentage data when compared to either the total distance or increase in distance due to reconfiguration. The slow, bumpy, tilted scenario had the lowest overall distance and the lowest increase in distance, but from a percentage standpoint it had the fifth highest change. The slow, easy, no tilt scenario had a high overall distance and high increase in distance, yet it had the second to lowest percentage change. The range of values for percentages is also much greater than value ranges for the raw numbers. The apparent randomness (as seen in the statistical analysis later) in the percentage results illustrates the large amount of variability that is inherent in the off-road vehicle traction problem. As noted in section 2, some aspects of terramechanic behavior are still not fully understood. Models that have been built based on collected data have limited accuracy in part due to the large amount of variability in the data. This data variability is attributed to constantly changing terrain conditions and the highly sensitive relationships that exist with those conditions. Those conditions were all present as part of this testing and therefore it is not surprising that even though patterns in the actual data can be observed, there is still a significant amount of randomness in the percentage data.

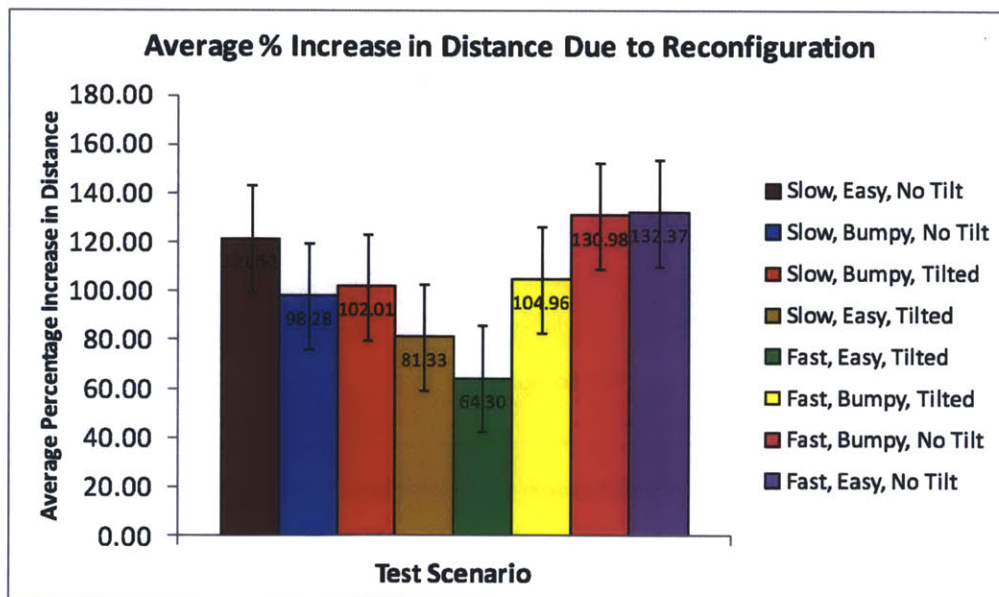


Figure 45 – Average percentage increase in distance due to reconfiguration for test scenarios

The same calculations made for distance were made for power. Graphs of this data can be seen in Figures 46–48.

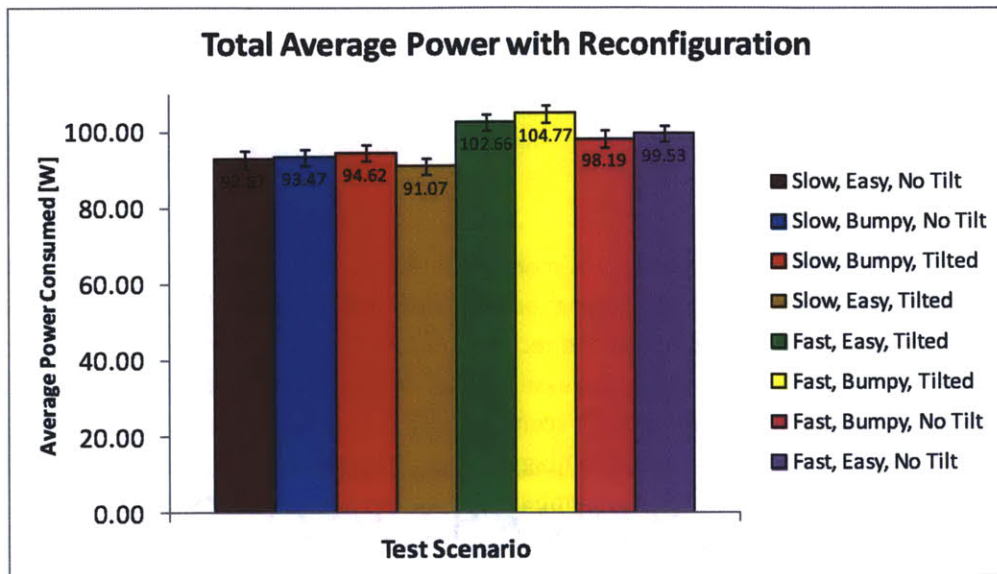


Figure 46 - Average power consumed with reconfiguration for test scenarios

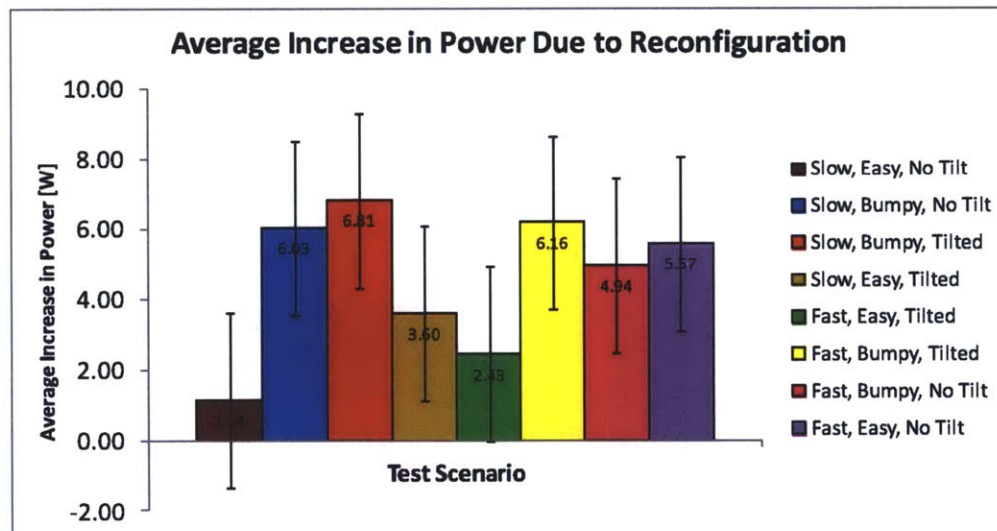


Figure 47 - Average increase in power due to reconfiguration for test scenarios



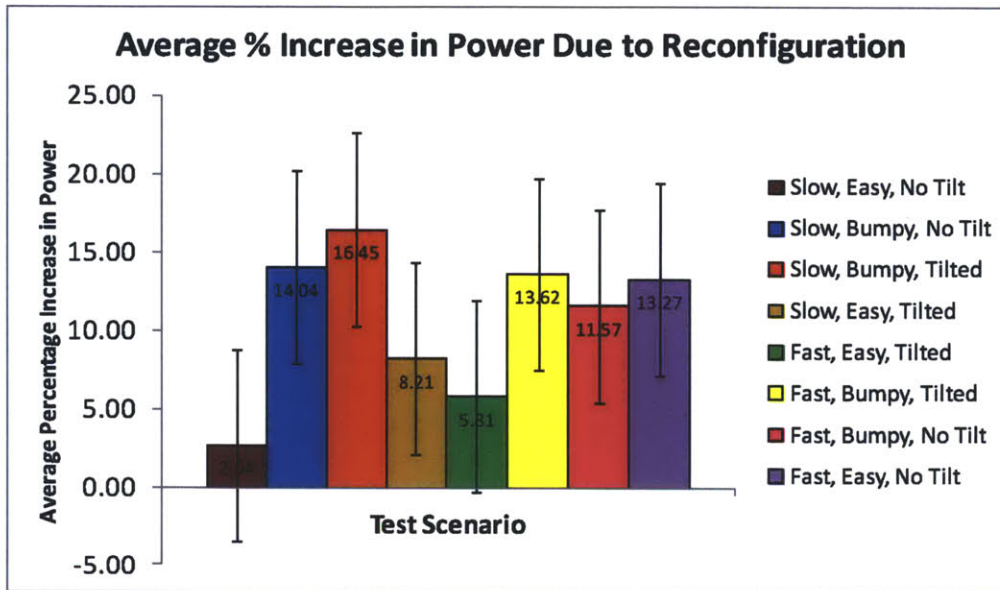


Figure 48 - Average percentage increase in power due to reconfiguration for test scenarios

Ranking the scenarios from least to greatest based on their total average power yields the following results:

- 1) slow, easy, tilted
- 2) slow, easy, no tilt
- 3) slow, bumpy, no tilt
- 4) slow, bumpy, tilted
- 5) fast, bumpy, no tilt
- 6) fast, easy, no tilt
- 7) fast, easy, tilted
- 8) fast, bumpy, tilted

There is a very clear pattern to this ranking. The scenarios are ranked primarily according to speed with the slow speeds using the least amount of power. The slow speed scenarios are ranked secondly by terrain and thirdly by inclination. It is the opposite for the fast speed scenarios. These are ranked secondly by inclination and thirdly by terrain. It is not surprising that speed is the primary factor for power consumption. Higher speeds require more motor torque and therefore more power. The order of the secondary and tertiary factors being opposite for the slow speeds versus fast speeds suggests that there is a small power sensitivity difference between these factors. A look at the actual values supports this notion. Similar to the overall distance values, the net power values can be divided into two groups— a low power group consisting of scenarios 1–3 and a high power group of scenarios 4–8. The difference in values is much greater for fast versus slow speeds than it is for easy versus bumpy terrain or an inclined versus a non-inclined setup.

Figure 47 shows the average increase in power needed for the reconfigurable system compared with the non-reconfigurable system. There is a large range of values for this data. Ranking the scenarios from lowest to highest average power increase yields different results than the net amount of power consumed:

- 1) slow, easy, no tilt
- 2) fast, easy, tilted
- 3) slow, easy, tilted
- 4) fast, bumpy, no tilt
- 5) fast, easy, no tilt
- 6) slow, bumpy, no tilt
- 7) fast, bumpy, tilted
- 8) slow, bumpy, tilted

These rankings are filtered almost entirely by terrain difficulty. The explanation for this is similar to the explanation for the increased distance rankings. The rover requires more power to start roving again after it has stopped (i.e., in the reconfigurable system) than it does to initially start moving forward (i.e., in the non-reconfigurable system). It is still true that the overall power usage is dominated by rover speed. However, when examining these results and comparing the non-reconfigurable system to the reconfigurable system, the large range in values and the obvious patterning according to terrain difficulty suggest that the amount of additional power needed to navigate the surface is more heavily dependent on terrain conditions than on rover speed. One would then expect to see patterning based on inclination, yet no such patterning appears. One explanation for the absence of this pattern is that the test bed was only raised by 2 inches so the inclination was perhaps not significant enough to cause noticeable power changes. Another explanation is that the amount of power consumed is influenced by local terrain conditions much more than global terrain conditions. The inclined test bed is a type of global terrain—the change is gradual and constant over the entire length of the test bed. The bumpy terrain presents localized challenges, so although it does not occur everywhere, the effect is more pronounced in places where it does occur. Most likely both of these explanations are true. A steeper inclination would probably induce a more pronounced change in power values, but in general, local terrain conditions account for power changes more than global terrain conditions.

The rankings according to power increase by percentage are exactly the same as for the average power increase except that scenarios 6 and 7 are flipped. The range of values for percentage increase of power is wide but not nearly as wide as the range of percentages for increased distance. As noted in the terramechanic equations, power relies much less on terrain conditions than does drawbar pull. In general, modeling power can be more accurate than modeling traction and there is typically less variability in the data. That is certainly the case in these results as well.

It is important to examine the power and distance values not just individually but also together. De Weck et al. did this by creating an objective function (Equation 9) that weighted the opposing metrics of

drawbar pull and torque. Those two metrics were not able to be directly measured in this experiment so an alternative objective function has been defined for use here:

$$J^* = \alpha D^* - (1 - \alpha)P \quad (23)$$

where  $D^*$  is distance,  $P$  is power, and  $\alpha$  is a weighting function between 0 and 1. The  $J^*$  values for each test were calculated with normalized distance and power values. The results for each testing scenario were averaged together and are shown in Figure 49.

The data shows that for  $\alpha = 0.5$ , all the test scenarios have negative  $J^*$  values. The negative values suggest that the net gain in distance is outweighed by the amount of power consumed, so for  $\alpha = 0.5$ , maximizing distance is just as important as minimizing power. For  $\alpha = 0.6$ , all but one of the testing scenarios have positive  $J^*$  values. As  $\alpha$  continues to increase, so do the  $J^*$  values. The  $J^*$  value is useful because it shows the limits of effectiveness for the reconfigurable wheels. The negative values seen when distance and power have equal weighting indicate that the ability of the reconfigurable wheels to minimize power is not as effective as their ability to maximize distance. This does not render the concept impractical however. For scenarios where distance achieved is more heavily weighted than power consumed, there is a net benefit. It is reasonable to weigh distance maximization more heavily than power minimization. If the rover is not able to navigate the terrain, mission objectives are limited or compromised. If a modest amount of additional power is required for the rover, the vehicle design can be adapted to meet this need.

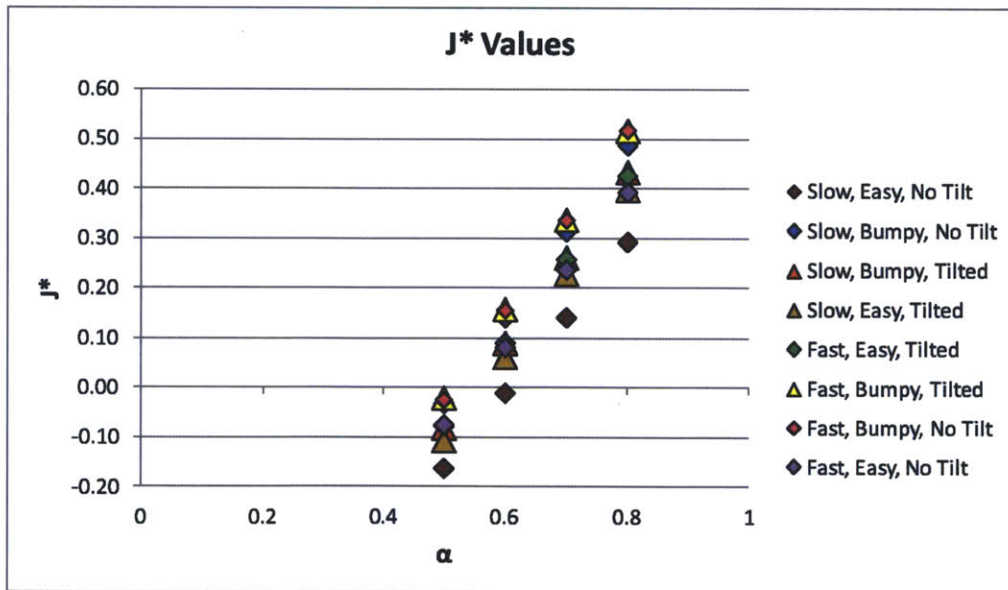


Figure 49 -  $J^*$  values for different alpha values in test scenarios

The  $J^*$  values also reveal that the reconfigurable wheel concept is not equally effective in all the testing scenarios. This can be inferred by ranking the values from lowest to highest:

- 1) slow, easy, no tilt
- 2) slow, easy, tilted
- 3) slow, bumpy, tilted
- 4) fast, easy, tilted
- 5) fast, easy, no tilt
- 6) slow, bumpy, no tilt
- 7) fast, bumpy, no tilt
- 8) fast, bumpy, tilted

When comparing the net effectiveness of maximizing distance and minimizing power, inclination seems to have had the smallest effect, and ease of terrain the largest. Easy terrains had lower values while bumpy terrains had higher values. It seems counterintuitive that the more difficult terrain yielded higher objective function values, but a plausible explanation for this is that the effectiveness of the reconfigurable wheels is more pronounced in challenging terrain environments than easy terrain environments. That idea suggests that the additional power required for larger wheels in the more difficult terrain is worth the extra cost.

Another way to assess the efficiency of the reconfigurable wheel concept is to look at the ratio of distance to power. Figure 50 shows the total distance divided by the total power consumed for each test scenario. The higher this ratio, the higher the net return based upon the net cost. Again, there seems to be a natural breakpoint in concept efficiency based upon terrain type. All of the bumpy terrain scenarios had lower readings than the easy terrain scenarios. The bumpy terrain scenarios were filtered secondly by speed and the easy terrain scenarios by inclination.

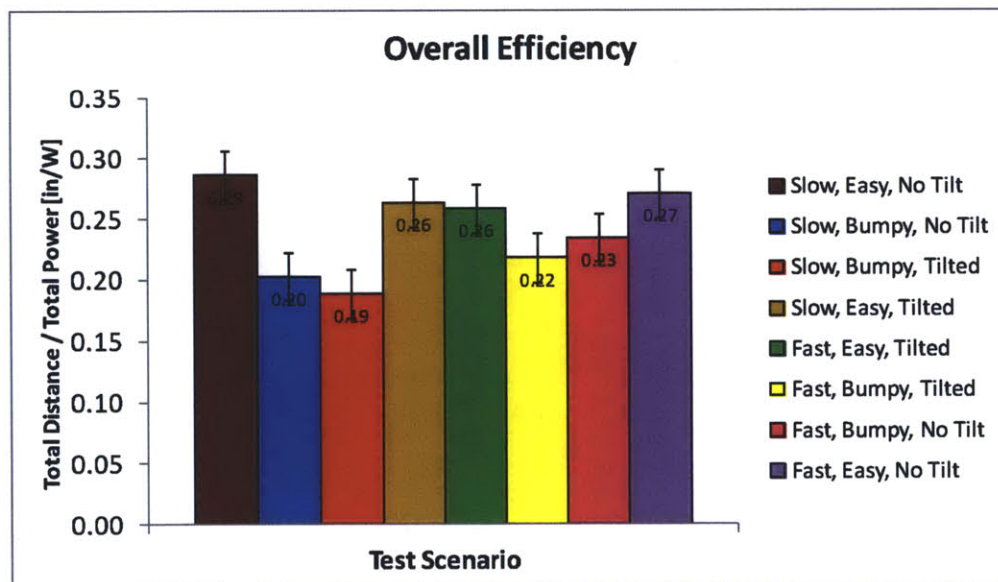


Figure 50 - Efficiency calculations for all testing scenarios

A more interesting effectiveness measurement is the relative efficiency. Recall from section 3 that as part of the initial design analysis, a relative performance efficiency metric was developed (Equation 21). This metric compares the performance efficiency of a reconfigurable system to the performance efficiency of a non-reconfigurable system. The performance efficiency of each system was defined as the ratio of drawbar pull to power (Equation 22). A similar metric is defined here except that the performance efficiency for each system is defined as the ratio of distance to power. The relative efficiency is still defined as the ratio of the reconfigurable system efficiency to that of the non-reconfigurable system; those values are displayed in Figure 51. A relative efficiency value greater than one indicates that the reconfigurable system is more efficient than the non-reconfigurable system, and vice versa for a value less than one. There does not appear to be any particular characteristic that dictated the relative efficiency of the scenarios. The range of values is relatively small and the differences in the values are gradual. Only three of the test scenarios had a relative efficiency that was greater than one. Although it would be ideal for relative efficiency values for all scenarios to be greater than one, these results do not necessarily mean that the concept is ineffective. They corroborate the results from the  $J^*$  values in suggesting that when power and distance are weighed equally the net benefit is not necessarily a positive one. As explained earlier, however, maximizing distance is typically a higher design objective than minimizing power.

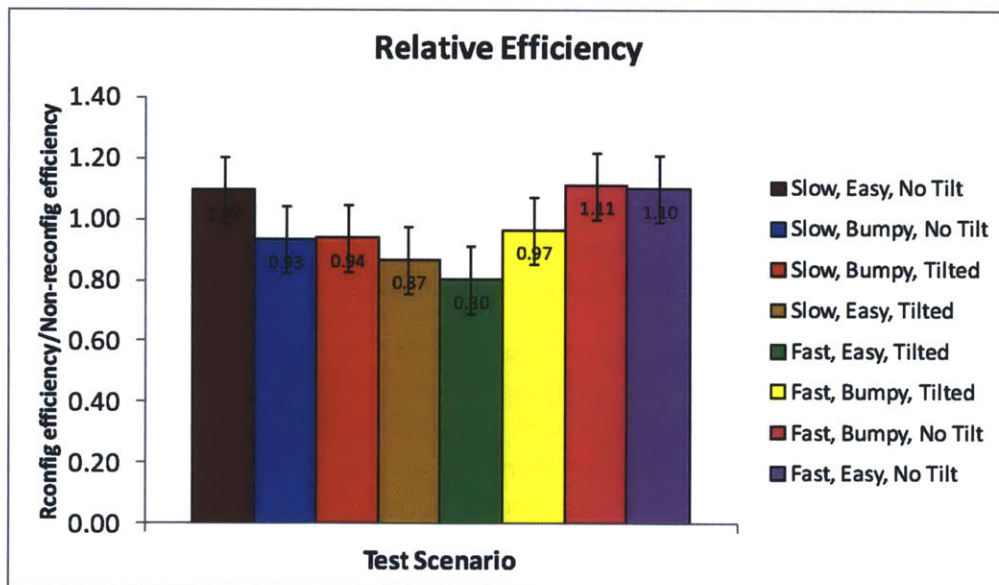


Figure 51 - Relative efficiency values for all test scenarios

As a final assessment, it is interesting to look congruently at the scenario rankings. In Table 8, the scenarios are listed on the left and relevant values discussed are shown horizontally along the top row. For each value, the scenarios are ranked from lowest to highest. The rankings are color coded as a visual aid. It is interesting to see the patterns that do exist and the patterns that do not exist. The scenarios that had the largest distances did not necessarily also consume the most power. The overall efficiency ranking closely followed the increase in distance ranking while the relative efficiency ranking more

closely matched the percentage increase in distance ranking. The objective function ranking does not closely coincide with any of the other value rankings. In summary, the data show several trends that can be explained using terramechanic models, however it is also clear that there is limited understanding in those models such that they cannot adequately explain all the behaviors exhibited in the data.

**Table 8 - Scenario Rankings for All Values**

Scenario	Total Distance	Increase in Distance	% Increase in Distance	Total Power	Increase in Power	% Increase in Power	J*	Overall Efficiency	Relative Efficiency
slow, bumpy, tilted	1	1	4	4	8	8	3	1	4
slow, bumpy, no tilt	2	2	3	3	6	7	6	2	3
fast, bumpy, tilted	3	5	5	8	7	6	8	3	5
fast, bumpy, no tilt	4	6	7	5	4	4	7	4	8
slow, easy, tilted	5	3	2	1	3	3	2	6	2
slow, easy, no tilt	6	7	6	2	1	1	1	8	6
fast, easy, tilted	7	4	1	7	2	2	4	5	1
fast, easy, no tilt	8	8	8	6	5	5	5	7	7

## 6.4 Error Analysis

It is important to identify potential sources of error or explanations for inconsistencies in the data for this project. One of the main sources of inconsistency was the terrain. Each time the rover would travel through the popcorn, it would disrupt the surface. Effort was made to return the surface to its original state after each test, but despite this effort the terrain conditions were not exactly the same for each test. This undoubtedly caused inconsistencies in the data; however, any rover on the Martian or lunar surface will certainly experience a wide range of surface conditions even if the soil type isn't changing, so the variability in testing conditions may have helped to produce more realistic results.

Another source of error was in the reconfiguration process. Each test began with the wheel in the smallest width configuration and then eventually the wheels reconfigured to the largest width configuration. The reconfiguration from small width to large width was controlled by microcontrollers, but at the end of every test the reconfiguration from large width back to small width was done by hand. This could have also been done with the microcontroller, but manually reconfiguring the wheels rather than autonomously reconfiguring them saved time. The wheels had approximately the same starting position each time, but there was undoubtedly some variation in the starting positions between wheels and between tests.

Perhaps the largest source of error was in measuring the electrical current in each test. This was done by connecting a multimeter in series with the electrical circuit used to power the drive motors. During each test, the current was measured by visually observing the readout on the multimeter. The current usage was not constant so the first measurement was typically the one that was recorded. A more accurate way to record current would have been to use a current probe that could record the current

consumption for the entire length of the test and then compute the average value. Unfortunately, a current probe was not available for use in the experiment so the multimeter was used instead.

For most of the testing scenarios, five tests were conducted. Analyzing the amount of error with a sample size of only five tests may be unreliable. Therefore, in an effort to quantify the amount of error inherent in the testing process, a set of 25 tests was conducted for the fast, easy, no tilt testing scenario. Statistical analysis for this larger sample set was completed, including calculating 90 percent confidence intervals. The results of this analysis are shown in Table 9 below.

**Table 9 - Statistical Values for Set of 25 Samples**

Variable Name	Mean	Standard Deviation	Min Value	Max Value	90% Confidence Interval
Reconfigurable (i.e. Total) Distance [in.]	26.84	5.41	18.00	38.00	+/- 1.85
Increase in Distance [in.]	14.56	4.74	6.00	26.00	+/- 1.62
% Increase in Distance	132.37%	63.57%	46.51%	305.88%	+/- 21.71%
Reconfigurable (i.e. Total) Power [W]	99.53	6.31	87.19	116.50	+/- 2.16
Increase in Power [W]	5.57	7.25	-7.63	20.95	+/- 2.48
% Increase in Power	13.27%	17.95%	-14.00%	63.26%	+/- 6.13%
J* ( $\alpha = 0.5$ )	-0.07	0.08	-0.23	0.10	+/- 0.027
J* ( $\alpha = 0.6$ )	0.08	0.09	-0.09	0.28	+/- 0.031
J* ( $\alpha = 0.7$ )	0.24	0.10	0.05	0.46	+/- 0.035
J* ( $\alpha = 0.8$ )	0.39	0.12	0.19	0.64	+/- 0.039
Overall Efficiency	0.27	0.06	0.16	0.41	+/- 0.020
Relative Efficiency	1.10	0.33	0.63	1.92	+/- 0.11

Most of the values are nominal, however, several important observations can be made from this table. The percentage increase in distance has a very large confidence interval. As mentioned earlier in the discussion, the values for the percentage increase in distance for all the testing scenarios appeared more random and had a much larger range than other values. The error analysis presented here concurs with the value comparison between the scenarios that suggested that there is naturally a large amount of variability within distance and drawbar pull data.

The power increase data is also interesting because its standard deviation is larger than its mean value. This is because in some of the tests, there was actually a decrease in power consumption between the reconfigurable and non-reconfigurable systems. It is uncertain whether the decrease in power between systems can be attributed to unusually large power readings for the non-reconfigurable system or unusually small power readings for the reconfigurable system. This uncertainty may be an outcome of the inaccuracies in the current measurements, however. More experimentation is necessary to know for certain the explanation for this drop in power.

Another important value to note is the confidence interval for the relative efficiency. This metric had a relatively high confidence interval of +/- 0.11. The relative efficiency value must be greater than one in

order to claim that the reconfigurable system is more efficient than the non-reconfigurable system. Only three of the scenarios had relative efficiencies that were greater than one, however of these three values the highest was 1.11, so the claim that in these three scenarios the reconfigurable system was more efficient than the non-reconfigurable system is thus questionable within the 90 percent confidence interval. Alternatively, many of the scenarios whose relative efficiencies were less than one actually had values within 0.11 of 1.0. Therefore, it is also plausible that in some of these scenarios, performing additional testing would yield greater efficiencies for the reconfigurable system than the non-reconfigurable system. Either way, the data suggests that it is difficult to claim that the reconfigurable system is substantially more efficient than the non-reconfigurable system, or vice versa.

None of the other error analysis results conflict with claims made from the data analysis discussion in the previous section. Scatter plots of all the data and tables of relevant statistical values for the other testing scenarios can be found in the appendix. Comparison of these statistical values between scenarios will not be discussed here because none of the findings are particularly relevant or interesting.

## **6.5 Summary of Results**

The major findings from the data can be summarized as follows:

- In all the test scenarios, the rover was able to autonomously reconfigure its wheels and achieve additional distance. However, the data indicates that the terrain and surface conditions had a major impact on the additional distance that the rover could achieve when using the reconfigurable wheels.
- As expected, results showed an increase in power when using the reconfigurable wheels. Power consumption seemed to be more sensitive to localized terrain challenges than global terrain challenges.
- When maximizing vehicle traction is more heavily weighed than minimizing power consumption, the use of reconfigurable wheels yields a net gain in performance.
- Error analysis of the results revealed no major concerns that compromise the observations and claims made here based on the collected data.



## **7.0 Summary and Conclusions**

### **7.1 Conclusion**

All objectives of this project were successfully met. New design concepts for reconfigurable wheels were explored; four working prototypes of the best design were built and integrated onto a rover platform; the rover's ability to autonomously reconfigure its wheels was successfully demonstrated; and the data collected from testing corroborates previous results and shows that the use of reconfigurable wheels enhances rover mobility in challenging terrain.

Any rover engineer would agree that designing, developing, building, testing, launching, and operating a real planetary rover takes enormous effort and tremendous teamwork. There is still a lot of design, development, and testing that must be completed before reconfigurable wheels can actually be implemented on real rovers, but the results of this project have hopefully brought that goal closer. Previous work from de Weck's research group showed that the concept of a reconfigurable wheel was beneficial from a theoretical standpoint, and results from the 62x project showed that in multiple soil types the amount of drawbar pull a wheel can produce was increased by changing the wheel size. As part of this project, two different reconfigurable wheel designs for various sized rovers have been developed. Although only one of the designs was built and tested, its successful integration with an entire rover platform shows that the reconfigurable wheel concept is practical from a systems perspective. The wheel is autonomously controlled and capable of supporting the weight of an entire rover, thus demonstrating that it can effectively function on the surface of another planet regardless of the absence of human assistance and control.

### **7.2 Future Work**

Many important lessons learned throughout the course of this project can help shape plans for future work. There were several structural problems when the wheel was integrated to the rover platform that required quick fixes and re-designs. Since every rover design is different, it is not possible to create a universal design to integrate the wheels onto any rover. However, this project has demonstrated that there are changes that can make the integration easier. The initial structural problems arose because the wheel axle was too small compared to the wheel. Due to various constraints, using different drive motors was not an option for this project; it is recommended that larger wheel axles and motor shafts be used.

The second structural problem was a result of misalignments between the hubcaps. In the current designs, the hubcaps are only connected via the linear actuator. In future designs, it is recommended that either a stronger linear actuator be used or that additional supporting structures that will maintain hubcap alignment be included.

The final recommendation regarding the wheel design is that there should be fewer gaps in the tire's surface area. In the 62x project the tire strips overlapped each other and caused friction problems when the tire strips tried to slide across each other. Consequently, the current wheel design was changed to have rectangular tire strips. This means that when the wheel is in its smallest width configuration there are often large gaps in between the strips. This has not caused any specific problems per se; however, a

greater surface area will most likely contribute to better wheel traction. Therefore, it is recommended that different shapes for the tire strips be experimented with in future designs.

The biggest opportunity for future research for this project lies in the area of autonomy and control. Multiple studies have now gathered data to support the concept of a reconfigurable wheel, but whether or not the concept can meet its full potential is dependent on the ability to properly control it. The control algorithm used in this project was very simplistic, since the testing procedure was designed to ensure that the wheel would experience slippage and need to change to a wider configuration. The optimal controller should be capable of changing the wheel to a wide configuration when the rover is losing traction, but also capable of changing the wheel to a narrow configuration when the rover has sufficient traction. Additional work should include configuration testing from large to small width. Additionally, the controller for this project used only two different wheel configurations—smallest width or largest width. Previous data suggests that in some soils intermediate configurations would be best, so an optimal controller would need to be capable of configuring to intermediate sizes as well. If new control algorithms are developed and implemented, the same series of tests conducted in this project could be carried out for the new controllers. The results could then be compared to see which algorithm was most effective. Another possibility would be to conduct the same series of tests outlined in the test matrix in Figure 42, but have a medium width state that the wheel can configure to before changing to the widest width state (Figure 52).

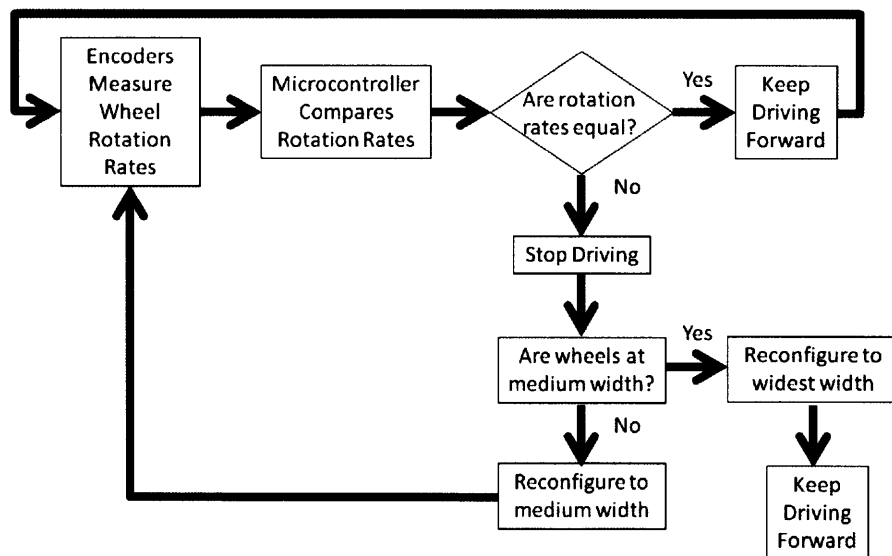


Figure 52 - Potential test diagram for future testing

Several other testing options can also be recommended. The testing for this project was done in popcorn seeds to avoid potential problems with sand and dust. If the problems with the wheel design can be addressed so that dust is less hazardous, then testing in sand would be advisable since sand is the most problematic soil type on the Martian surface. More variety can also be added to the testing environment. For example, the inclination of the testbed can be raised, and the tests can be conducted

at additional speed settings. New variables—moisture content, for example—can also be introduced to the test matrix. New tests that experiment with movement strategies can also be tried. For example, as discussed earlier, the rover often had more difficulty restarting after it stopped in the soil to reconfigure the wheels due to additional sinkage. Therefore it could be more effective to have the rover back-up a short distance before moving forward again to increase vehicle momentum. Overall, the data collected from this project is useful, but there are still many more opportunities for future testing and design improvements to enhance the concept.

### 7.3 Closing Statement

Designing wheels for Mars rovers has been a great challenge and a thrilling opportunity. The contributions made from this project are small compared to the vast reservoirs of knowledge required to successfully send a rover to another planetary surface. Although these contributions are small, it is hopeful that they will work to expand man's reach to understand other worlds and aid in the quest to explore the beauties and mysteries of space and the heavens.



Figure 53 - Image Collage: MER on the left, reconfigurable wheel rover on the right, Apollo 1 Hills in the background (MER and Apollo 1 Hills pictures courtesy of NASA)

## 8.0 References

- [1] "NASA's Opportunity Rover Rolls Free on Mars," <http://marsrovers.nasa.gov/newsroom/pressreleases/20050606a.html> (Accessed January 15, 2011).
- [2] M. Wall, "Spirit Rover Remains Silent as Mars Mission Begins 8<sup>th</sup> Year," <http://www.space.com/10425-spirit-rover-remains-silent-mars-mission-begins-8th-year.html> (Accessed June 3, 2011).
- [3] "NASA's Spirit Rover Completes Mission on Mars," [http://www.nasa.gov/mission\\_pages/mer/news/mer20110525.html](http://www.nasa.gov/mission_pages/mer/news/mer20110525.html) (Accessed June 3, 2011).
- [4] A. Young, *Lunar and Planetary Rovers: The Wheels of Apollo and the Quest for Mars*. Praxis Publishing Ltd., 2007.
- [5] A. Ball, J. R. C. Garry, R. D. Lorenz, and V. V. Kerzhanovich, *Planetary Landers and Entry Probes*. Cambridge University Press, 2007.
- [6] "Durable NASA Rover Beginning Ninth Year of Mars Work," [http://www.nasa.gov/mission\\_pages/mer/news/mer20120124.html](http://www.nasa.gov/mission_pages/mer/news/mer20120124.html) (Accessed January 25, 2012).
- [7] M. G. Bekker, *Introduction to Terrain-Vehicle Systems*. University of Michigan Press, 1969.
- [8] M. G. Bekker, *Theory of Land Locomotion*. University of Michigan Press, 1956.
- [9] J.Y. Wong, *Theory of Ground Vehicles*, 4<sup>th</sup> edition. John Wiley & Sons, 2008.
- [10] J.Y. Wong, *Terramechanics and Off-Road Vehicle Engineering: Terrain Behaviour, Off-Road Vehicle Performance and Design*, 2<sup>nd</sup> edition. Elsevier Ltd., 2010.
- [11] J.R. Matijevic et. al., "Characterization of Martian Surface Deposits by the Mars Pathfinder Rover, Sojourner," *Science*, Vol. 278, pp. 1765-1768, 1997.
- [12] A. Siddiqi, O.L. de Weck, and K. Iagnemma, "Reconfigurability in Planetary Surface Vehicles: Modelling Approaches and Test Study." *Journal of the British Interplanetary Society (JBIS)*, Vol. 59, pp. 450-460, 2006.
- [13] B. Baker and N. Steber, "Reconfigurable Wheels for Planetary Surface Rovers." 16.622 Final Report, Department of Aeronautics and Astronautics, Massachusetts Institute of Technology, 2008.
- [14] S. H. Crandall, N. C. Dahl, and T.J. Lardner, *An Introduction to the Mechanics of Solids: 2<sup>nd</sup> Edition with SI Units*. McGraw-Hill, 1999.

[15] R. Huston and H. Josephs, *Practical Stress Analysis in Engineering Design: 3<sup>rd</sup> Edition*. CRC Press, 2009.

[16] A. Siddiqi, O. de Weck, and J. Hoffman, "Sustainability in System Architectures Through Reconfigurability: A Case Study of Planetary Surface Vehicles." *International Astronautical Federation – 56<sup>th</sup> International Astronautical Congress* Vol. 8, pp. 5550-5562, 2005.

[17] A. Siddiqi and O. de Weck, "Reconfigurability in planetary surface vehicles." *Acta Astronautica* Vol. 64, pp. 589-601, 2009.

[18] K. Iagnemma, H. Shilby and S. Dubowsky, "Online Terrain Parameter Estimation for Wheeled Mobile Robots with Applications to Planetary Rovers." *IEEE Transactions on Robotics* Vol. 20, pp. 921-927, 2004.

[19] J.D. Terry and M.A. Minor, "Traction Estimation and Control for Mobile Robots using the Wheel Slip Velocity." *Proceedings of the IEEE/RSJ International Conference on Intelligent Robots and Systems*, Nice, France, September 2008.

## 9.0 Appendix

### Influence Diagram

Several iterations of the influence diagram were created. For one of the final versions, the names of relevant properties were replaced by the actual variables. That variable diagram and its accompanying influence diagram can be seen here.

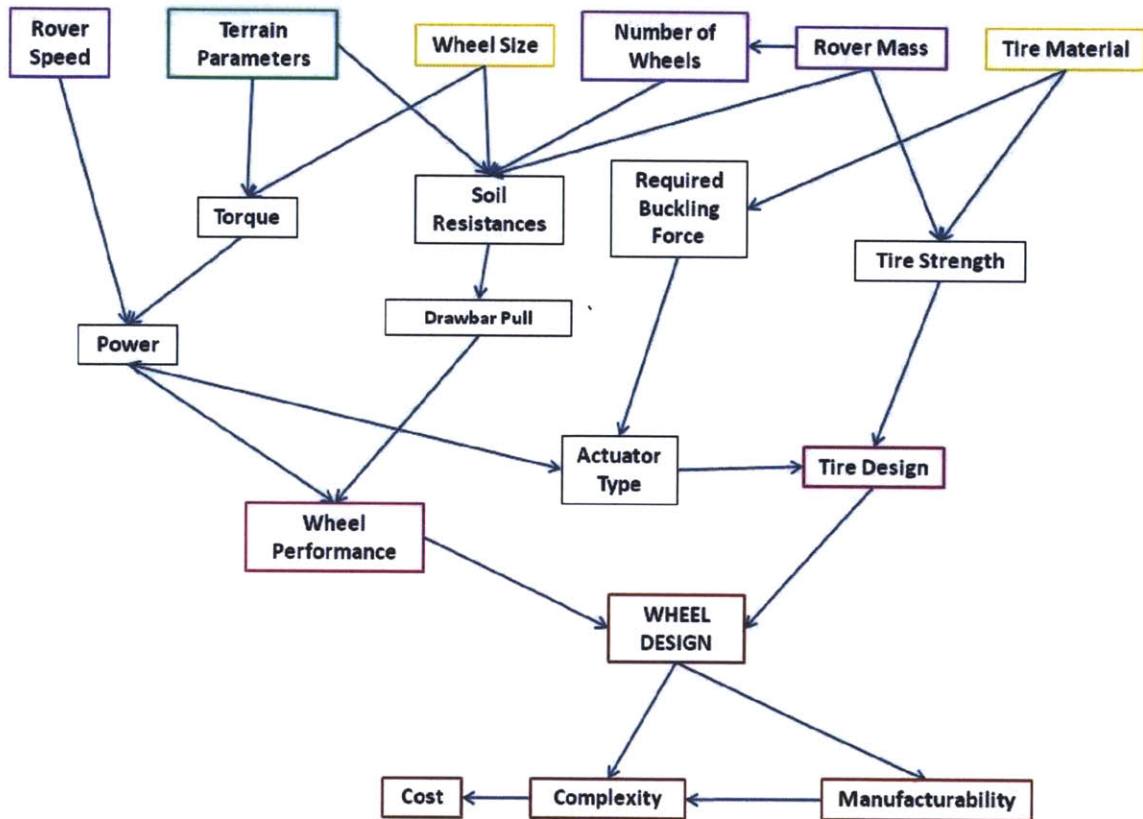


Figure 54 - Earlier version of the influence diagram

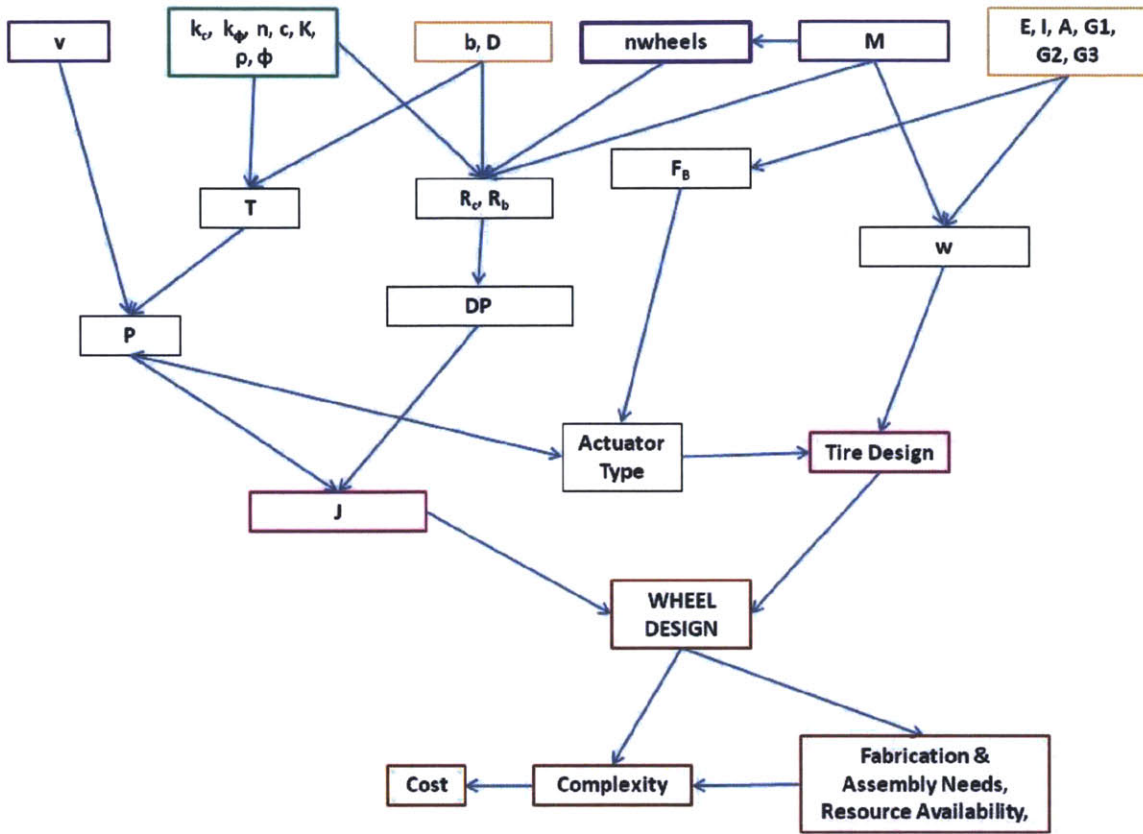


Figure 55 - Influence diagram with variables

## Incidence Matrix

In conjunction with the influence diagram, an incidence matrix was also created to show the relationships between variables. The variables listed horizontally on the top are inputs and the variables listed vertically on the side are outputs. An 'x' indicates that an output variable is influenced by an input variable. A black 'x' indicates a direct relationship and a red 'x' indicates an indirect relationship.

	wheel load (W)	terrain	rover lifetime	rover speed	slippage (i)	sinkage (z)	cost	wheel width (b)	wheel diameter (D)	surface contact area (A)	soil properties	motor efficiency	tire material	tire design (i.e. size/shape)	tire strength	actuator type	# of actuators	power required per actuator	tractive force (F)	soil resistances	power available	DP	effectiveness of controller	Consumed power
Fatigue/Wear	X	X	X	X	X	X		X	X		X	X	X										X	X
Deformation	X						X						X	X	X	X							X	
Power to reconfigure							X						X	X	X	X	X	X				X		
Tire material							X															X		
Tire Strength												X	X									X		
Surface Contact Area (A)								X					X	X	X							X		
Actuator Type							X						X	X	X							X		
Rover Speed																						X		
Power to drive	X	X		X	X	X		X	X		X	X	X	X								X		X
Sinkage (z)	X				X			X	X		X													
Slippage (i)	X	X		X		X					X		X	X								X	X	
DP	X	X		X	X	X	X	X	X	X	X		X	X	X	X			X	X		X		X
Tractive Force (F)	X	X		X	X	X	X	X	X	X	X		X	X	X	X						X		X
Bull-dozing Resistance	X					X		X	X		X													
Compaction Resistance	X					X		X	X		X													
Performance	X	X		X	X	X	X	X	X	X	X	X	X	X	X	X	X	X	X	X	X	X	X	X

Figure 56 - Incidence matrix showing dependencies between relevant variables



# Wheel Design Comparison

The three major wheel designs were compared on based on several figures of merit. Those comparisons are outlined in Table 10.

Table 10 - Wheel Design Comparison

Wheel Design	Strength	Loading Force (→ power)	Cost	Weight	Complexity	State of manufacturing	Susceptibility to environment	Failure modes/risk	Overall Comments
Eds version 2	Deflection values are very low... which I think signifies that wheel would not be strong enough to support tower.	Range is 10.09 - 13.31 N (for one spring steel strip)	No additional materials so no additional cost	This would weigh about the same as Eds wheel.	Simplest design	Hardest part of manufacturing was assembly.	Will need to protect actuator from sand somehow.	Based on Eds experience, actuator failure and fatigue issues are probably biggest concerns related to failure.	Experiences from Eds showed that this design worked fairly well, however after running the numbers major concern with this design is that it won't actually be strong to support an entire row.
3 hubcap	Deflection values are much more manageable. I think this design would be strong enough to support tower.	Range is 60.75 - 106.50 N (for one "pair" of spring steel strips)	Additional hubcap would require more cost. If actuator has to be stronger, actuator cost will likely be more.	Additional hubcap would require more weight. Actuator would likely weigh more and if more power is needed that also adds weight.	This is the most complex idea. It's hard to say how easy it will slide back to either configurations. Teflon pieces will also have to be made for each piece, and additional machining may also be required.	Each teflon piece will have to be made separately. Attaching each teflon piece will also be more challenging and time consuming.	will need to protect teflon pieces from sand. Best way to do this is probably having a wiper. Questionable how well teflon will slide in presence of sand. It will be difficult to get spring steel slide when its supporting weight of row.	No previous experience with this design, but sliding mechanism is probably biggest area of concern.	I really like this idea and I think it could make a lot of potential, but refining this design would probably require more time than I actually have so I think it might be better to stick to the Eds.
Sliding Spring Steel	I think deflection values for this would be about the same as 3 hubcap because we are only using one piece of spring steel.	This design de-complex width and diameter, loading force is dependent on which wheel can change in this design, so loading force would be in range of 14.59 - 132.9 N. Teflon structures will be readily there for teflon pieces. Sand in reality there you define mechanism which would add to overall power requirement.	Teflon devices would require extra cost.	If actuator doesn't need to be as strong, that would mean less weight.	I feel like sliding spring steel idea has the potential to be a more elegant solution but I'm not sure that there is enough time needed to make this idea work.	Similar to complexity criterion, sliding spring steel idea adds additional manufacturing challenges compared to other two designs.	First experience has shown that the sport environment poses many challenges. As such, the importance of minimizing the susceptibility to environment must not be underestimated.	After comparing options from several different angles, I think best choice is 3 hubcap idea. Greater power requirement is not ideal, but it's more important to have a wheel that is strong enough to support tower and requires more power than to have wheel that requires less power but can't support tower.	
General Comments	Using deflection equation to assess the strength is a very rough, first-order approximation. I hesitate to use that model to get exact size values (i.e. thickness of spring steel), but I think it does accurately reflect general concepts of strength. Based on results, I feel like 3 hubcap design is the only one strong enough to support tower weight.		Eds design would be cheapest. However, differences in cost for the three designs may not turn out to be very substantial.						

## Material Properties for Composite Tire Strips

Table 11 - Material properties for tire strips

<b>Material Properties of Spring Steel/Wire Mesh Combo</b>		
<i>Property</i>	<i>Value</i>	<i>Units</i>
Elastic Modulus	4.24*10 <sup>10</sup>	Pa
Poisson's ratio	0.287	NA
Density	0.283	lbs/in <sup>3</sup>
Tensile Strength	142	ksi
Yield Strength	80	ksi
Thermal Expansion Coefficient	8.1*10 <sup>-6</sup>	/° F
Thermal Conductivity	27	Btu/sq. ft./ft./hr./° F

## Deflection Results from Beam Modeling

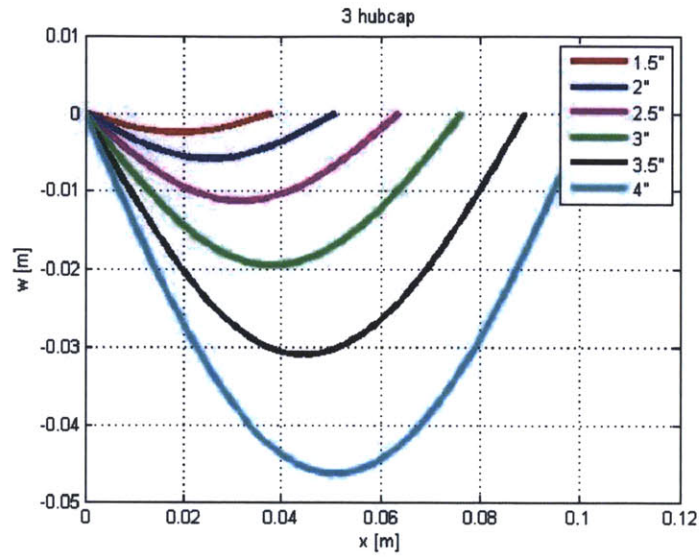


Figure 57 - Simple beam theory deflection results for 3hubcap wheel design. The different colors represent different tire strip lengths. The x-axis is the distance along the length of the tire strip and the y-axis is the amount of deflection.

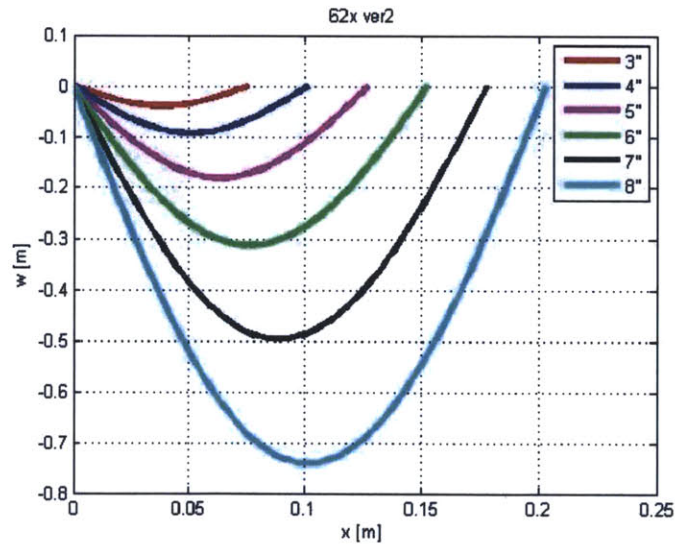


Figure 58 - Simple beam theory deflection results for 62x\_ver2 wheel design. The different colors represent different tire strip lengths. The x-axis is the distance along the length of the tire strip and the y-axis is the amount of deflection.

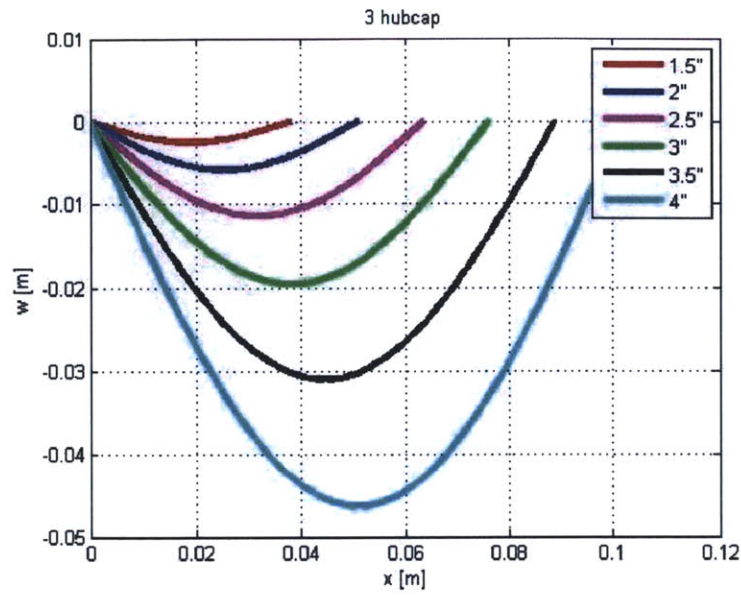


Figure 59 - Thin curved beam theory deflection results for the 3hubcap wheel design. The different colors represent different tire strip lengths. The x-axis is the distance along the length of the tire strip and the y-axis is the amount of deflection.

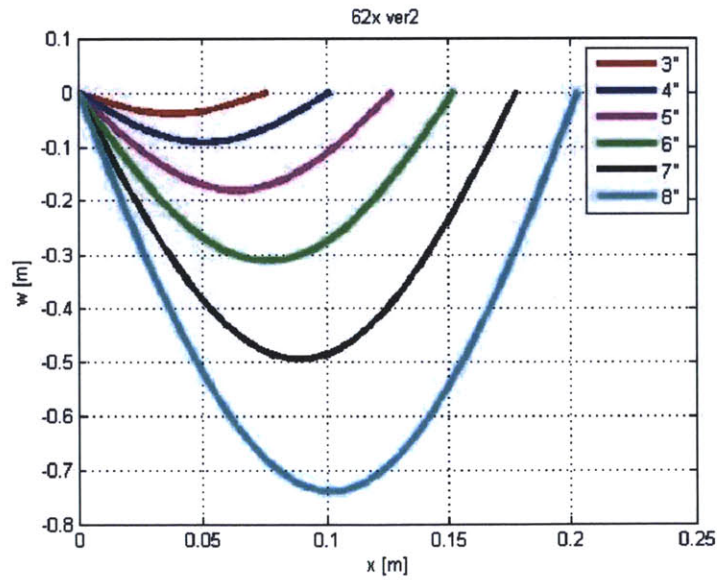


Figure 60 - Thin curved beam theory results for the 62x\_ver2 wheel design. The different colors represent different tire strip lengths. The x-axis is the distance along the length of the tire strip and the y-axis is the amount of deflection.

## Manufacturability Assessment

After the wheel design selection, the manufacturability of the reconfigurable wheel was evaluated based on whether or not parts were commercially available (COTS), material costs, fabrication needs, assembly needs, and the availability of resources to meet the assembly and fabrication needs.

**Table 12 – Manufacturability assessment for the 62x\_ver2 and 3hubcap wheel designs**

Parts List	COTS?	Material Cost	Fabrication Needs	Assembly Needs	Resource Availability
Hubcaps	No	37.5	Pieces have to be cut using water jet, drilled for screws and actuator using mill, tapped by hand		Aero/Astro Machine Shop Capability
Wire Mesh	No	105	Pieces have to be cut by hand	spring steel and wire mesh has to be "sewn" by hand	Aero/Astro Machine Shop Capability
Spring Steel	No	30	Pieces have to be cut using water jet	spring steel and wire mesh pieces have to be secured to hubcaps	Aero/Astro Machine Shop Capability
Actuator	Yes	?	Set screws for linear actuator need to be made	Actuator has to be mounted to hubcaps	Aero/Astro Machine Shop Capability
Retaining Ring/Flange	No	37.5	Pieces have to be cut using water jet, drilled using mill, tapped by hand		Aero/Astro Machine Shop Capability
Screws	Yes	5			
Microcontroller	Yes	250		Programming for microcontroller, all of the	Laptop Computer and OpenSource Software
Encoders	Yes	40			Purchase from VEX Robotics

## List of Major Parts

Table 13 - Parts List

Parts	Materials (if part was made)	Manufacture and Part No. (if part was purchased)	Dimensions (if appropriate)
Hubcaps and Hubrings	T6061 Aluminum	McMaster	Hubcaps were 4.5" in dia. Hubrings were donut shaped. Outside hubrings, outer dia. was 4.5" and inner dia. Was 2.5". Inner hubrings, outer dia. 4.5" and inner dia. 3.25"
Tire Strips	Spring Steel, Copper Wire Mesh, Steel Wiring	Copper Wire Mesh Purchased from TWP Inc., 010X010C0250W36T, Spring Steel McMaster 9075K183	Copper strips were 6.5" long and 1" wide. Spring steel was 6.5" long and 0.25" wide.
Electric Slip Rings	Copper Plates	All Electronics Corp., PCB-612	Slip Rings were also donut shaped. Outer diameters: 1st ring - 1.5", 2nd ring - 2.5", 3rd ring - 3.5", 4th ring - 4.5". For all rings, inner diameter was 0.5" less than outer diameter
Electric Brushes		OmegaShielding	
Electric Brush Mounts	Lexan	McMaster	
Wheel Axle	1/8" square steel stock	McMaster	Length of wheel axle: 1.25" (?)
Wheel Axle Flange	T6061 Aluminum	McMaster	Tapered Flange. Large piece was 0.875" in dia. and 0.25" long, small piece was 0.375" in dia. and 0.375" long (See Diagram)
Hollow Connector Tube	1" Steel Tube (Hollow with 1/16" wall thickness)	McMaster	Tube Length: 3.25"
Actuator/Stepper Motor		Anaheim Automation, TSFNA57-075-26-023-LW6	
Inside Wheel Collars		McMaster 6432K12	
Horizontal Support Bars	T6061 Aluminum		Length: 14.5", Width: 2"
Bearings for Steel Tube		McMaster 6455K88	
Casing for Steel Tube Bearings	T6061 Aluminum		See Diagram
Frictionless Rails		McMaster 6709K33	
Frictionless Guides		McMaster 6709K12	
Support Arms	T6061 Aluminum	McMaster	See Diagram
Support Arm Mounts	T6061 Aluminum	McMaster	Approx. 1.5" x 1.5"
Outside Wheel Collars	T6061 Aluminum	McMaster	See Diagram
Bearings for Outside Collars		McMaster 6680K36	
Vertical Arms for Outside Collar Bearings	T6061 Aluminum		See Diagram
Wheel Covers	Spandex		
Rover Platform		VexRobotics Robot Starter Kit 276-1750-G	
Wheel Encoders		VexRobotics 276-2156	

Arduino Uno Microcontroller		SparkFun DEV-09950	
Stepper Motor Drivers		Marlin P. Jones Assoc., 18187MS	
LiPo Batteries (for Drivers)		Hobby Lobby International Inc., YTB13004	

# Dimensional Drawings for some of the Custom-Made Parts

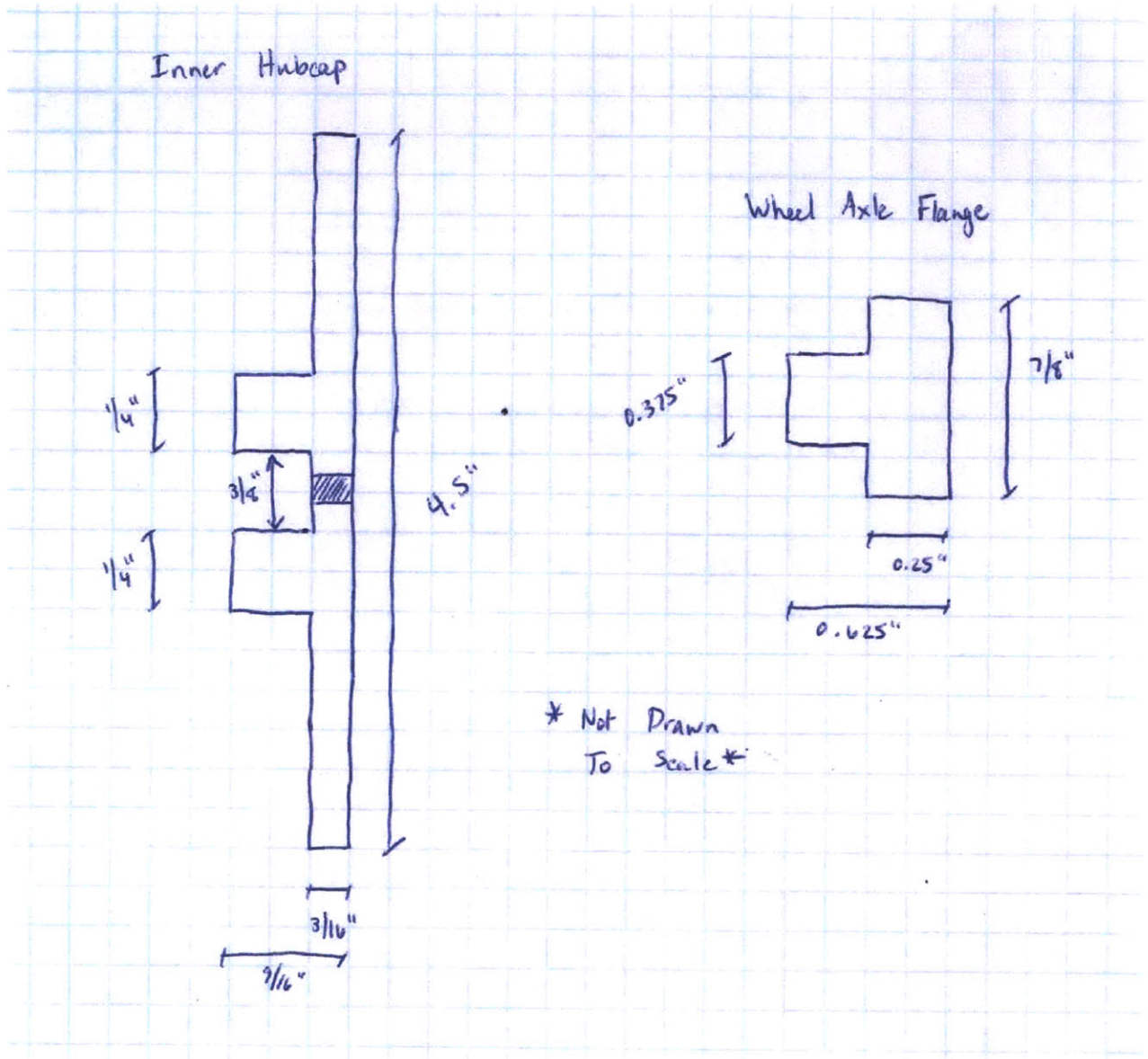


Figure 61 - Dimensional drawings of inner hubcap and aluminum plug



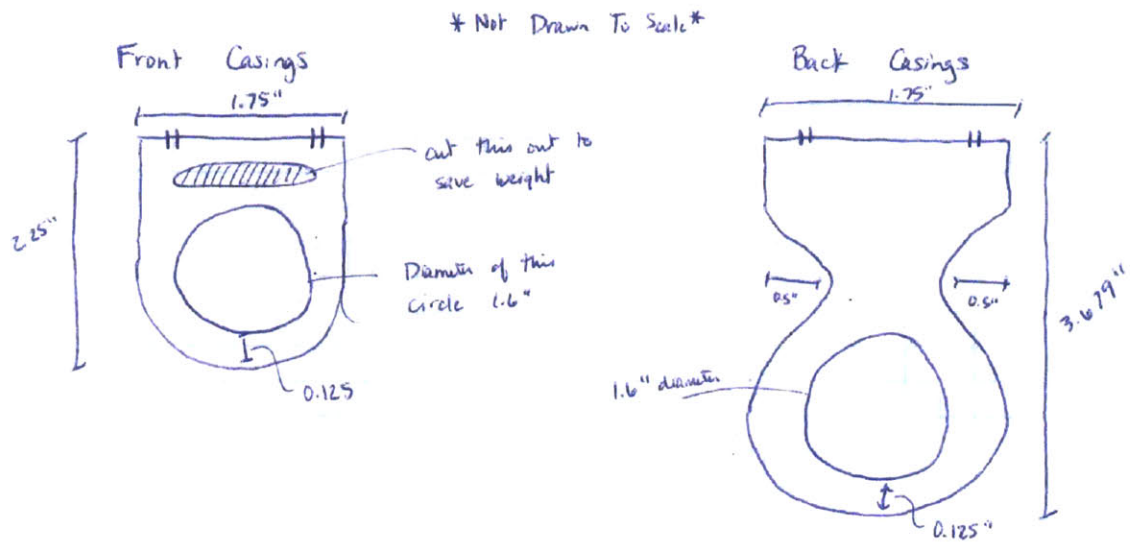


Figure 62 - Dimensional drawing for bearings for hollow steel tube

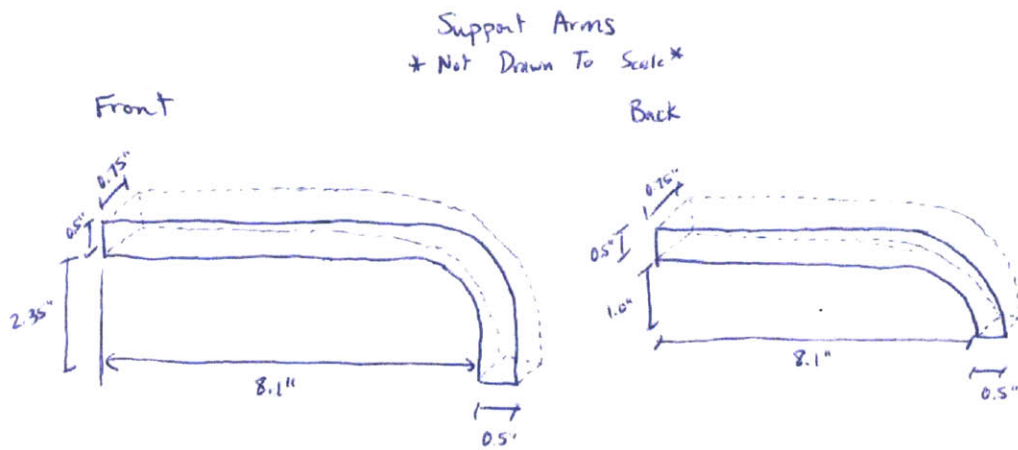


Figure 63 - Dimensional drawing for support arms

Collar and Vertical Arm  
 \* Not Drawn To Scale \*

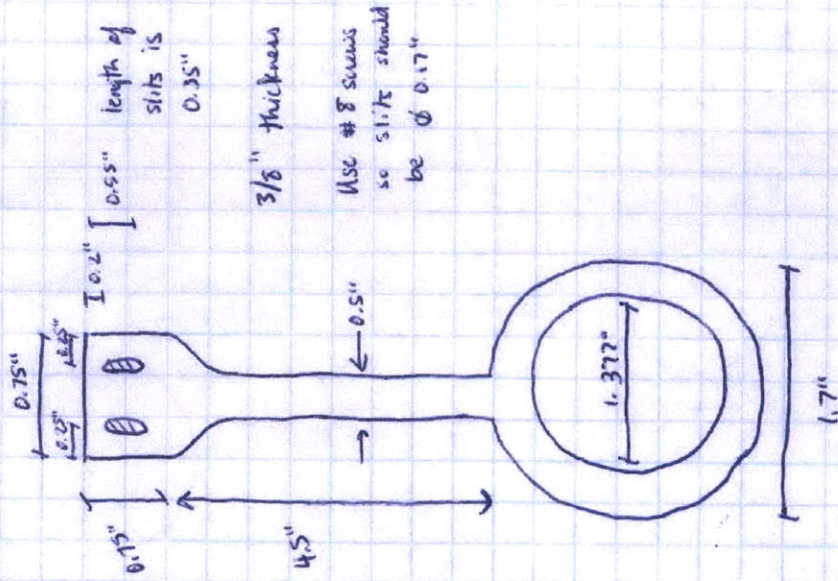
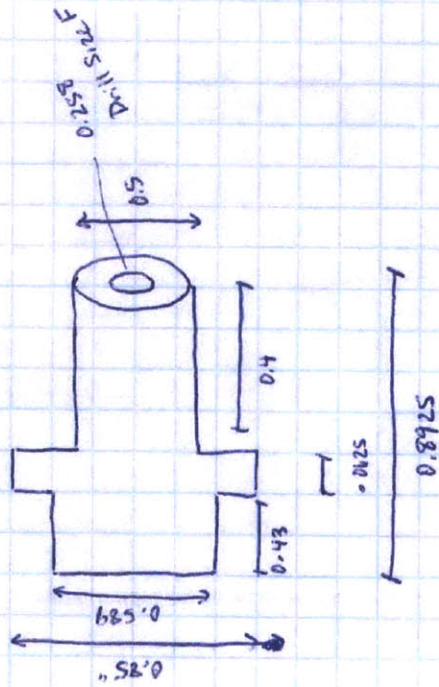


Figure 64 - Dimensional drawing of collars and vertical mounts for outside hubcaps


## Specs for Major Hardware Components

ANAHEIM  
AUTOMATION

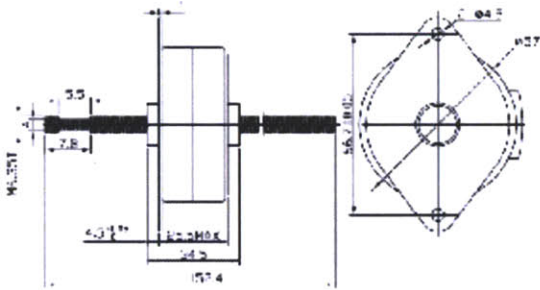
### TSFNA57 Series Linear Actuator

FEATURES

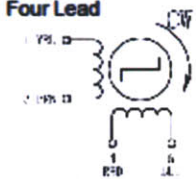
- **Cost Effective Linear Actuator**
- **Step Motor with Internal Conversion to Linear Output**
- **Up to 24 lb of Thrust**
- **Can be Customized for**
  - Screw Options
  - Leadwires
  - Cables and Connectors
- **CE Certified and RoHS Compliant**



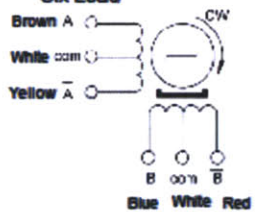
DIMENSIONS



**Four Lead**



**Six Lead**



Brown A      White com      Yellow A  
Blue B      White B      Red B

SPECIFICATIONS

The TSFNA57 Linear Actuator is the perfect choice for cost effective linear motion. The stepper motor internally converts rotary motion to linear motion via a rotating bronze nut and a leadscrew. This actuator eliminates the need for other rotary-to-linear conversions such as belt and pulleys, rack and pinions, or external ball screws. Motion designs can be simplified, production costs lowered and product life enhanced. The motors can be customized to fit your machine requirements. The motor comes in a standard 6-lead or 4-lead configuration. We can also customize the winding to perfectly match your voltage, current, and maximum operating speed. Special screw modifications, cables and connectors are also available upon request.

Item #	Motor Size	Force (lb)	Bipolar Current (A)	Bipolar Voltage (V)	Unipolar Resistance (Ohms)	Unipolar Inductance (mH)	Travel Per Fullstep (inch)	# of Lead Wires	Weight (lbs)
TSFNA57-075-26-042-UW4	57mm	24	0.5	12	24	31	.005"	4	0.66
TSFNA57-075-26-023-UW6	57mm	24	0.32	16	50	116	.00098"	6	0.66

**L010717**

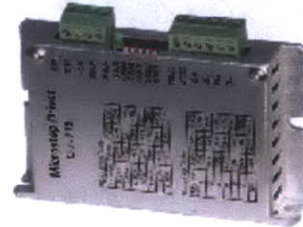
910 East Orangefair Ln. Anaheim, CA 92801 Tel. (714) 992-0990 Fax. (714) 992-0471 www.anaheimautomation.com

Figure 65 - Specification sheet for linear actuator

## 18187-MS 2 PHASE 1.8° STEPMOTOR DRIVER QJ-215

### SPECIFICATIONS:

**Power Input:** 12-32VDC (36V Absolute Max)  
**Control Inputs:** +5V TTL <20mA Optically Isolated  
**Output Drive Current:** 0.2-1.5A  
**Stepping: Basic:** 1/1=1.8°  
**Microstepping:** 1/2-1/4-1/8-1/16-1/32-1/64  
**Protection:** Overheat/50% Current lock  
**Connections:** Terminal Strips  
**Physical:** L: 3-7/8" W: 2-1/2" T: 3/4" WT: .25lb



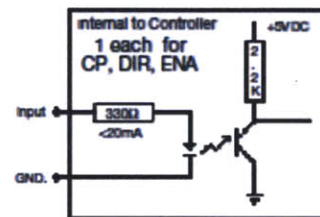
### INPUT/OUTPUT CONNECTIONS:

#### Outputs:

**A+** Motor Winding Phase A+  
**A-** Motor Winding Phase A-  
**B+** Motor Winding Phase B+  
**B-** Motor Winding Phase B-

#### Inputs:

**Vcc+:** Input Power Positive  
**GND-:** Input Power & Logic Negative  
**+5VDC** Logic Power for Opto-Couplers  
**ENA** Turns Outputs ON/OFF  
**CP** Step Pulse  
**DIR** "1"/"HIGH" Forward  
 "0"/"LOW" Reverse



### NOTES:

CP, DIR & ENA are +5V logic levels CP is + edge triggered  
 DO NOT SHORT motor wires; Damage will occur to Driver  
 When used above 1.05A output or Above 30°C, Module must be mounted to Heatsink/metal panel or use fan to provide Axial air flow  
 Internal timer sets output to 1/2 of programmed Current after no input signal is received for 1/2 Second to prevent motor heating.  
 Should motor oscillate/show erratic rotation/torque/reversing problems, Check motor wiring to driver

### MICRO STEP SELECTION

Switch: 0="ON" lever Down  
 1="OFF" Lever Up

STEP	S4	S5	S6
1	0	0	0
1/2	1	0	0
1/4	0	1	0
1/8	1	1	0
1/16	0	0	1
1/32	1	0	1
1/64	0	1	1

### OUTPUT CURRENT LIMIT SELECTION

Switch: 0="ON" lever Down  
 1="OFF" Lever Up

I <sub>OUT</sub>	S1	S2	S3
.21A	0	0	0
.42A	0	0	1
.63A	0	1	0
.84A	0	1	1
1.05A	1	0	0
1.26A	1	0	1
1.5A	1	1	0

Figure 66 - Specification sheet for stepper motor driver

## Stepper Motor Overview

Stepper motors operate differently than regular DC motors. As diagramed in the lower left of Figure 67, stepper motors are built from two electromagnets (marked as 1 and 2 in the diagram) and a 6-pole magnetic rotor. As the electromagnets are energized in sequence, the rotor turns. Figure 67 also includes a timing diagram and phase diagram as visualization tools. The axes in the phase diagram represent the input signals for each electromagnet. The timing diagram also show the input signals for each electromagnet but here they are shown separately as a function of time. As can be seen from either diagram, four different states are possible (marked as 0, 1, 2, or 3). Both electromagnets can be high, both can be low, or they can be opposite each other. The frequency of the signal determines the speed that the motor turns at and the sequence of the signals determines the direction. This type of design allows for precise positioning without the need for feedback. In order to control the stepper motors, a direction command and a square pulse wave is sent to the motor driver. The motor driver then translates those commands into the proper sequence of pulses to move the motor. The motor driver is analogous to a compiler. The user writes the source code but then the driver translates that code into the assembly language that the motor needs to run.

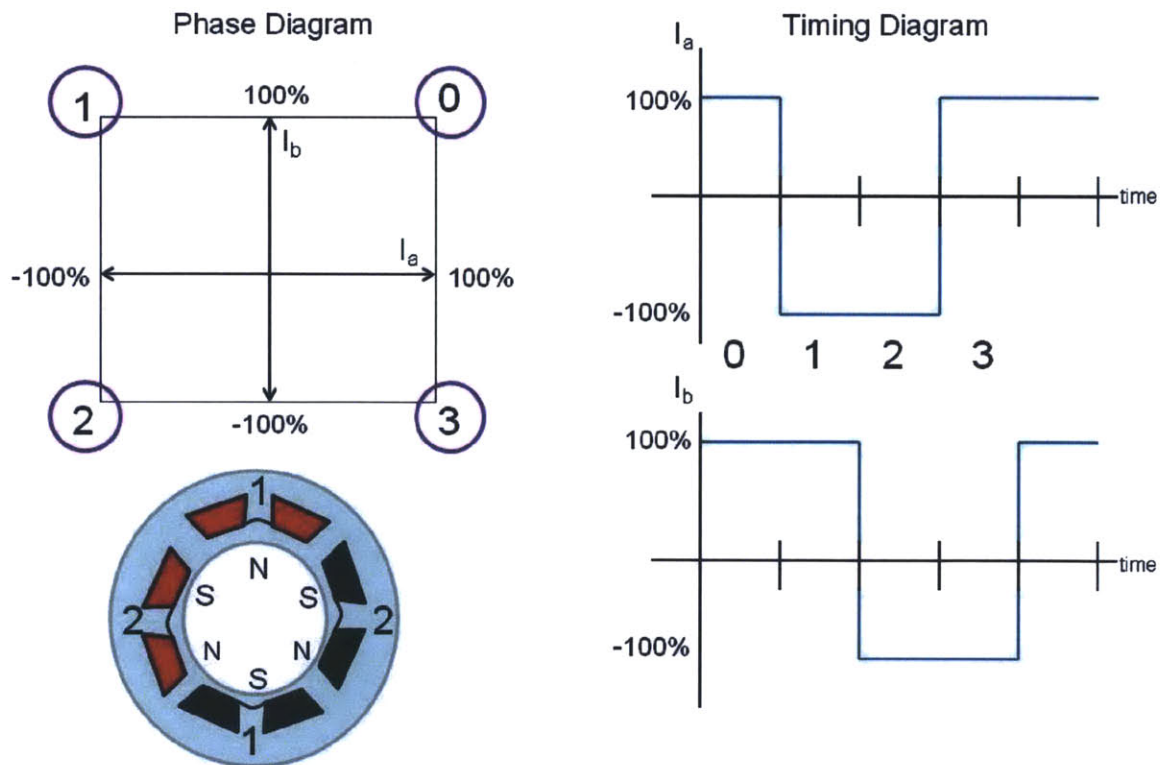


Figure 67 - Stepper motor diagrams

# Electrical System Setup

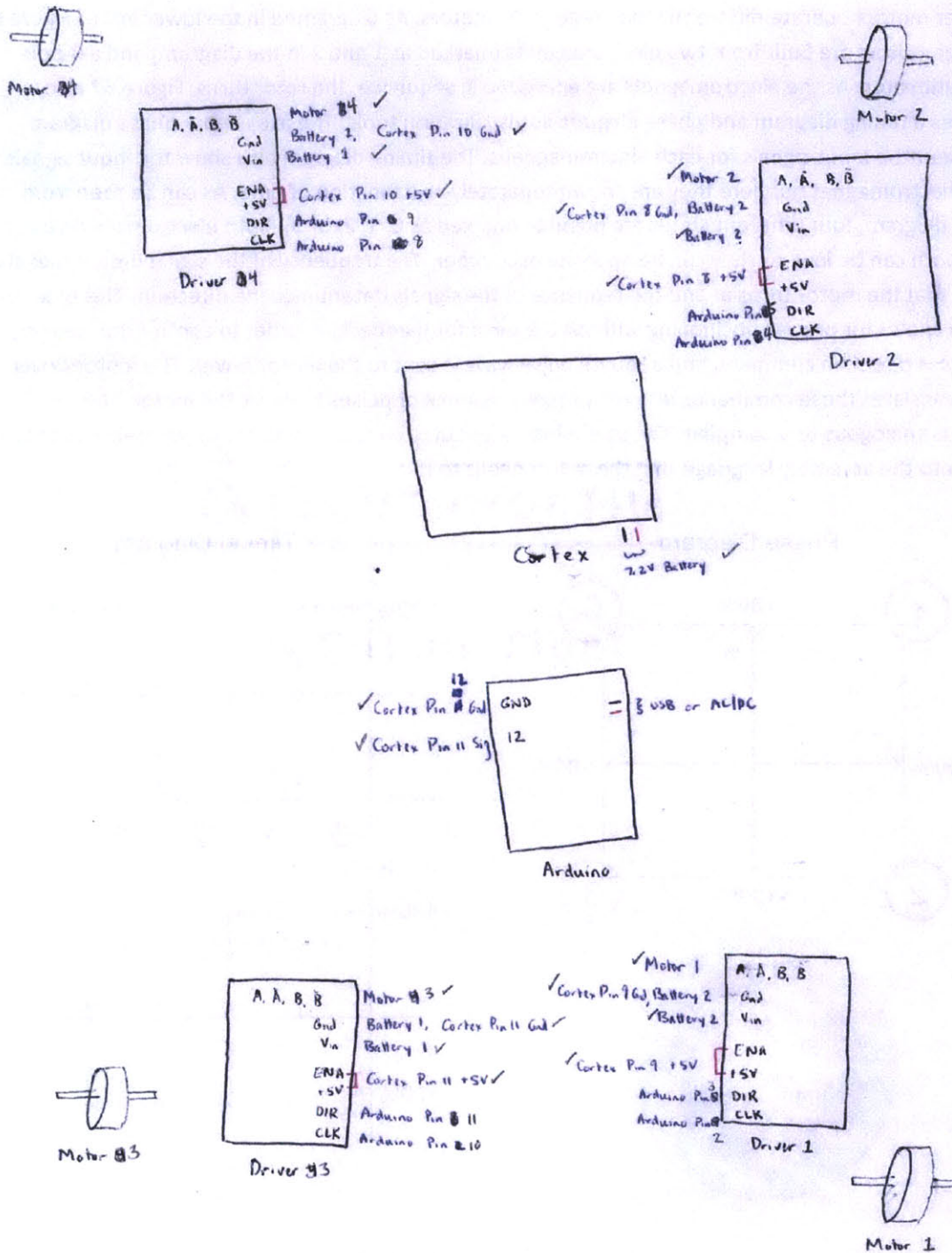


Figure 68 - All of the connections for the electrical system

## Test Plan

The testing procedure is outlined below.

1. Make sure all rover electronics are unplugged and turned off
2. Remove voltmeter
3. Manually put wheels in smallest width configuration
4. Replace voltmeter and turn it on
5. Position rover at starting point in trench
6. Connect Cortex microcontroller to laptop using USB to USB cord
7. Mark starting location of rover
8. Run robotC code from laptop
9. While rover is moving forward, observe and record average current reading from voltmeter
10. Once rover stops, measure and record how far rover has traveled
11. Reconfigure wheels to widest width
  - a. Remove voltmeter
  - b. Plug in driver batteries
  - c. Plug in Arduino microcontroller
  - d. After wheels have reached widest width unplug microcontroller
  - e. Unplug driver batteries
  - f. Replace voltmeter
12. Mark location of rover
13. Run robotC code from laptop
14. While rover is moving forward, record average current reading from voltmeter
15. Once rover stops, measure and record how far rover has traveled (measurement taken from point in step 12)

## Scatter Plots and Statistical Tables

Scatter plots showing the data for all different test scenarios are shown below. The scatter plots show the power and distance results for the non-reconfigurable and reconfigurable systems. Tables showing statistics for other relevant values are also shown for each scenario.

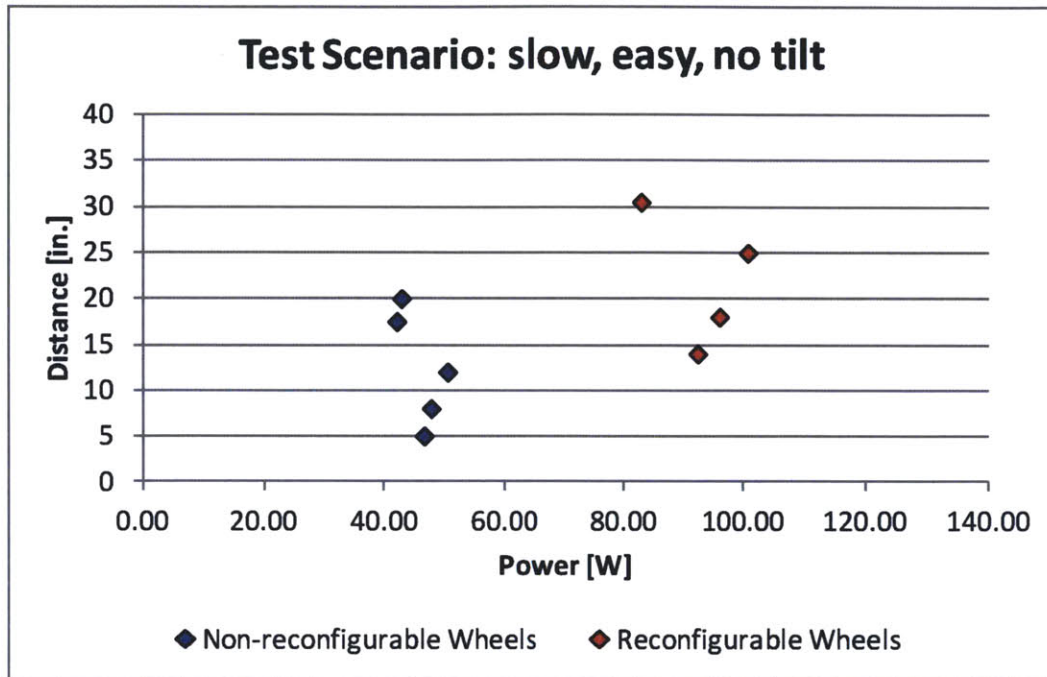


Figure 69 - Power and distance data for slow, easy, no tilt scenario

Table 14 - Statistics for slow, easy, no tilt scenario

Variable Name	Mean	Standard Deviation	Min Value	Max Value
Reconfigurable (i.e. Total) Distance [in.]	26.3	11.76	14	44
Increase in Distance [in.]	13.8	5.97	9	24
% Increase in Distance	121.52%	38.21%	74.29%	180.00%
Reconfigurable (i.e. Total) Power [W]	92.87	6.59	82.87	100.80
Increase in Power [W]	1.14	3.18	-1.08	6.70
% Increase in Power	2.64%	7.44%	-2.57%	15.66%
J* ( $\alpha = 0.5$ )	-0.16	0.15	-0.30	0.04
J* ( $\alpha = 0.6$ )	-0.01	0.17	-0.18	0.23
J* ( $\alpha = 0.7$ )	0.14	0.19	-0.05	0.43
J* ( $\alpha = 0.8$ )	0.29	0.22	0.07	0.62
Overall Efficiency	0.29	0.13	0.15	0.48
Relative Efficiency	1.09	0.20	0.88	1.41



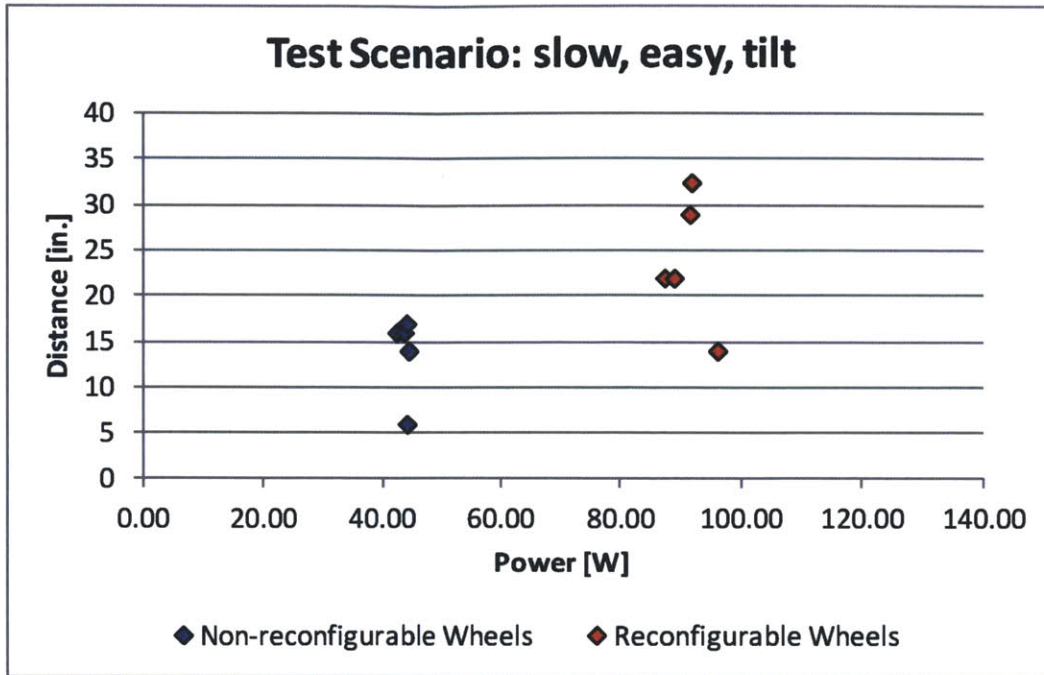


Figure 70 - Power and distance data for slow, easy, tilted scenario

Table 15 – Statistics for slow, easy, tilted scenario

Variable Name	Mean	Standard Deviation	Min Value	Max Value
Reconfigurable (i.e. Total) Distance [in.]	23.9	7.16	14	32.5
Increase in Distance [in.]	10.1	4.77	6	15.5
% Increase in Distance	81.33%	42.75%	37.50%	133.33%
Reconfigurable (i.e. Total) Power [W]	91.07	3.35	87.26	96.05
Increase in Power [W]	3.60	2.44	1.58	7.78
% Increase in Power	8.21	5.50	3.63	17.62
J* ( $\alpha = 0.5$ )	-0.11	0.12	-0.28	0.02
J* ( $\alpha = 0.6$ )	0.06	0.14	-0.14	0.22
J* ( $\alpha = 0.7$ )	0.23	0.16	0.00	0.41
J* ( $\alpha = 0.8$ )	0.40	0.18	0.14	0.61
Overall Efficiency	0.26	0.08	0.15	0.35
Relative Efficiency	0.87	0.19	0.67	1.07

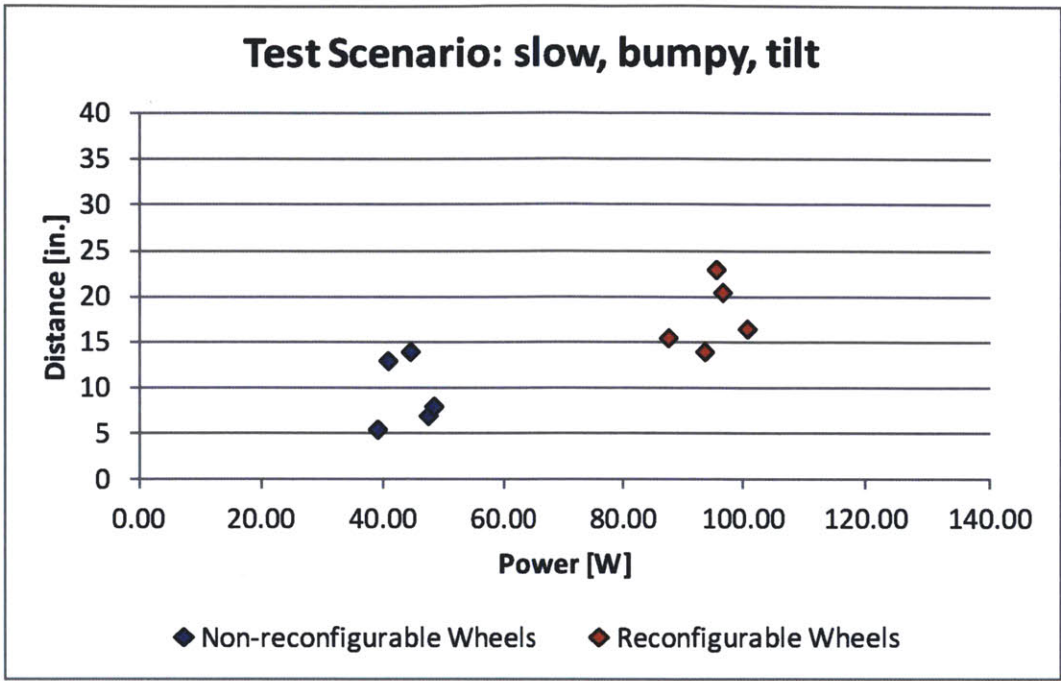


Figure 71 - Power and distance data for slow, bumpy, tilted scenario

Table 16 - Statistics for slow, bumpy, tilted scenario

Variable Name	Mean	Standard Deviation	Min Value	Max Value
Reconfigurable (i.e. Total) Distance [in.]	17.9	3.73	14	23
Increase in Distance [in.]	8.4	1.19	7	10
% Increase in Distance	102.01%	49.44%	57.69%	181.82%
Reconfigurable (i.e. Total) Power [W]	94.62	4.79	87.41	100.51
Increase in Power [W]	6.81	6.05	-1.15	15.05
% Increase in Power	16.45%	15.08%	-2.44%	36.99%
J* ( $\alpha = 0.5$ )	-0.08	0.08	-0.16	0.03
J* ( $\alpha = 0.6$ )	0.09	0.09	-0.01	0.22
J* ( $\alpha = 0.7$ )	0.26	0.11	0.15	0.42
J* ( $\alpha = 0.8$ )	0.43	0.13	0.30	0.61
Overall Efficiency	0.19	0.04	0.15	0.24
Relative Efficiency	0.94	0.23	0.67	1.26

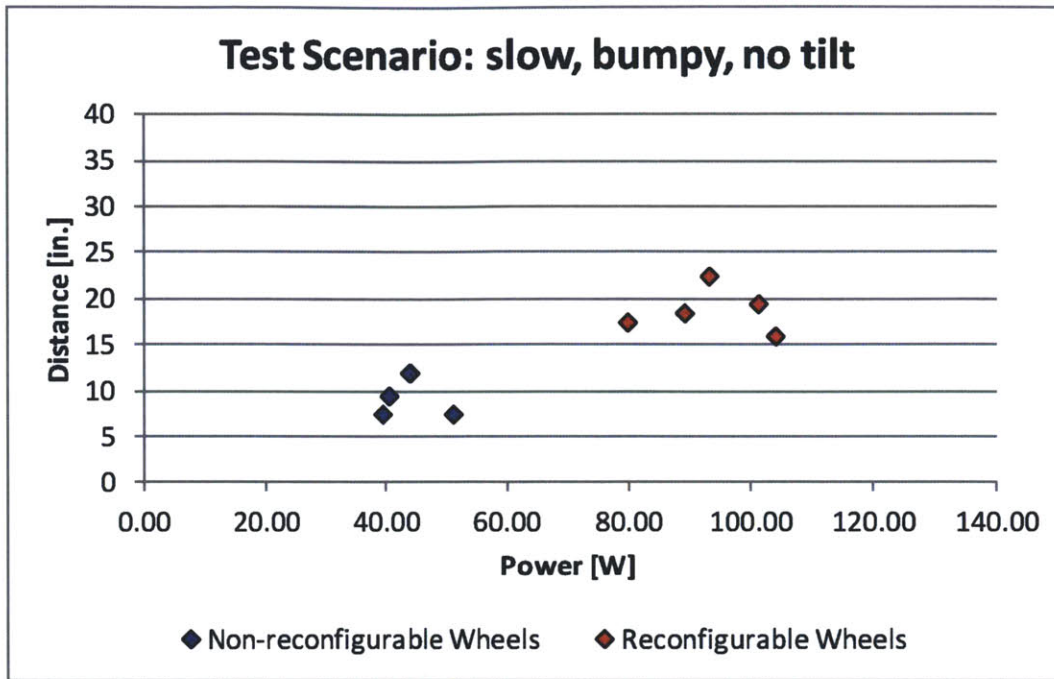


Figure 72 - Power and distance data for slow, bumpy, no tilt scenario

Table 17 - Statistics for slow, bumpy, no tilt scenario

Variable Name	Mean	Standard Deviation	Min Value	Max Value
Reconfigurable (i.e. Total) Distance [in.]	18.8	2.44	16	22.5
Increase in Distance [in.]	9.1	1.19	7.5	10.5
% Increase in Distance	98.28%	26.76%	62.50%	133.33%
Reconfigurable (i.e. Total) Power [W]	93.47	9.73	79.78	104.04
Increase in Power [W]	6.03	5.18	1.15	13.68
% Increase in Power	14.04%	12.08%	2.93%	31.25%
J* ( $\alpha = 0.5$ )	-0.03	0.07	-0.14	0.05
J* ( $\alpha = 0.6$ )	0.14	0.08	0.03	0.24
J* ( $\alpha = 0.7$ )	0.32	0.08	0.20	0.43
J* ( $\alpha = 0.8$ )	0.49	0.09	0.37	0.62
Overall Efficiency	0.20	0.03	0.15	0.24
Relative Efficiency	0.93	0.17	0.70	1.15

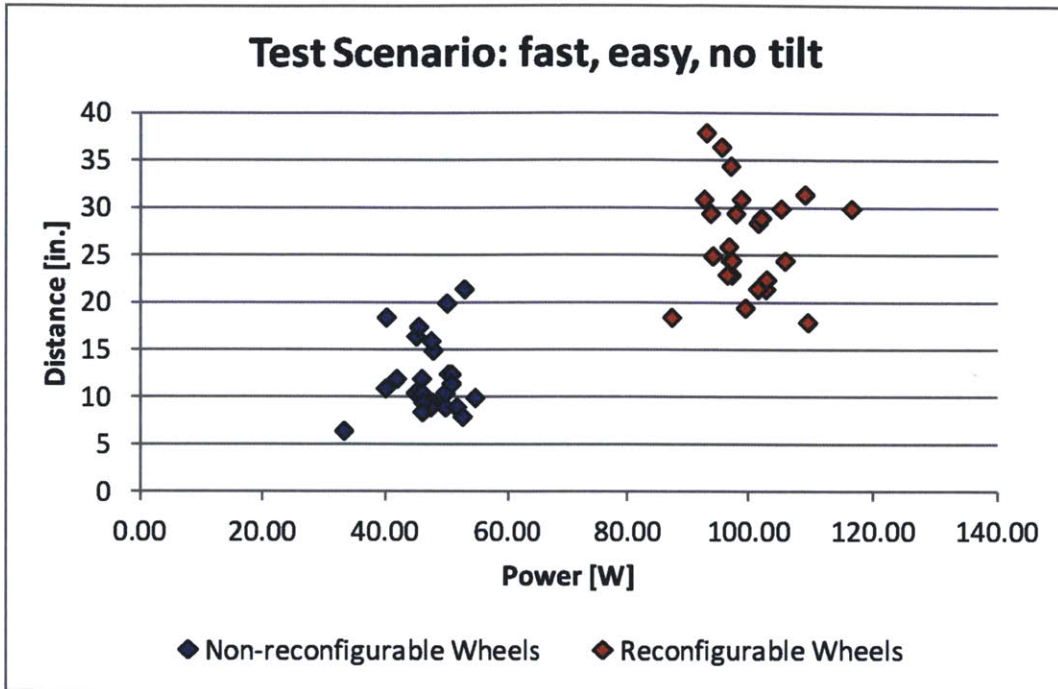


Figure 73 - Power and distance data for fast, easy, no tilt scenario

\*Note: In the fast, easy, no tilt scenario 25 tests were completed so that an error analysis could be completed.

Table 18 - Statistics for fast, easy, no tilt scenario

Variable Name	Mean	Standard Deviation	Min Value	Max Value	90% Confidence Interval
Reconfigurable (i.e. Total) Distance [in.]	26.84	5.41	18.00	38.00	+/- 1.85
Increase in Distance [in.]	14.56	4.74	6.00	26.00	+/- 1.62
% Increase in Distance	132.37%	63.57%	46.51%	305.88%	+/- 21.71%
Reconfigurable (i.e. Total) Power [W]	99.53	6.31	87.19	116.50	+/- 2.16
Increase in Power [W]	5.57	7.25	-7.63	20.95	+/- 2.48
% Increase in Power	13.27%	17.95%	-14.00%	63.26%	+/- 6.13%
J* ( $\alpha = 0.5$ )	-0.07	0.08	-0.23	0.10	+/- 0.027
J* ( $\alpha = 0.6$ )	0.08	0.09	-0.09	0.28	+/- 0.031
J* ( $\alpha = 0.7$ )	0.24	0.10	0.05	0.46	+/- 0.035
J* ( $\alpha = 0.8$ )	0.39	0.12	0.19	0.64	+/- 0.039
Overall Efficiency	0.27	0.06	0.16	0.41	+/- 0.020
Relative Efficiency	1.10	0.33	0.63	1.92	+/- 0.11

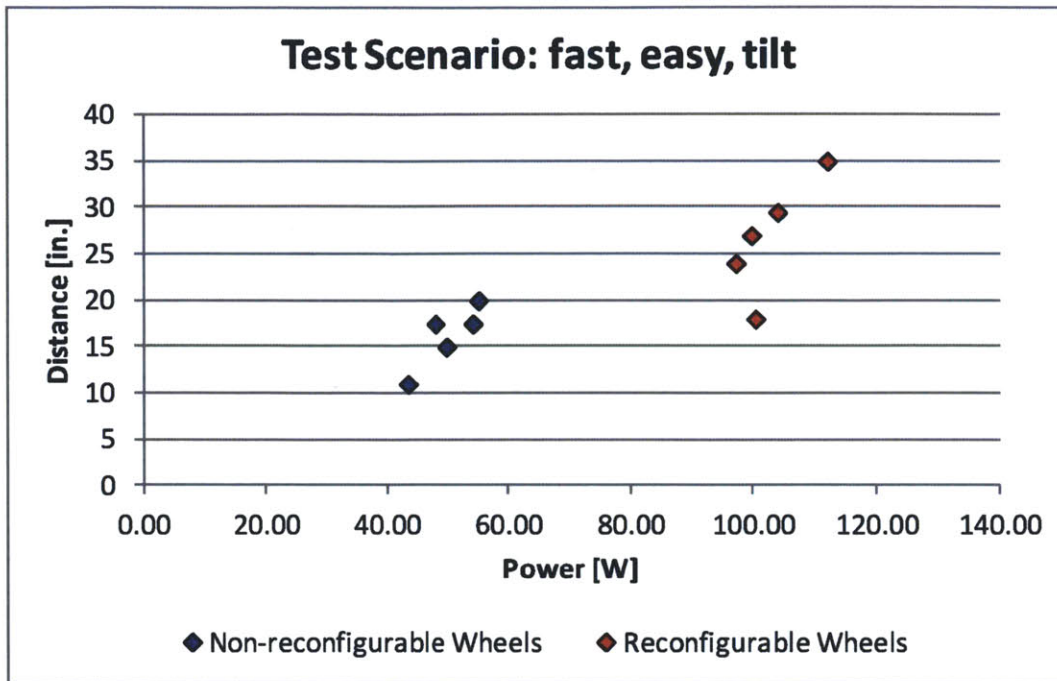


Figure 74 - Power and distance data for fast, easy, tilted scenario

Table 19 - Statistics for fast, easy, tilted scenario

Variable Name	Mean	Standard Deviation	Min Value	Max Value
Reconfigurable (i.e. Total) Distance [in.]	26.7	6.32	18.00	35.00
Increase in Distance [in.]	10.5	3.08	7.00	15.00
% Increase in Distance	64.30	7.94	54.29	75.00
Reconfigurable (i.e. Total) Power [W]	102.66	5.77	97.20	112.03
Increase in Power [W]	2.43	7.00	-4.32	13.54
% Increase in Power	5.81	15.52	-7.98	31.18
J* ( $\alpha = 0.5$ )	-0.08	0.07	-0.19	0.00
J* ( $\alpha = 0.6$ )	0.09	0.09	-0.05	0.20
J* ( $\alpha = 0.7$ )	0.26	0.11	0.09	0.40
J* ( $\alpha = 0.8$ )	0.43	0.14	0.23	0.60
Overall Efficiency	0.26	0.05	0.18	0.31
Relative Efficiency	0.80	0.07	0.71	0.88

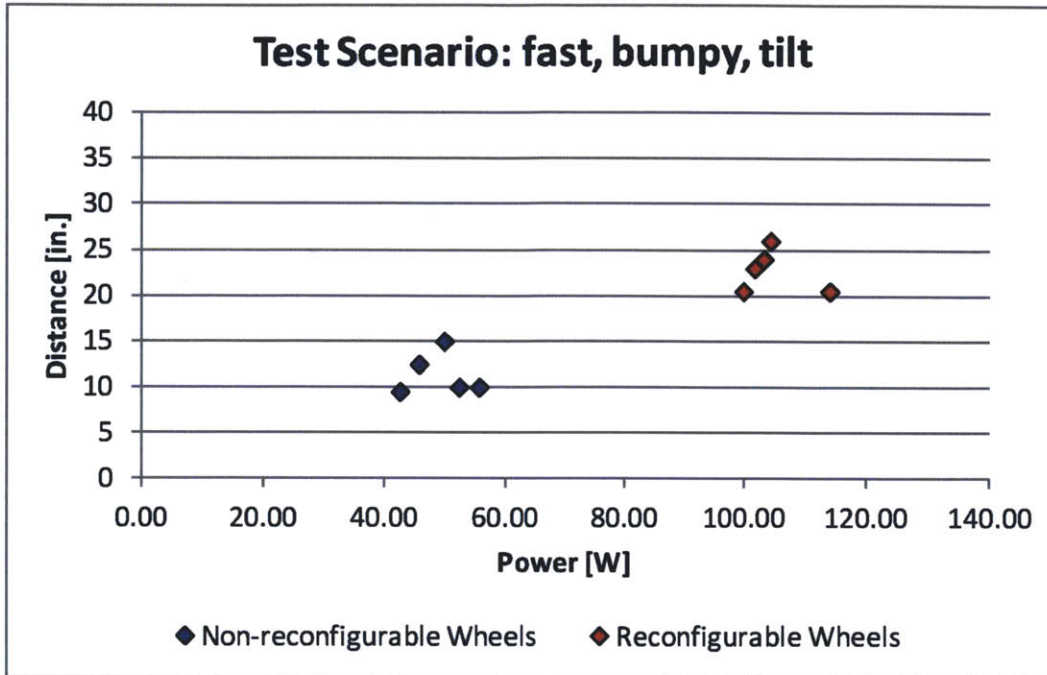


Figure 75 - Power and distance data for fast, bumpy, tilted scenario

Table 20 - Statistics for fast, bumpy, tilted scenario

Variable Name	Mean	Standard Deviation	Min Value	Max Value
Reconfigurable (i.e. Total) Distance [in.]	22.8	2.36	20.5	26
Increase in Distance [in.]	11.4	2.68	9	16
% Increase in Distance	104.96%	37.44%	60.00%	160.00%
Reconfigurable (i.e. Total) Power [W]	104.77	5.49	100.01	114.12
Increase in Power [W]	6.16	6.19	-0.36	14.76
% Increase in Power	13.62%	14.56%	-0.69%	34.63%
J* ( $\alpha = 0.5$ )	-0.02	0.06	-0.11	0.04
J* ( $\alpha = 0.6$ )	0.16	0.06	0.07	0.23
J* ( $\alpha = 0.7$ )	0.34	0.07	0.25	0.43
J* ( $\alpha = 0.8$ )	0.52	0.08	0.43	0.62
Overall Efficiency	0.22	0.03	0.18	0.25
Relative Efficiency	0.97	0.21	0.77	1.30

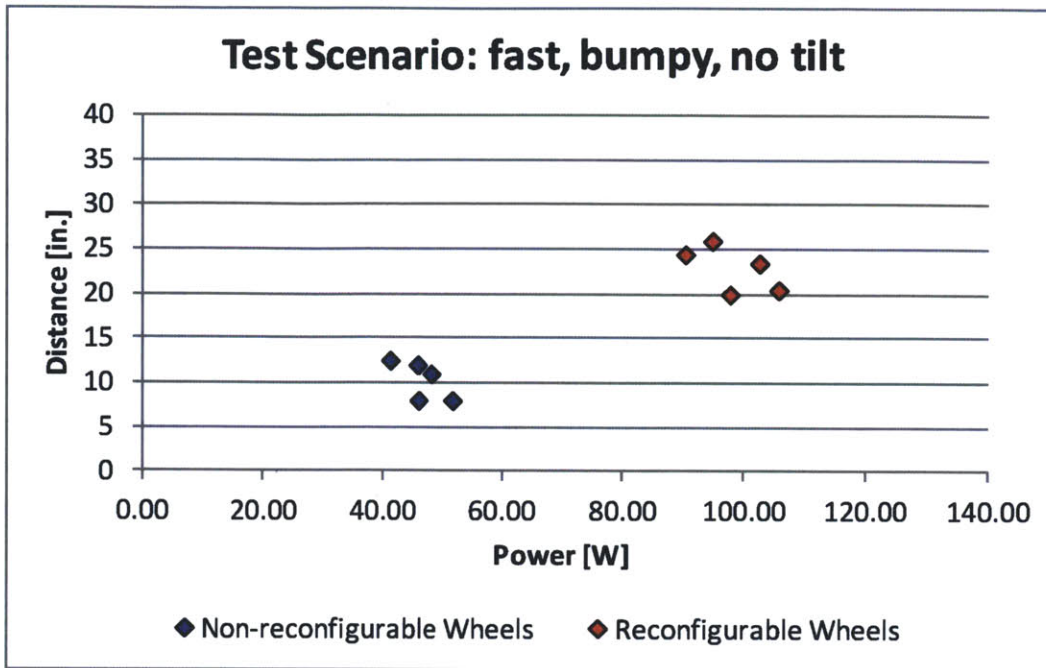


Figure 76 - Power and distance data for fast, bumpy, no tilt scenario

Table 21 - Statistics for fast, bumpy, no tilt scenario

Variable Name	Mean	Standard Deviation	Min Value	Max Value
Reconfigurable (i.e. Total) Distance [in.]	22.9	2.58	20	26
Increase in Distance [in.]	12.6	3.31	9	18
% Increase in Distance	130.98%	59.90%	81.82%	225.00%
Reconfigurable (i.e. Total) Power [W]	98.19	6.12	90.29	105.70
Increase in Power [W]	4.94	9.02	-8.93	13.68
% Increase in Power	11.57	18.99	-17.22	29.73
J* ( $\alpha = 0.5$ )	-0.02	0.07	-0.11	0.05
J* ( $\alpha = 0.6$ )	0.16	0.08	0.07	0.24
J* ( $\alpha = 0.7$ )	0.34	0.08	0.25	0.43
J* ( $\alpha = 0.8$ )	0.52	0.09	0.43	0.62
Overall Efficiency	0.23	0.04	0.19	0.27
Relative Efficiency	1.11	0.38	0.88	1.78

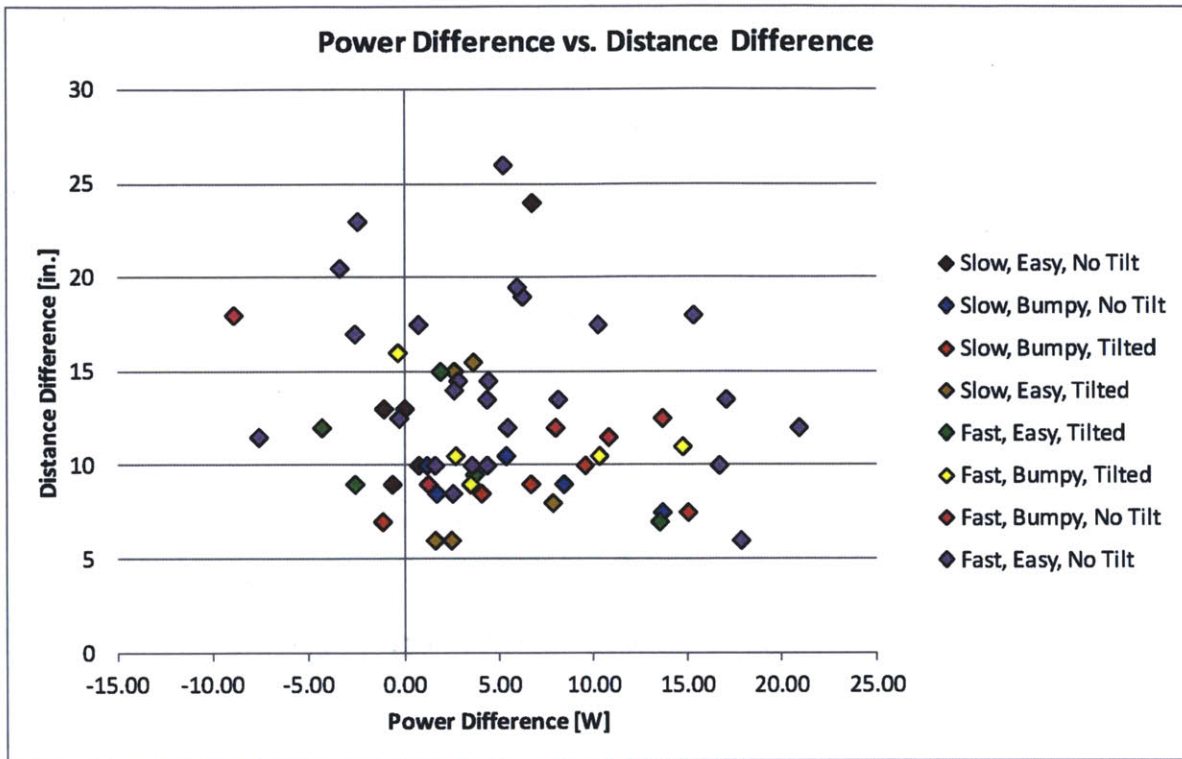


Figure 77 - Power difference vs. distance difference for all tests